A DIAGNOSTIC QUASI-DIMENSIONAL MODEL OF HEAT TRANSFER AND COMBUSTION IN COMPRESSION-IGNITION ENGINES

ALAN CHRISTOPHER HANSEN

Submitted in partial fulfilment of the
requirements for the degree of
Ph.D.

Department of Agricultural Engineering
University of Natal
1989

ABSTRACT

Investigations into the combustion of alternative fuels in compression-ignition engines in South Africa have underlined the inadequacies of existing zero-dimensional combustion models. The major aspect of concern in these models was the computation of heat transfer which had been singled out by a number of researchers as the leading cause of inaccuracies in heat release computations.

The main objective of this research was to develop a combustion model that was less empirically based than the existing zero-dimensional models for use in evaluating the combustion and resulting thermal stresses generated by alternative fuels in diesel engines. Particular attention was paid to the development of a spatial and temporal model of convective heat transfer that was based on gas flow characteristics and to the introduction of a radiation heat transfer model that made use of fuel properties and fuel-air ratio. The combustion process was divided into two zones representing burnt and unburnt constituents and the resulting temperatures in each zone were used in the calculations of convective and radiative heat transfer. The complete model was formulated in such a way that it could be applied with the aid of a micro-computer.

Calibration and verification of the gas flow sub-models which involved the squish, swirl and turbulence components necessitated the use of published data. Good agreement for the squish and swirl components was obtained between the present model and the experimental data from three engines, two with a bowl-in-piston and the other with a flat piston. These gas flow components dominated the gas velocities in the combustion chamber and provided a reliable foundation for the calculation of convective heat transfer. In spite of the well documented difficulties of characterising turbulence, after calibration the model generated turbulence levels with acceptable trends and magnitudes.

Tests were carried out on a naturally aspirated ADE 236 engine involving the measurement of cylinder pressure and heat flux at a single point. Motored engine data were used to verify the convective heat transfer rates and to ascertain the effects of soot deposition on the heat flux probe. Close correlation between predicted and measured heat flux was achieved after accounting for the effects of chamber geometry at the probe site. Soot deposition on the probe caused a significant attenuation of the heat flux within a short period of the engine running under fired conditions.

The results from fired engine tests showed that the two zone combustion model was providing plausible trends in the burnt and unburnt zone temperatures and that the model generated combined heat transfer rates which were credible not only on a global basis but also in terms of point predictions in the combustion chamber. The results also highlighted the considerable variation in heat transfer that could occur from one point in the chamber to another. Such variations added considerable weight to the objective of moving away from a zero-dimensional model to a quasi-dimensional type where predictions could be made on a more localised rather than global basis. It was concluded that the model was a definite improvement over zero-dimensional models and competed favourably with existing quasi-dimensional models with advantages in both simplicity and accuracy.

I wish to certify that the work reported in this thesis is my own original and unaided work except where specific acknowledgement is made. In addition I wish to declare that this thesis has not been submitted for a degree in any other university.

Signed.....

A C HANSEN

Acknowledgements

The author wishes to record his sincere appreciation for the assistance given by the following:

Professor P. Meiring, Head of the Department of Agricultural Engineering, University of Natal, for his supervision of the work and his encouragement and support for this venture.

Dr C.E. Goering, Division Head of Power and Machinery, Department of Agricultural Engineering, University of Illinois, Urbana, Illinois, USA, for his considerable advice and support during the course of the project.

Mr P.W.L. Lyne, Senior Lecturer, Department of Agricultural Engineering, University of Natal, for his encouragement and support.

Mr A.B. Taylor, Engineer, SasTech (Pty) Ltd, Sasolburg, for his assistance on certain aspects of the project.

Mr R.W. Haines, Mr R.P. North and Mr C.C. Tredrea for their assistance during the engine tests.

Mrs K. Temple and Miss J. Whyte for their assistance in preparing the document.

The University of Natal, who provided funding for the project.

My wife, Jan, for typing the first draft of the thesis and for her continuous encouragement, patience and sacrifice, without which this document would not have been completed.

TABLE OF CONTENTS

TABLE OF CONTENTS (continued)

LIST OF TABLES

LIST OF FIGURES

LIST OF FIGURES (continued)

LIST OF FIGURES (continued)

LIST OF FIGURES (continued)

1. INTRODUCTION

Investigations into the combustion of alternative fuels in compression-ignition engines in South Africa have underlined the inadequacies of existing zero-dimensional combustion models that assume homogeneous conditions in the combustion chamber. With the country's substantial commitment to meeting its own liquid fuel requirements in the face of relatively severe economic and political pressures, it is vitally important that valuable data obtained from combustion tests are analysed with the most advanced technology available in order to reach credible and accurate conclusions. A much greater level of sophistication in the diagnostic type of combustion model is therefore required.

The major aspect of concern in the existing models is the computation of heat transfer which has been singled out by a number of researchers as the leading cause of inaccuracies in heat release computations (Taylor, 1987; Timoney, 1987a; Timoney, 1987b; Taylor, Hansen, Lyne and Meiring, 1989). In an analysis of stress from the combustion of alternative fuels, Taylor et al. (1989) employed a zero-dimensional heat release model to determine bulk gas temperatures and then made certain assumptions based on published data to arrive at suitable boundary conditions for the piston. As the object of the study was to determine relative differences rather than absolute values, the level of accuracy achieved by Taylor et al. (1989) was acceptable. However, future work concerning stress levels in engines that are generated by alternative fuels will require higher levels of accuracy as the differences can be small and still remain significant. There is therefore a strong need for models of heat transfer and combustion that incorporate spatial as well as temporal computations and that can account for engine to engine differences more accurately than a zero-dimensional heat release model. Such a model would be an invaluable tool for the engine manufacturer, fuel producer and the researcher.

The main objective of this research was to develop a combustion model that was less empirically based than the existing zero-dimensional models for use in evaluating the combustion and resulting thermal stresses generated by alternative fuels in diesel engines. Particular attention was paid to the development of a spatial and temporal model of convective heat transfer that was based on gas flow characteristics and to the introduction of a radiation heat transfer model that made use of fuel properties and fuel-air ratio. The combustion process was divided into two zones representing burnt and unburnt constituents and the resulting temperatures in each zone were used in the calculations of convective and radiative heat transfer. The complete model was formulated in such a way that it could be applied with the aid of a micro-computer.

The advantages of this approach to the modelling were that the heat release computations would be more accurate than achieved with the zero-dimensional model and would reflect more closely the influences of combustion chamber geometry with special reference to convective and radiative heat transfer. In addition fairly accurate boundary conditions would be generated for structural calculations in finite element models, the results of which depend critically on the applied thermal loads. More realistic product temperatures would be generated than would be obtained from a zero-dimensional model, thus allowing the expanded model to form the basis of sub-models for nitric oxide formation, soot kinetics and flame radiation. The revised model would still be driven to a large extent by cylinder pressure data and therefore would remain diagnostic in nature. Finally the gas flow model could be used to gauge the effects of varying engine geometry on fuel-air mixing.

In this thesis a literature review of in-cylinder flow processes, heat transfer and combustion modelling is presented with emphasis being placed on those aspects of modelling that are directly relevant to the proposed model. Details of the proposed model and its formulation and structure are then provided. The

calibration and verification of the model with published data and with new experimental data is presented and discussed.

2. LITERATURE REVIEW

Prior to the formulation and verification of the model that was developed in this study it was necessary to review the research that had been carried out on related topics. This review provides the background to the three important subjects of in-cylinder gas flow processes, heat transfer modelling and combustion modelling. Each of these subjects on their own has been investigated extensively. However, the purpose of this review was to provide an indication of the scope of the work completed and the relative complexities involved. In addition, particular attention was paid to those aspects that were relevant to the formulation of the model and its justification.

2.1 In-Cylinder Gas Flow Process

In-cylinder air motion in diesel engines plays a major role in the combustion process and in heat transfer. Owing to the non-stationary character of this air motion caused by the reciprocating piston movement, analysis of the flow processes is complex. The application of the Navier-Stokes equations to these flow processes and the generation of a satisfactory solution on a three-dimensional basis requires not only considerable computer resources but also experimental data to verify such solutions. Arcoumanis and Whitelaw (1987) stated that to achieve a totally predictive ability either the numerical methods had to be improved so that computing time was greatly reduced or computers with much larger storage capacity and speed had to emerge. It has been acknowledged by a number of researchers that model development has overtaken the availability of appropriate data to verify the output of these models. Hence there is still a fairly heavy reliance on empirically based models with the inclusion of physically related phenomena where possible.

In spite of these complexities of air motion the flow models that are presently applied provide results which correspond

remarkably well with the experimental data that are available. The flow patterns are normally divided into mean flow components and fluctuating flow components, the latter being termed turbulence. While it is possible to model the mean flow components fairly accurately, the subject of turbulence remains somewhat nebulous because of the lack of experimental data.

High speed direct injection diesel engines rely heavily on swirl and squish as flow mechanisms for mixing the injected fuel with air. The interaction of these two mean flow components is also important during the compression and expansion strokes as high swirl may inhibit squish induced flow leading to less effective mixing (Arcoumanis and Whitelaw,1987).

In spite of its complexity, turbulence cannot be ignored when characterising the flow processes in a diesel engine as it contributes significantly to heat transfer and to combustion. Tabaczynski (1983) reported that two of the major features of turbulent flow were its definite structure in the flow field and its tendency to be governed by chamber geometry near top dead centre of compression. Turbulence models presently in use provide reasonable levels of accuracy in terms of expected trends. However, they generally employ procedures which provide ensemble-averaged solutions and can only be validated by ensemble-averaged velocity data (Arcoumanis and Whitelaw, 1987).

2.1.1 Swirl and squish

Air motion in direct injection diesel engines during the compression and expansion strokes is dominated by swirl and squish. These flow processes have a major influence on the mixing of injected and evaporated fuel with air.

Swirl is generated initially during the intake stroke by the use of either helical or directed ports. A helical port creates swirl upstream of the intake valve while a directed port is mainly responsible for swirl downstream of the valve. The

magnitude of the resulting swirl is dependent on the slope of the port relative to the cylinder head, the velocity characteristics at the valve exit and the port eccentricity from the cylinder axis. Figure 1 illustrates the variation of swirl during the four phases of the cycle for a bowl-in-piston arrangement. The chamber in this example was divided into three regions, the volume directly above the piston crown, the bowl volume and the volume directly above the bowl as shown in Figure 2. The swirl during the intake stroke rises sharply initially to a maximum and then begins to decay because of wall friction and reduced angular momentum flux.

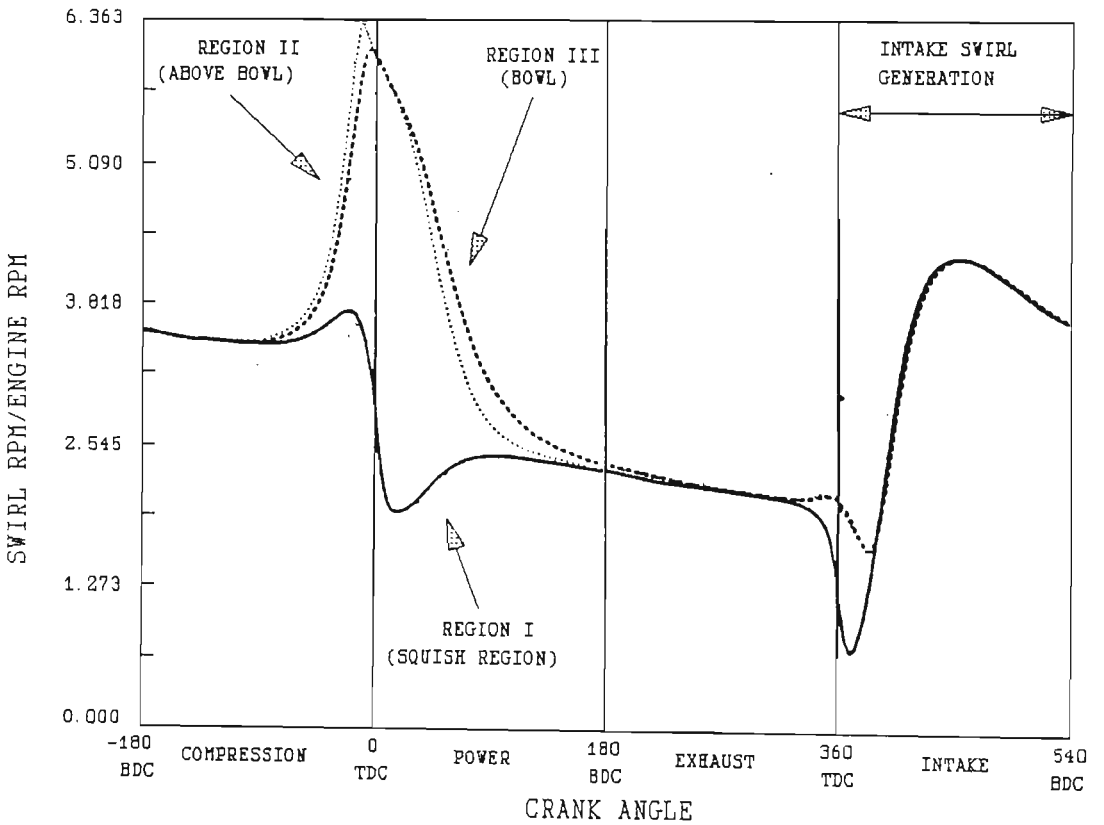

Figure 1 The variation of swirl velocity in three regions of the combustion chamber of a DI diesel engine (after Morel and Keribar, 1985).

At inlet valve closure (IVC) the initial conditions of swirl for the subsequent compression process are established and reflect the inlet port/valve geometry and the small effect of piston geometry on flow development during induction (Arcoumanis and Whitelaw, 1987). As the piston approaches top dead centre (TDC)

of compression the effect of inlet geometry diminishes and the geometry of the piston and cylinder head plays the dominant role in the structure of both mean and turbulent velocity fields (Arcoumanis and Whitelaw, 1987).

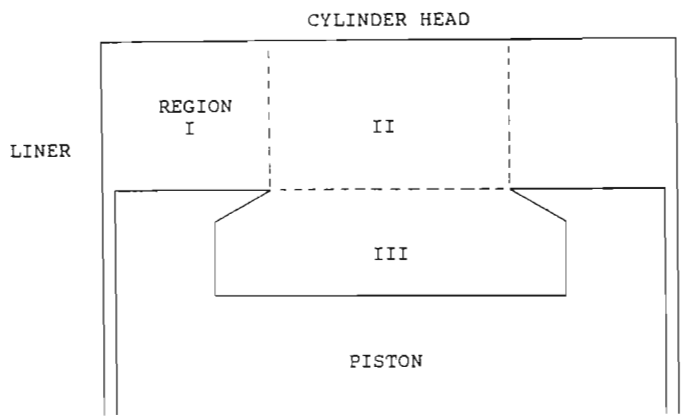

Figure 2 Division of a typical bowl-in-piston combustion chamber into three flow regions (after Morel and Keribar,1985).

During compression the swirling flow tends to be transformed into an organised structure with a velocity distribution which resembles solid body rotation. Measurements in the cylinder by a number of researchers support this finding for bowl-in-piston engines (Dent and Derham, 1974; Arcoumanis, Bicen and Whitelaw, 1983; Fansler, 1985; Murakami, Hiroyasu and Arai, 1986).

Murakami, Arai and Hiroyasu (1988) carried out measurements of tangential velocity distributions for different piston bowl diameters and heads. On the basis of their findings they proposed that the volume in the combustion chamber should be divided into two regions for analysis of the swirling flow fields as shown in Figure 3.

The centre of the bowl in the piston is generally offset from the piston axis in practice. However, Murakami et al. (1988) found that the centre of the swirl motion tended to move around

the cylinder axis during compression independent of the geometry and eccentricity of the inlet valve. This effect is shown in Figure 4 for four crank angle positions and three engine speeds of 250, 500 and 1000 r/min at an axial position 10 mm from the face of the cylinder head.

According to Arcoumanis and Whitelaw (1987) as the piston approached TDC after IVC the overall angular momentum of the swirling air decayed by 30 - 50% depending on swirl distribution and piston geometry. This decay was attributed to wall friction which accompanied an increase of the surface to volume ratio. With bowl-in-piston arrangements the swirl was amplified as TDC was approached because of the conservation of angular momentum and the transfer of an increasing proportion of total mass to the bowl. The increase in angular velocity was proportional to the square of ratio of the cylinder to bowl diameters (Arcoumanis and Whitelaw, 1987).

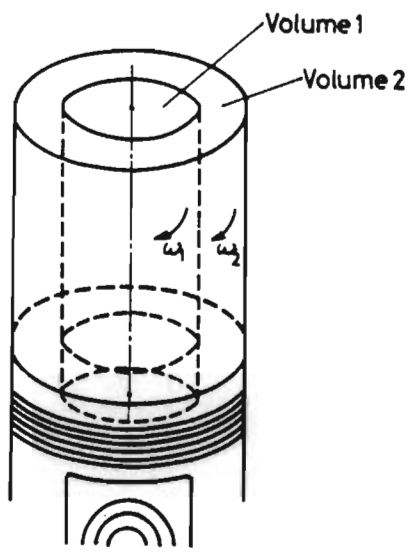

Figure 3 Division of the combustion chamber volume into two regions (Murakami et al., 1988).

Referring to Figure 1, the conservation of angular momentum is illustrated by the increase in swirl velocity for the bowl. Swirl in the region above the piston crown decreases rapidly close to TDC as a result of loss of angular momentum through wall friction.

Compression or squish effect also induces a radial inward motion towards the piston-bowl axis in the clearance gap between the cylinder head and piston crown. The magnitude of the squish velocity, which reaches a peak approximately 10° before TDC (BTDC) and again 10° after TDC (ATDC) when there is reverse squish as shown in Figure 5, is dictated by the piston crown to head clearance and the ratio of bowl to bore diameters. It is also affected by air leakage through the piston rings, the dimensions of the crevice volume and heat losses to the wall and cylinder head (Arcoumanis and Whitelaw, 1987).

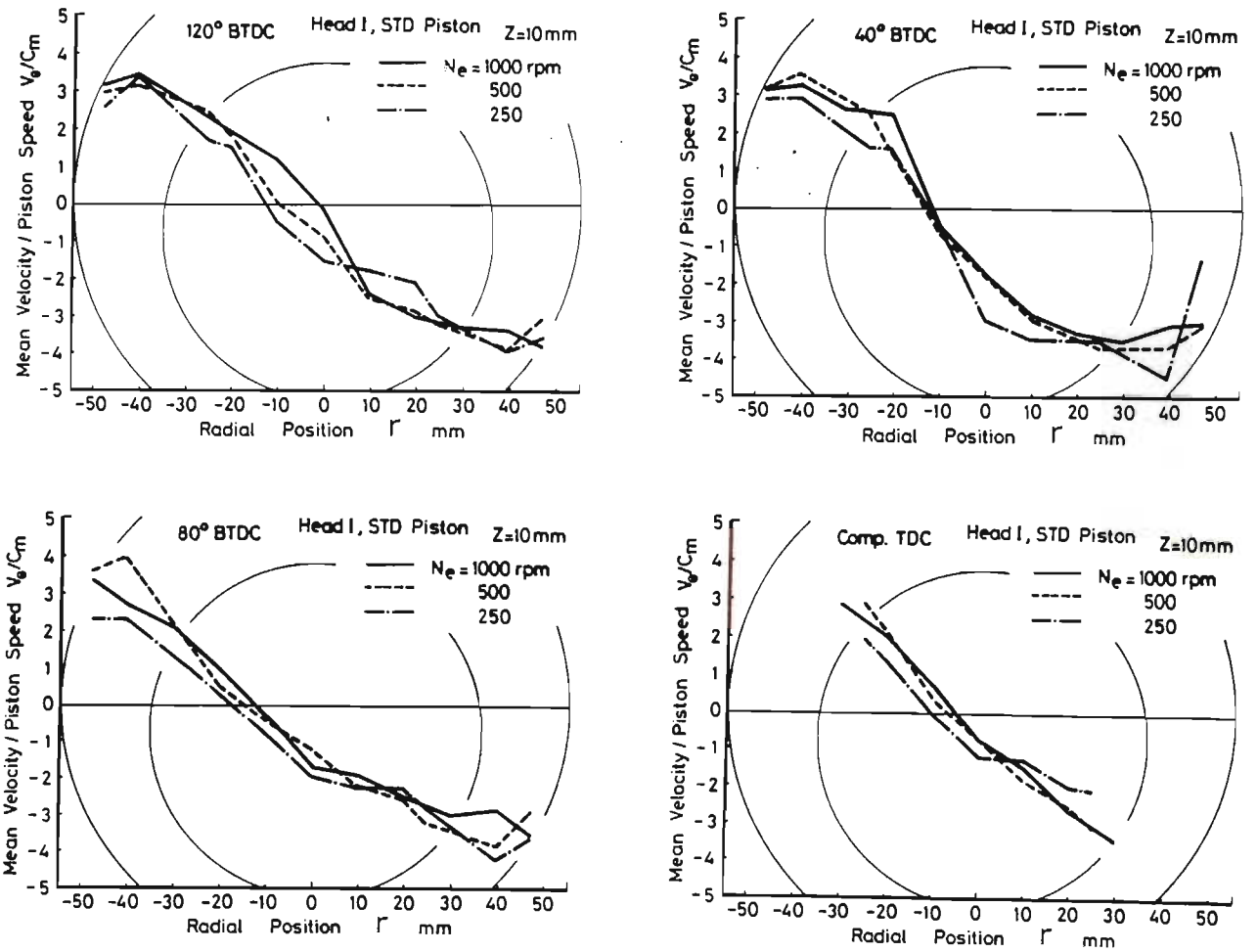

Figure 4 The variation of swirl motion relative to the cylinder axis for four crank angle positions and three engine speeds (Murakami et al., 1988).

Arcoumanis and Whitelaw (1987) also pointed out the competing requirements of the centrifugal forces associated with swirl and the opposing inward squish motion as TDC was approached. Arcoumanis et al. (1983) found that in the absence of swirl an anti-clockwise rotating vortex shown in Figure 6 was generated inside the piston bowl. In the presence of swirl the vortex changed rotational direction as a result of reduced penetration, inhibited by swirl, of squish towards the cylinder axis. This effect of reduced penetration was also reflected in the work of Arcoumanis, Begleris, Gosman and Whitelaw (1986) for a bowl-in-piston configuration.

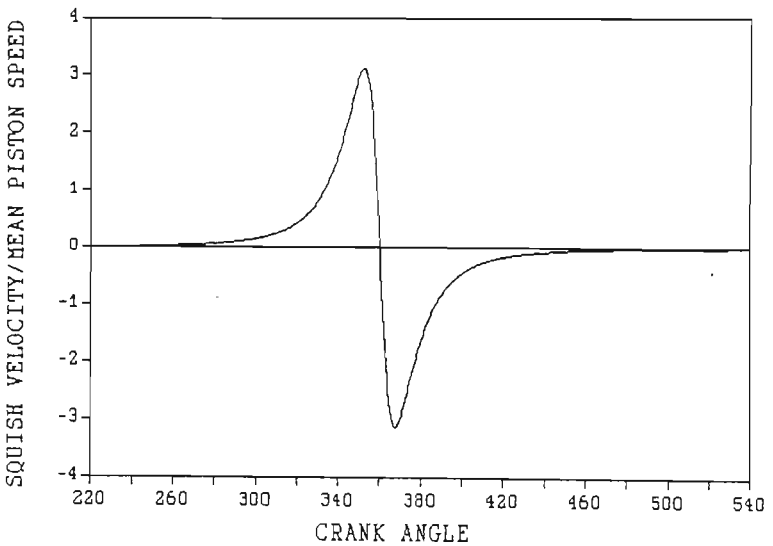

Figure 5 The variation of squish velocity with crank angle during the compression and expansion strokes for a typical DI diesel engine.

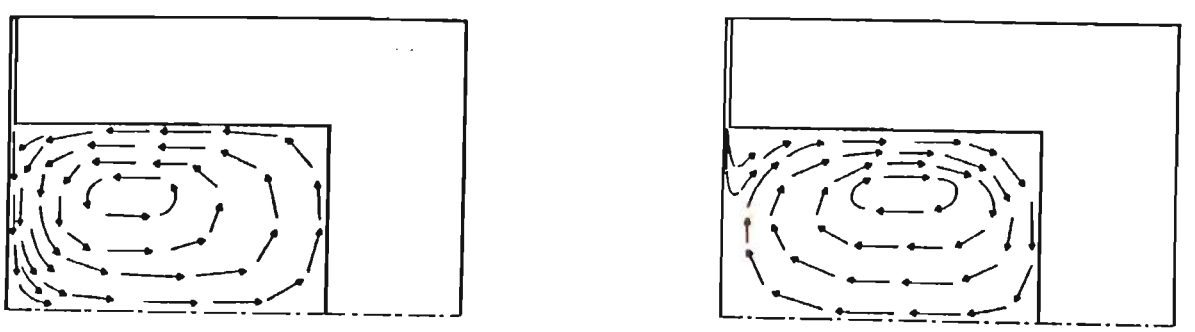

No Swirl With Swirl

Figure 6 Schematic diagram of air flow in the piston bowl at TDC with and without swirl (after Arcoumanis et al., 1983).

Models that have been developed for evaluating air swirl and squish generally apply the principle of conservation of momentum to the contents of the engine cylinder (Dent and Derham, 1974; Borgnakke, Davis and Tabaczynski, 1981; Morel and Keribar, 1985; Murakami et al., 1988). It is first of all necessary to predict swirl at the end of the induction period so that, at IVC, the initial swirl conditions for the start of compression are established. Swirl during the compression and expansion strokes is then determined by taking into account angular momentum fluxes from squish, wall friction and shear within the flow.

The Ricardo Engineers predicted swirl at the end of the induction period using the Ricardo Momentum Summation Method (Lilly, 1984). Calculations were based on measurements from a steady state flow rig to which was attached the cylinder head and valve assembly and a cylinder liner of correct diameter in an inverted position. Early rigs made use of a light vane which was made to rotate by the swirling air and was placed within the cylinder liner one bore diameter from the valve. The speed of rotation was then measured.

Doubts about the accuracy of this technique because of the possibility of spiralling air motion down the cylinder bore resulted in the development of an impulse meter. This meter consisted of a honeycomb structure which was fitted in place of the rotating vane and suspended in the bore. With the swirling air charge moving up the cylinder, the axial holes in the honeycomb, through which the air had to pass to escape, absorbed the swirl effect destroying the total angular momentum flux to produce a torque reaction on the suspended honeycomb. Measurement of this reaction was equivalent to the angular momentum of the swirl. The swirl ratio was determined by equating the angular momentum of the charge at the end of induction to the sum of the angular momentum flux generated by the inlet port over the induction period (Lilly, 1984).

Dent and Derham (1974) assumed that during the induction period the moment of momentum of the air entering the inlet port was equal to the rate of change of angular momentum of the cylinder contents. The moment of momentum was obtained from an equation including the instantaneous mass flow rate of air through the inlet port, the velocity of air at the valve seat and the relative position and angle of the port in relation to the cylinder. The rate of change of angular momentum was given by the differential with respect to time of the product of the moment of inertia of the cylinder contents and the angular velocity. The latter velocity was therefore obtained by integrating a function made up of terms obtainable from engine geometry and from measurements on a steady flow rig. Wall friction was neglected for the induction process as viscosity effects in the late induction period were predicted to be small due to the low surface-to-volume ratio (Dent and Derham, 1974). A comparison of the computed results with experimental data indicated acceptable agreement for both air swirl motion and inward radial flow.

Borgnakke et al. (1981) and Morel and Keribar (1985) formulated differential equations for angular momentum for each of the flow regions into which the cylinder was divided. Borgnakke et al. (1981) divided the total cylinder volume into two regions as shown in Figure 7. The interface between the two coincided with the cylindrical area of the same diameter as the bowl. The equation included fluxes of angular momentum entering and leaving the chamber.

Borgnakke et al. (1981) also proposed three different profiles for angular velocity varying with cylinder radius so as to provide more flexibility than obtained with the assumption of solid body rotation (see Figure 8). The accuracy of the model was established by comparing the model output for three engine types and three different intake port configurations. Good agreement was obtained after the friction coefficient was adjusted for correct calibration at one point in the cylinder.

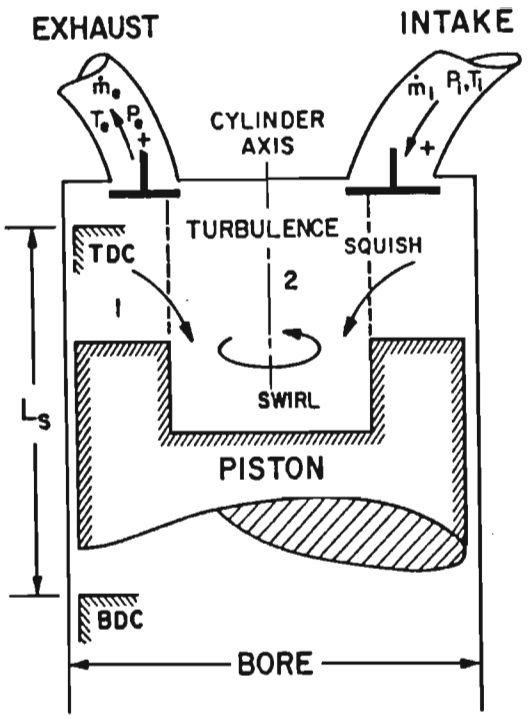

Figure 7 Idealised combustion chamber geometry showing division of cylinder volume (Borgnakke et al., 1981).

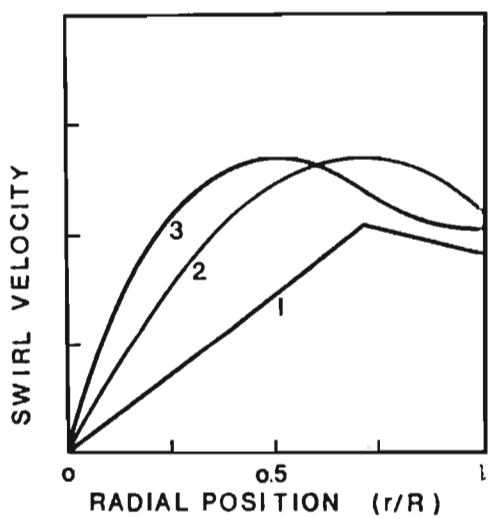

Figure 8 Examples of various tangential velocity profiles investigated (Borgnakke et al., 1981).

Morel and Keribar (1985) assumed solid body rotation in each of three regions divided in a similar way to that of Borgnakke et

al. (1981) except for the addition of a third region being the bowl volume. Their equations included terms representing convection from region to region, diffusion from one region to another by the action of turbulence also referred to as inter-regional friction, intake flux of angular momentum, exhaust flux out and wall friction. The swirl model was verified by comparing its output for a high swirl engine with pancake combustion chamber geometry against the data measured by Johnston, Robinson, Rorke, Smith and Witze (1979). The rate of swirl decay was particularly high and therefore provided a good indication of the skin friction correlation. Excellent agreement was obtained.

The model for swirling flow formulated by Murakami et al. (1988) was applied to the compression and expansion strokes. The division into two flow regions was the same as employed by Borgnakke et al. (1981). Two differential equations were presented for the variation of angular momentum with time for each region equated to the wall friction moment for each surface in the chamber, the angular momentum flux transmitted between regions by viscous shear and the angular momentum flux transported between regions by squish flow. The two regions were modelled as solid bodies rotating with different angular velocities. The results obtained from the model were compared to experimental data for different piston and head configurations. For the majority of the tests an error of less than 10% of the measured value was achieved.

Swirl and squish remain two dominant velocity components that must be considered in any gas flow model for diesel engines. Models such as those of Morel and Keribar (1985) and Murakami et al. (1988) can provide the precision necessary in this project for generating swirl and squish velocities. However, a further gas velocity component that should not be overlooked is turbulence intensity.

2.1.2 Turbulence intensity

It has been generally accepted that the shear flow past the intake valve is the major source of turbulence in engine cylinders and that this turbulence persists throughout the cycle (Tabaczynski, 1983 ; Rao and Bardon, 1985). After IVC viscous shear stresses perform deformation work which increases the internal energy of the fluid at the expense of kinetic energy of the turbulence. Turbulence therefore requires a continuous supply of energy to make up for these viscous losses (Tennekes and Lumley, 1972). Viscous dissipation therefore tends to reduce turbulence intensity during the cycle.

An example of the relative magnitude and trends that can be expected for a diesel engine with bowl-in-piston is illustrated in Figure 9 representing the output from the model of Morel and Keribar (1985) in which the combustion chamber was divided into three regions. The dominating peak of turbulence generated early in the intake stroke shown in Figure 9 decays fairly rapidly for the remainder of the intake stroke and approximately half way into the compression phase as a result of viscous dissipation. As the intake valve closes the sharp shear layers disappear but the turbulence generated by them remains (Reynolds, 1980). The initial conditions of turbulence for the subsequent compression process are established at this point as for swirl.

The piston bowl to bore diameter ratio and the piston crown-head clearance at TDC are factors which have a significant effect on the in-bowl flow field and hence on the generation of turbulence. Production and dissipation of turbulence during compression is governed by four main factors excluding the initial generation of turbulence during the intake stroke. Shear within the combustion chamber is created by angular velocity gradients caused by swirl deviating from solid body rotation. This shear process is a mechanism for generating and dissipating turbulence. Shear at the boundary layer adjoining the chamber walls has a similar mechanism and is also taken into account.

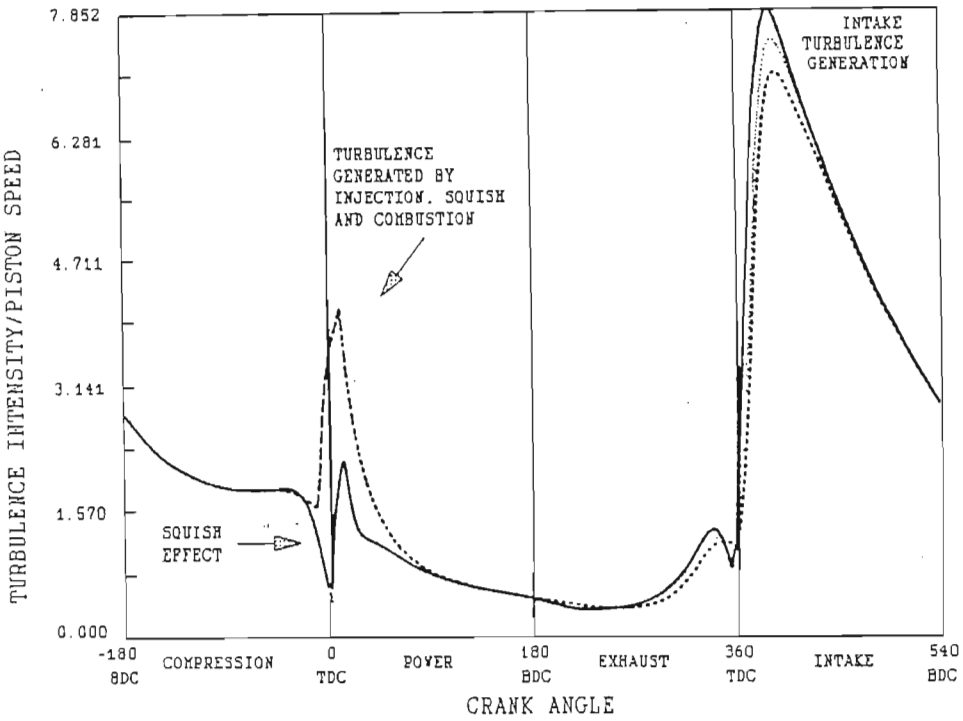

Figure 9 Turbulence intensity in the three flow regions (after Morel and Keribar, 1985).

A third contributor to production and dissipation of turbulence is the result of compression. During the compression and combustion processes the turbulent kinetic energy is amplified due to the rapid distortion that the cylinder charge undergoes with rising cylinder pressures. This effect is illustrated in Figure 9 by the small rise in turbulence intensity towards the end of compression. According to Wong and Hoult (1979) piston motion during compression caused an amplification of turbulence based on the rapid distortion theory. This effect was also referred to by Arcoumanis and Whitelaw (1987) as turbulence production by compressive strain.

The last factor is squish which can have a major effect on the production of turbulence as shown in Figure 9. In the cup region, Morel and Keribar (1985) catered for a large increase in turbulence resulting from the inflow of gases as well as injection and combustion contrary to the findings of Rao and Bardon (1985). In Figure 9 turbulence in the squish region above the piston crown decreases abruptly close to TDC because of the

small clearance between head and piston increasing viscous dissipation. However, immediately after TDC there is a sharp rise in turbulence caused by reversed squish. It should be noted that the turbulence remains uniform for all regions of the chamber over most of the compression stroke with differences occurring from 20 - 30° BTDC onwards. The curves emerge again further on in the expansion stroke.

The turbulence also tends to be isotropic during the compression and expansion strokes. Fansler (1985) concluded that near-TDC peaks in rms fluctuation intensity were dominated by squish-induced velocity fluctuations which tended to decrease with increasing bowl-bore diameter ratio.

The model most extensively used in engines for turbulence is the $k - \epsilon$ model which takes into account the rate of turbulent kinetic energy production and the rate of viscous dissipation. Davis and Tabaczynski (1988) provided an equation for the production and dissipation of turbulence kinetic energy which included variables responsible for production due to compression, squish and intake generated turbulence respectively. These terms were offset by a dissipation variable.

As the intention of this project is to examine and model the events taking place from the point of IVC through the compression and expansion strokes to the point of exhaust valve opening (EVO), a factor that had to be considered was a starting value for the turbulence intensity. Rao and Bardon (1985) indicated that reported values for turbulence intensity at intake valve closure varied between 20-50% of mean piston speed. They suggested a representative value for the turbulence kinetic energy/unit mass at the start of the compression stroke of 12,5% of the square of the mean piston speed. These observations were largely based on measurements in cylindrical chambers with flat pistons having relatively low compression ratios.

For chambers with flat pistons and no squish, turbulence levels of 0,3 - 0,5 times the mean piston speed have been measured at TDC under different conditions with tendencies towards homogeneity and isotropy (Arcoumanis and Whitelaw (1987). Hayder et al. (1985) concluded from computations and measurements in engines with pancake chambers that the maximum value of the TDC turbulence intensity was about one half the mean piston speed when the intensity of turbulence was defined as the intensity of the high frequency components of the velocity fluctuations.

It was apparent from the research published that turbulence remained a variable that was difficult to measure and model accurately. However, some guidelines for models had been established which afforded acceptable levels of accuracy and which provided expected trends.

2.2 Heat Transfer

The gross heat loss to the coolant during combustion in internal combustion engines normally lies in the range of 10-35% of the fuel energy and depends on engine type, size, efficiency, load and speed (Lilly 1984; Goering, 1986). Energy is lost from the gases in the combustion chamber thus reducing the amount of piston work and affecting engine performance. Gas temperatures are also affected and through them combustion rate, emissions formation, knock and other related factors. Further areas of importance are the thermal loading of engine structural components and the optimisation of engine cooling systems (Morel, Wahiduzzaman, Tree and DeWitt, 1987). The researcher involved in engine design, optimisation of engine performance or investigations of alternative fuels therefore requires a representation of the heat transfer processes that will achieve an acceptable level of accuracy.

Heat losses from the combustion chamber occur as a result of heat transfer from gases to the walls and of heat conduction through the structure and to the coolant. It is generally

accepted that, given the correct boundary conditions, the heat conduction portion of the heat losses can be calculated to any desired accuracy using finite element models (Morel et al., 1987). Gas-to-wall heat transfer correlations have to rely on models for the processes taking place in the combustion chamber. These correlations in turn are used to establish the boundary conditions for the heat conduction calculations. Hence an accurate description of the heat flux rates and their spatial and temporal variations within the cylinder is very important.

Heat transfer from the gases to the walls is due both to convection and radiation. In the past, greater emphasis was placed on the convection component as radiation was considered by some researchers to contribute a negligible portion of the heat transfer. However, measurements of time-averaged heat transfer indicated that 20-40% of the total cylinder flux was due to radiation (Borman and Nishiwaki, 1987).

Hohenberg (1979) stated that the conditions in the internal combustion engine were so complex and also locally different that no generally valid mathematical formulation of the heat transfer could be established. Borman and Nishiwaki (1987) indicated that a satisfactory predictive model for heat transfer had not yet evolved even though heat transfer modelling for engines had begun in the late 1920's and both experimental and theoretical analyses had progressed considerably.

Heat transfer in the combustion chamber of a direct injection diesel engine varies considerably on both a spatial and temporal basis. Heat flux to the surface of the chamber can vary from zero to as high as 10 MW/m^2 and back to zero again in less than 10 ms while portions of a surface only 10 cm apart can receive peak fluxes differing by as much as 5 MW/m^2 (Borman and Nishiwaki, 1987). The combination of substantial variations in temperature and pressure of the contents of the combustion chamber and the cyclic movement of the piston leading to varying

three-dimensional geometry confronts the researcher with a complex problem.

Timoney (1987a) reporting on heat release rates calculated from the First Law of Thermodynamics in a direct injection diesel engine for different swirls, injection rates, bowl shapes and engine speeds, concluded that heat transfer estimates were the root cause of doubts about accuracy. The usefulness of the heat release analysis was therefore restricted. This problem, which was also referred to by Taylor (1987), highlights the need for reliable instantaneous heat transfer calculations when interpreting small differences in heat release rates at various stages in the cycle.

Timoney (1987b) attributed the main cause of errors in his heat transfer analysis to be inadequate treatment of radiative effects. His results indicated that net radiative heat transfer in the cylinder of a direct injection diesel engine at high load could be of the same order as the net convective heat transfer.

The evaluation not only of engines but also different fuels in terms of heat transfer effects has received relatively scant attention. Callahan, Yost and Ryan (1985) selected heat transfer models for ease of programming and adaptability to a wide range of engine-fuel combinations. It could be expected that convective and radiative heat transfer rates with different fuels in the same engine would vary according to fluctuations in gas temperatures. In addition fuel chemical and physical properties would influence the radiative component in terms of soot formation during combustion. For instance an alcohol-based fuel would cause relatively little radiative heat transfer because of a tendency towards clean burning.

The different approaches that are used in modelling to analyze in-cylinder heat transfer vary from global or one-zone thermodynamic to multi-dimensional numerical fluid-dynamic. As the objective of this study was to develop a combustion model

requiring limited computing power this review was restricted to global models and the zonal thermodynamic models which involved more than one zone as defined by Borman and Nishiwaki (1987).

2.2.1 Global heat transfer

Borman and Nishiwaki (1987) provide a comprehensive review of global models for heat transfer applied to internal combustion engines in general. Only the models relevant to direct injection diesel engines will be examined in this study. These models are based on empirical heat transfer coefficients which are assumed to apply for all the heat transfer surfaces in the engine. The basis of these models is the quasi-steady expression:

$$Q = h.A.(T-T_w) \qquad \text{-----(1)}$$

where Q = heat transfer rate, kW
h = heat transfer coefficient, $kW/m^2.K$
A = surface area, m^2
T = mass averaged bulk mean gas temperature, K
T_w = wall surface temperature, K.

If local differences in temperature are to be incorporated equation (1) becomes:

$$Q = h \sum_{i=1}^{N} A_i \, (T - T_{w_i}) \qquad \text{-----(2)}$$

where N = number of individual areas A_i with a uniform surface temperature T_{w_i} (Borman and Nishiwaki, 1987).
The model of Nusselt (1923), cited by Borman and Nishiwaki (1987) was the first formulated for engine heat transfer. Later Eichelberg (1939) put forward a model which is still widely used and has the form :

$$h = a\ (C_m)^{0,333}(P.T)^{0,5} \qquad \text{-----(3)}$$

where a = constant fitted to experimental data

C_m = mean piston speed, m/s

P = cylinder pressure, kPa

T = bulk gas temperature, K.

Both these models were empirical and were not dimensionless.

Working from a simplified energy equation and applying dimensional analysis less empirical models were developed for convective heat transfer of the form:

$$Nu = C.Re^n \qquad \text{-----(4)}$$

where Nu = Nusselt number = $h.D/k_g$

Re = Reynolds number = $\rho.v_o.D/\mu$

C = constant

k_g = gas thermal conductivity

v_o = reference velocity

ρ = density

μ = dynamic viscosity

D = bore diameter

The model formulated by Annand (1963) is one of the most widely used models based on steady turbulent convection heat transfer. It includes a second term representing radiant heat flux:

$$q = a.\frac{k}{D}.Re^{0,7}(T - T_w) + b.(T^4 - T_w^4) \quad kW/m^2 \qquad \text{------(5)}$$

where a = constant ranging from 0,35 to 0,8 depending on intensity of charge motion

b = constant = $3,3 \cdot 10^{-11}$ $kW/m^2.K^4$ for diesel engines

Re = Reynolds number based on mean piston speed and bore diameter with gas properties taken at the bulk mean temperature and not the average of T and T_w.

Annand and Ma (1970) extended equation (5) to include additional terms after examining experimental results obtained in a DI diesel engine which used induction swirl:

$$q = \frac{k}{D}.Re^{0,7}[a(T - T_w) + \frac{a'}{\omega}.\frac{dT}{dt}] + b.\sigma(T^4 - T_w^4) \text{ kW/m}^2 \quad \text{-----(6)}$$

where ω = angular velocity of engine crankshaft

σ = Stefan-Boltzmann constant

a,a',b = constants obtained for test engine and dependent on engine speed and fuel-air ratio

dT/dt = time derivative of bulk mean temperature to compensate for unsteady nature of flow.

The reference velocity in Re was an energy-mean-velocity calculated from the mean kinetic energy per unit mass of gas.

Another correlation which is also used extensively in heat release analysis, was developed by Woschni (1967) and was based on equation (4) and given as:

$$Nu = 0,035\ Re^{0,8} \quad \text{-----(7)}$$

The heat transfer coefficient was then given by the following correlation:

$$h = 0,82\ D^{-0,2}P^{0,8}W^{0,8}T^{-0,53} \quad \text{kW/m}^2\text{.K} \quad \text{-----(8)}$$

The reference velocity, W, represented the mean gas velocity and was given by :

$$W = [C_1.C_m + C_2.\frac{V_s.T_1}{P_1.V_1}.(P - P_o)] \text{ m/s} \quad \text{-----(9)}$$

where C_m = mean piston speed, m/s

P_o = pressure obtained for motoring, MPa

V_s = displacement volume, m^3

subscript 1 = pressure, temperature and volume at IVC.

For the compression process, C_1 = 2,28, C_2 = 0 and for the combustion and expansion process, C_1 = 2,28, C_2 = 0,00324. Both convection and radiation effects were lumped together in equation (8). In order to improve the representation of velocity in equation (8) a swirl term was included later by modifying C_1 in equation (9) to the form(Woschni, 1970, cited by Borman and Nishiwaki, 1987):

$$C_1 = 2,28 + 0,308\ C_u/C_m$$

where $C_u = \pi.D.\omega_r$, and

ω_r = rotation speed of paddle wheel in a steady swirl test rig.

Hohenberg (1979) examined each term in equation (8) critically and proposed modifications to give better predictions of time-averaged heat fluxes. Instantaneous cylinder volume was used instead of cylinder bore and changes were made to equation (9) and to the exponent of the temperature term. Hohenberg (1979) stated that heat transfer between gas and combustion chamber wall depended mainly on convection and hence on the pressure, temperature and velocity of the gas. He regarded radiation as relatively small. The gas pressure and temperature could be determined fairly accurately, however, gas velocity varied locally and per unit time owing to intake swirl, combustion chamber shape, combustion system and especially turbulence of combustion. Hohenberg (1979) suggested that one mean velocity be defined for the entire combustion chamber and that the factors affecting the magnitude of the velocity be taken into account by varying the constants or by additional terms.

Hohenberg (1979) also indicated that the surface of the piston land above the top compression ring should be included to some extent in calculations of heat transfer. Under motored conditions the heat transfer coefficient in the top land amounted to about 40% of that in the combustion chamber. The lower heat transfer was due to the lower gas temperatures and lower gas velocities. Under fired conditions the coefficient would be

reduced, a theoretical estimate being 25% of that in the combustion chamber.

Another important application of equation (4) was that of Sitkei and Ramanaiah (1972) who concluded from available data that the exponent n should be equal to 0,7 as opposed to the value of 0,8 used by Woschni (1967). Their equation as represented by Borman and Nishiwaki (1987) for the heat transfer coefficient used in the convection component was of the form:

$$h = 0{,}000236\ (1 + b).P^{0,7}.C_m^{0,7}/(T^{0,2}.d_e^{0,3})\ kW/m^2.K \quad --(10)$$

where d_e = equivalent diameter, m

= 4V/A

V = cylinder volume, m^3

A = heat absorbing area, m^2

P = cylinder pressure, MPa

b = dimensionless constant included in consideration of additional turbulent velocity and ranges from 0 to 0,35 depending on type of combustion chamber.

With reference to equation (4) Kamel and Watson (1979) indicated that the problem was not only to define the values of the empirical constants C and n, but also to establish appropriate but convenient expressions for the gas viscosity and density in Re, gas conductivity in Nu, a characteristic length in Nu and Re and a characteristic velocity in Re.

Convenient definitions for these terms were applied such as cylinder bore for characteristic length, mean piston speed for velocity and bulk gas temperature and pressure for the evaluation of gas properties. In their own study Kamel and Watson (1979) attempted to improve the gas velocity variable by considering the swirling fluid flow to act as a rotating disc and proposed friction torque coefficient to be used in determining the reduction in kinetic energy of the disc and hence the decay of swirl during the cycle.

While the global models do not provide details of local and unsteady heat transfer they have often been used in engine cycle simulations for examining the state of the whole cylinder gas and for predicting overall engine performance in terms of fuel consumption, total heat loss, thermal loading, exhaust temperature and other global variables (Borman and Nishiwaki, 1987). These models are also relatively simple to implement as the variables that are necessary for their application are easily measured or calculated.

2.2.2 Zonal heat transfer

The next step in improving the resolution of the global heat transfer models is to divide the chamber gas volume into a number of control volumes each with its own temperature history and heat transfer coefficient. The portion of surface area exposed to each gas volume is also estimated.
Zonal models were first developed and applied to spark ignition (SI) engines because of the theoretical simplicity in defining a flame front and hence burnt and unburnt zones in the combustion chamber assuming a homogeneous fuel-air mixture. The zonal models used for diesel engines were largely spawned from the SI engine models. However, owing to the heterogeneous nature of the fuel-air mixing in diesel engines, definition of the discrete gas volumes was far more complex. Borman and Nishiwaki (1987) stated that because zonal models had been developed only recently, they had not yet been sufficiently evaluated. However, in principle the zonal models were expected to be superior to the global models and to cover a wider range of applications.

Morel and Keribar (1985) formulated one of the first comprehensive zonal convective heat transfer models for a direct injection diesel engine. As indicated by Morel, Keribar and Blumberg (1988) their approach was to retain the essential practicality of the global approach to engine simulation but to introduce a level of spatial resolution previously not available. Morel et al. (1987) stated that a successful convective heat

transfer model should take into account all of the key in-cylinder fluid motions such as intake flows, swirl, squish, turbulence and injection and combustion generated motions. Also the model had to provide spatial resolution capable of differentiating between various in-cylinder surfaces.

In the model of Morel and Keribar (1985) the bowl-in-piston combustion chamber was divided into three flow regions for the calculation of flow velocities as shown earlier in Figure 2. In each of the regions the model solved an equation for conservation of angular momentum and two equations for a $k - \epsilon$ turbulence model thus providing the swirl and turbulent velocity components. Calculation of mass conservation and piston kinematics gave the radial and axial velocity components.

Well established boundary layer concepts were applied in the model to determine the heat transfer coefficient. The Colburn analogy based on the Reynolds analogy between momentum and heat transfer was used to link the heat transfer across the thermal boundary layer to the flow velocity at the outer edge of the momentum boundary layer. The resulting heat transfer coefficient was primarily a function of a skin friction coefficient for the boundary layer, the average gas properties of the boundary layer with particular reference to the density, and the effective velocity at the edge of the boundary layer. The skin friction coefficient was modelled by a correlation obtained in flat plate boundary layers and fully developed pipe flow. The effective velocity was determined from the resultant of two velocity components parallel to the surface and the tubulence kinetic energy provided by the $k - \epsilon$ model.

Morel and Keribar (1985) divided the combustion chamber into six surfaces for each of which an instantaneous transfer coefficient was determined. They also generated a burnt and unburnt zone in the combustion chamber, each with a different gas temperature. The relative proportion of these zones in the chamber determined the convective temperature at the boundary layer.

Morel et al. (1987) illustrated the variation in heat transfer coefficient within the cylinder by Figure 10 for a piston. The head centre curve represents the area-averaged value for the bottom of the bowl. The head perimeter curve is the area-averaged value for the piston crown and the liner curve is also area-averaged. Significant variations in heat transfer coefficient were therefore obtained for the particular engine modelled reflecting the changes in flow velocities adjoining the respective surfaces.

Morel et al. (1987) also compared the area-averaged heat transfer coefficient for all the surfaces in the combustion chamber to the global Annand correlation. This is illustrated in Figure 11, where the coefficient of the Annand's correlation had been adjusted in order to give the same cycle-integrated heat rejection for the whole cylinder. Higher heat transfer coefficients were calculated with the flow based model near firing TDC owing to squish, compression generated turbulence and injection and combustion motions. In addition low heat transfer coefficients were computed during the relatively quiescent expansion and exhaust periods.

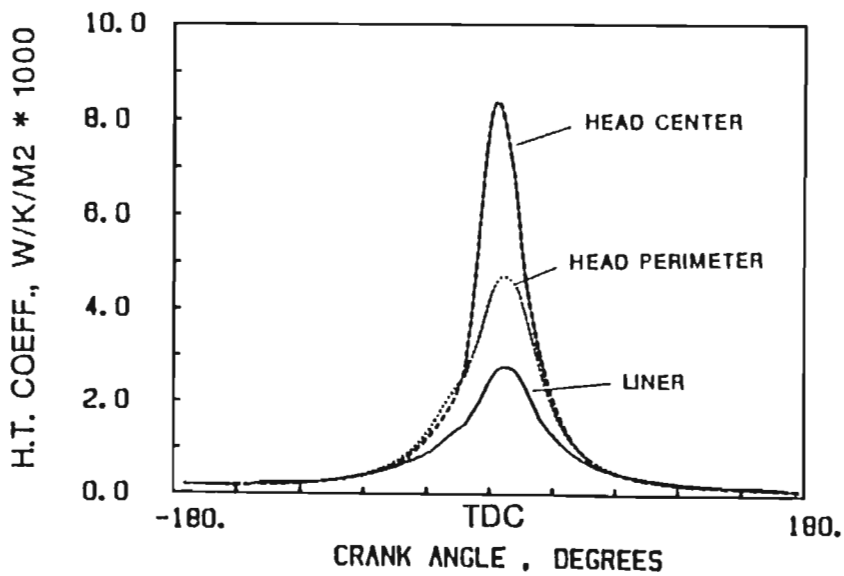

Figure 10 The variation of heat transfer coefficients with crank angle on three in-cylinder surfaces (Morel et al., 1987)

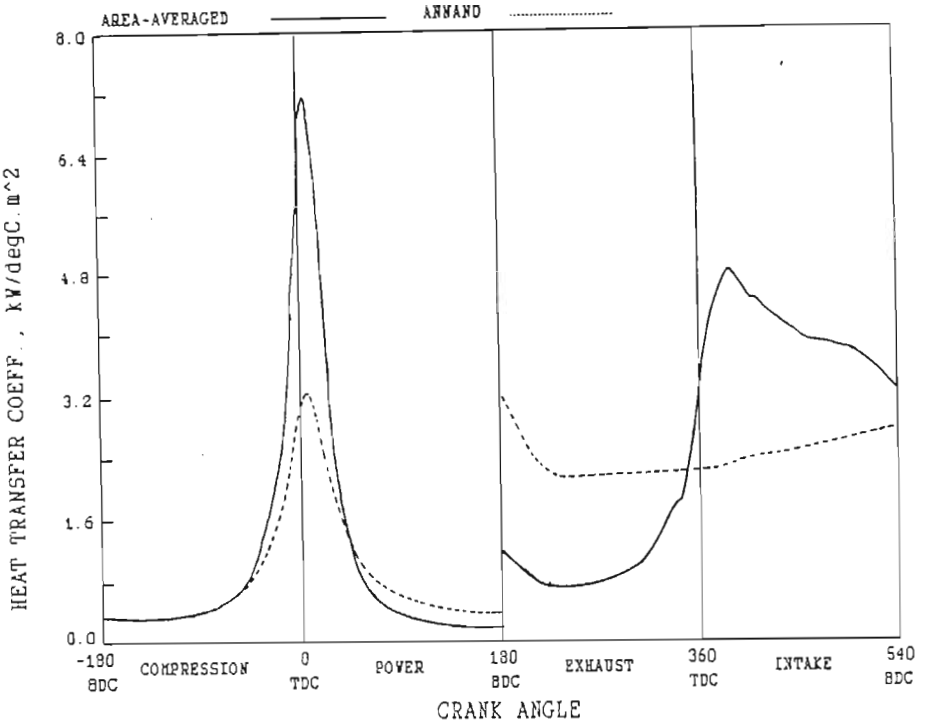

Figure 11 The variation of area-averaged heat transfer coefficients calculated from a flow-based model and from Annand's correlation (after Morel et al., 1987).

The discrepancies between the global models and the flow based model were illustrated further by Morel et al. (1987) using experimental data. Figures 12 to 14 compare the Annand correlation, Woschni correlation and the flow-based model to data obtained for the crown and bowl regions at rated conditions for a DI diesel engine. The correlations of Annand and Woschni deviate substantially from the actual values while the flow-based model reproduces the maximum values at each location in addition to providing a good similarity in shape.

A two stage heat-release model developed at the General Motors Research Laboratories by Szekely and Alkidas (1986) was applied to an open-chamber diesel engine to determine the fuel burning rates and product temperatures from measured cylinder pressure-time profiles. The model assumed that combustion in the first stage occurred at an equivalence ratio above the cylinder-averaged equivalence ratio, and that in the second stage it occurred at an equivalence ratio below the cylinder-averaged

ratio. These stages were referred to as rich and lean zones. With combustion in progress each of these two zones was subdivided into burnt and unburnt zones giving a maximum of four zones in the combustion chamber.

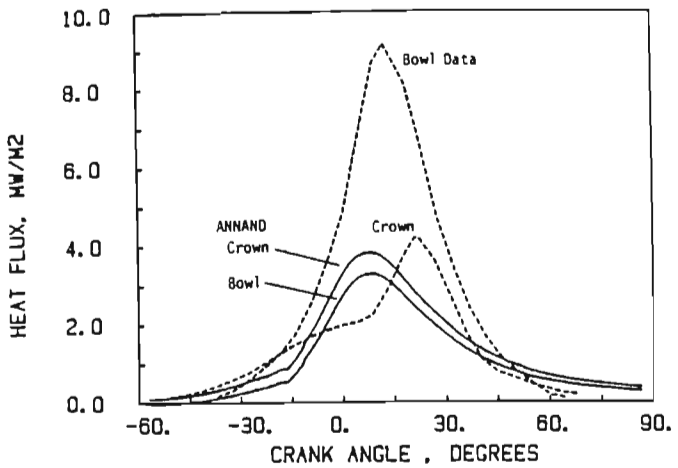

Figure 12 The variation of heat flux at rated conditions based on Annand's correlation compared to experimental data (Morel et al., 1987).

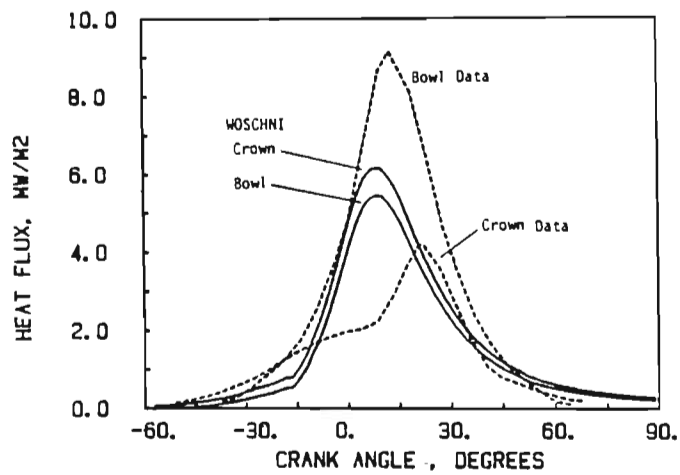

Figure 13 The variation of heat flux at rated conditions based on Woschni's correlation compared to experimental data (Morel et al., 1987).

Further postulates were that the zone which began to react first was consumed completely prior to reaction of the second zone, and that no mixing occurred between any of the four zones. The equivalence ratios of the two combustion stages were empirically

determined from measured NO emission levels for several engine operating conditions.

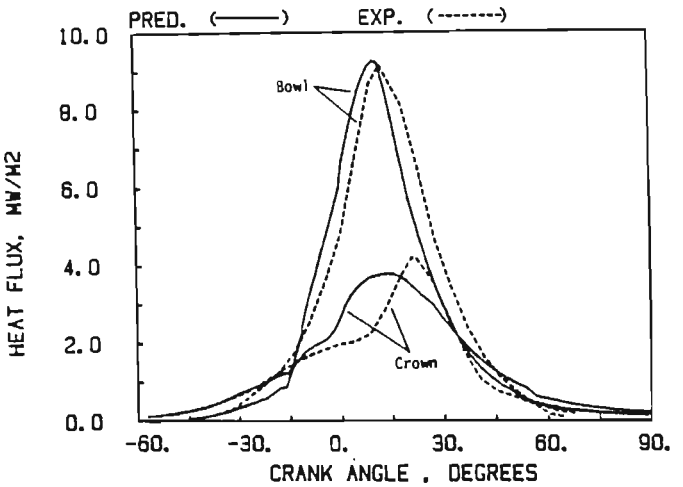

Figure 14 The variation of heat flux at rated conditions based on a gas flow model compared to experimental data (Morel et al., 1987).

The instantaneous convective heat transfer rate for each zone was determined by applying an equation similar to equation (2). Gas temperatures were determined for each zone according to the fuel energy present. The representative surface area was calculated with the aid of an area-fraction value set equal to the volume fractions of the zone. The instantaneous convective heat transfer coefficient was based on Woschni's correlation and a heat transfer multiplication factor was applied, the value of which was adjusted so that the calculated final fuel-mass-burned fraction was equal to the value estimated from exhaust emissions and measured fuel consumption.

Good agreement between the results of the model of Szekely and Alkidas (1986) and the corresponding single stage model was obtained for heat release and heat transfer histories. It was also concluded that more realistic gas temperature histories were calculated for the modelling of NO kinetics.

Another class of models that have been developed and applied by researchers such as Gosman and Harvey (1982) are multi-

dimensional simulations. These models resolve the entire contents of the combustion chamber into a fine grid mesh and solve governing differential equations at each point. This approach removes many of the empirical relationships used in the global models but retains empirical relationships concerning the effects of turbulence and of chemical reactions. These models were regarded by Morel, Keribar and Blumberg (1988) as still highly research oriented, constrained by computation time and cost and, hence, were not yet applicable in the product engineering environment. Borman and Nishiwaki (1987) concluded from their review of the literature that predictions by multi-dimensional models were not guaranteed to be more accurate at present than those by the global or zonal models.

It can therefore be concluded that zonal models made up of carefully selected and tested submodels should provide a level of accuracy which surpasses that of the global models but which should still generate cost and time effective solutions directly applicable to engineering problems.

2.2.3 Radiation

There are two primary sources of radiative heat transfer in a diesel engine. The first and smaller source is non-luminous radiation from the high temperature combustion gases. This gas radiation is mainly due to emission contributions from the tri-atomic molecules of CO_2 and H_2O. Many of the intermediate chemical species formed during combustion also emit radiation, however, their concentration levels are small and therefore their contribution to radiation is negligible (Morel and Keribar, 1986). The second more significant source in diesel engines is luminous radiation from soot particles which are formed as an intermediate step in the turbulent, diffusion-controlled diesel flame.

The radiation emitted and absorbed by the gas species is concentrated in narrow bands of wavelength as opposed to the

radiation from soot which is broad band. The gas radiation has been neglected by some researchers because its contribution is smaller than soot radiation. Morel and Keribar (1986) stated that the error introduced by this neglect was likely to be most important during the latter part of combustion when soot levels decreased rapidly due to soot burn-up, but during the early stages of combustion the soot absorption and emission dominated the radiation process and the error was small.

Borman and Nishiwaki (1987) mentioned that measurements of radiation during the engine cycle indicated that it was important only during the heat release period. Furthermore, the radiation peaked just after the end of premixed burning approximately 5 - 10° CA after the start of combustion, with the peak values being roughly one half of the total heat transfer. In well optimised diesel engines Morel and Keribar (1986) suggested that the radiation heat transfer during the diffusion phase of combustion could be of the same order of magnitude as the convective heat transfer. However, the split between radiation and convection heat transfer was highly dependent upon the engine design and operating conditions. The composition and properties of the fuel should also be included as a factor affecting this split.

Borman and Nishiwaki (1987) provide a plausible explanation of the events in the combustion chamber leading up to and during soot formation and radiation. As the fuel is injected into the cylinder the spray begins to break up immediately into very small droplets. A narrow core of churning liquid fuel penetrates down the spray centreline often reaching the piston bowl surface before the end of injection. Even when a moderately high swirl ratio of 4 or 5 is present the spray is not deflected very much by the swirl. However, droplets and vapour may be swept out of the spray by the swirl.

When ignition takes place the cloud of mixed fuel vapour and air surrounding each spray plume burns rapidly at an average mixture strength close to stoichiometric. Only a small amount of

particulates or radiation is generated by this premixed burning phase. However, the rapid burning causes each spray plume to be surrounded by a sheath of hot products. This in turn causes a reduction in oxygen entrainment and a rapid rise in pressure and temperature of the typically rich remaining spray plume. These conditions produce soot both by pyrolysis and by rich combustion. The hot particulate laden cloud at a temperature of 2200 - 2500 K then radiates strongly, giving a rapid rise in radiant flux, peaking at 1,2 - 1,6 MW/m^2 and then dropping at a rate determined by the rate of mixing and burning.

Attempts at measuring radiation have been made by a number of researchers with varying degrees of success (Flynn, Mizusawa, Uyehara and Myers, 1972; Oguri and Inaba, 1972; Sitkei and Ramanaiah, 1972; Dent and Sulaiman, 1977). The major conclusions from these measurements were summarised by Borman and Nishiwaki (1987) as follows:

(a) A soot-covered transducer received more net radiation than a clean transducer indicating that the emissivity effect overpowered the resistance-capacity effect of the deposit.

(b) Radiation was found to be very important during the combustion period with peak instantaneous radiant flux levels as high as 50 - 60% of the total flux.

(c) Time-averaged rates of radiation increased with increases in speed, fueling rate, inlet pressure and injection advance.

(d) The premixed portion of the combustion produced little radiation, but a very rapid increase in radiation took place near the end of the premixed burning.

(e) For naturally aspirated conditions a decrease in cetane number reduced radiation, provided the cetane number was not lowered by addition of aromatic or other highly soot-producing fuels.

Models of radiation heat transfer are generally based on the Stefan-Boltzmann law which states that the energy radiated by a black body is proportioned to the fourth power of its absolute temperature:

$$E_b = \sigma.T^4 \qquad \text{-----(11)}$$

where E_b = energy radiated per unit area per unit time
σ = Stefan-Boltzmann constant = $5,68 \cdot 10^{-8}$ $J/s.m^2.K^4$.

Under practical conditions, surfaces radiate less than a black body at the same temperature and may be referred to as a grey body. The ratio of energy radiated by a grey body, E_g to that radiated by a black body at the same temperature is called its emissivity, ϵ (Benson and Whitehouse, 1979). Hence:

$$E_g = \epsilon.\sigma.T^4 \qquad \text{-----(12)}$$

Some correlations for heat transfer used in single zone combustion models such as that of Woschni (1967) lump the radiation with convection heat transfer while models such as Annand (1963) provide separate terms for the two modes of heat transfer. In models of the latter type the problem is to use the appropriate emissivity and radiant temperature in equation (12). With the fourth power relationship, an error of only 50°C in radiant temperature results in a 10% error in heat flux while use of the molar-average temperature gives an error of almost 200% (Borman and Nishiwaki, 1987). Calculations of radiant heat transfer therefore rely fairly heavily on a valid radiant temperature.

Borman and Nishiwaki (1987) suggested that, to compute the radiation temperature, a two or three zone heat release model could be used with one zone being the combustion products. This products zone would have been cooled primarily by radiation and its temperature could be taken as the radiation temperature for

the heat transfer model. From their survey of the available data Borman and Nishiwaki (1987) indicated that the radiation temperature resulting from such a model should initially be close to the adiabatic flame temperature for a rich limit mixture in the range 2200 - 2400 K. This temperature should be relatively insensitive to load. Furthermore, after the peak the temperature should decrease almost linearly, reaching the average gas temperature near the end of combustion. The timing of the peak temperature should coincide with the start of diffusion combustion as determined from the shape of the heat release curve.

Kunitomo, Matsuoka and Oguri (1975) considered the temperature in the luminous flame to be nearly constant while combustion was in progress. They fixed the radiation temperature at 2400 K for the first 90% of heat release and then decreased it linearly to merge with the mass average gas temperature at the end of heat release. Kamel and Watson (1979) assumed that the radiation temperature was 2200 K at the beginning of heat release and then decreased to equal the bulk mean gas temperature at the end of heat release.

Callahan et al. (1985) at the Southwest Research Institute, San Antonio, Texas, USA, who formulated a radiation heat transfer model similar to those of Kunitomo et al. (1975) and Kamel and Watson (1979) pointed out that no adjustment to the flame temperature for different fuels was proposed by either group of researchers. They therefore assumed that the flame temperature was equal to the adiabatic flame temperature when the mass fraction of fuel burned was less than 90%. Beyond 90% the flame temperature was assumed to approach the bulk gas temperature as illustrated in Figure 15.

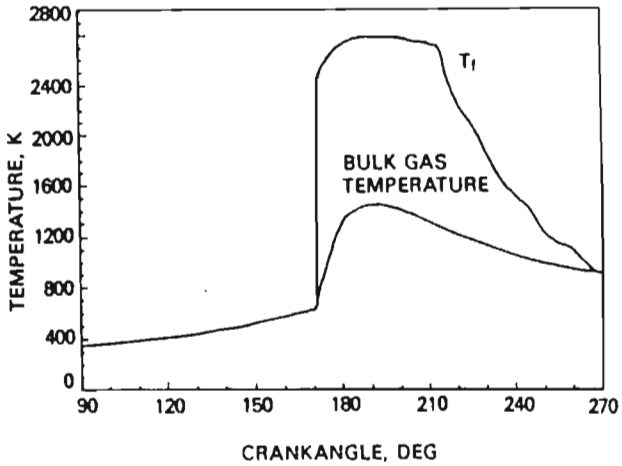

Figure 15 Assumed flame temperature (Tf) and bulk gas temperature profiles for a particular fuel (Callahan et al., 1985).

After studying the results of Flynn et al. (1972), Assanis and Heywood (1986) suggested that the adiabatic flame temperature could be modelled as the temperature of the slightly greater than stoichiometric zones of hydrocarbon-air combustion products with an equivalence ratio of 1,1. However, they pointed out that this adiabatic flame temperature became considerably higher than the apparent radiant temperature. They obtained a better estimate of radiant temperature which was in reasonable agreement with the data of Flynn et al. (1972), by using the mean of the adiabatic flame temperature and the average bulk gas temperature. A comparison of the adiabatic flame temperature, radiant temperature and mean gas temperature is shown in Figure 16 for the expansion process. In addition Figure 17 shows typical apparent radiant temperature values obtained by Flynn et al. (1972) for three paraffinic fuels of cetane numbers 30, 40 and 50 respectively.

The measurements of flame temperature in an indirect injection diesel engine carried out by Peterson and Wu (1986) indicated that the stoichiometric adiabatic flame temperature equalled the maximum measured temperature within a tolerance of approximately 100 K when the initial conditions were estimated by assuming

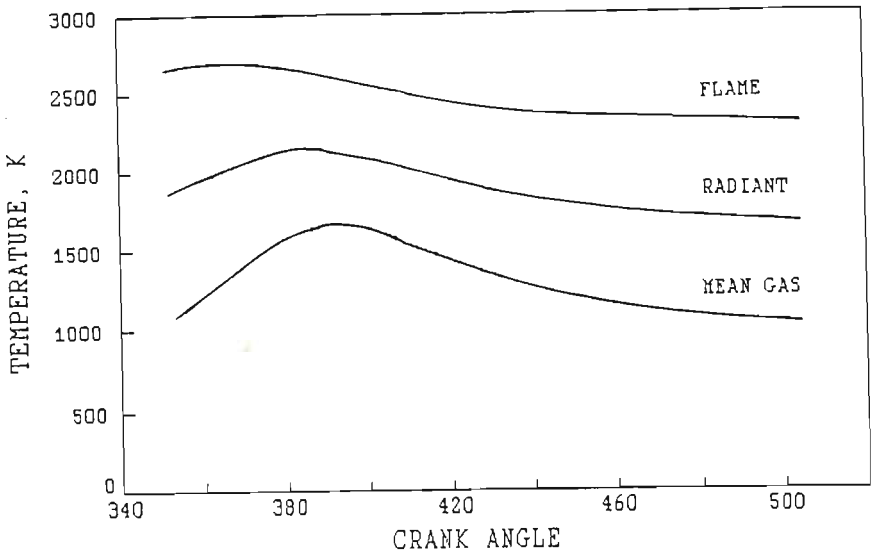

Figure 16 The variation of adiabatic flame temperature, radiant temperature and mean gas temperature with crank angle for the expansion process (after Assanis and Heywood, 1986).

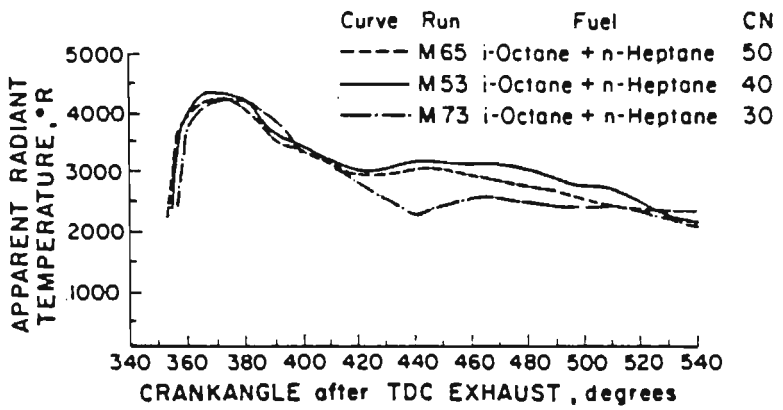

Figure 17 The variation of apparent radiant temperature with crank angle for three paraffinic fuels of cetane numbers 30, 40 and 50 respectively (after Flynn et al., 1972).

infinite mixing between previously produced combustion products and air. Figure 18 shows the variation with crank angle of the measured ensemble-averaged flame temperatures in the pre-chamber for two different intake pressures. The maximum temperatures are approximately 200 K higher than those modeled by Assanis and

Heywood (1986). Similar magnitudes of temperature to those obtained by Peterson and Wu (1986) were measured by Wahiduzzaman, Morel, Timar and DeWitt (1987) in a DI diesel engine. Figure 19 illustrates predicted and measured radiation temperatures for four loads at 2100 r/min. At maximum load the maximum measured radiation temperature is close to 2500 K decreasing down to approximately 2300 K at 25% load.

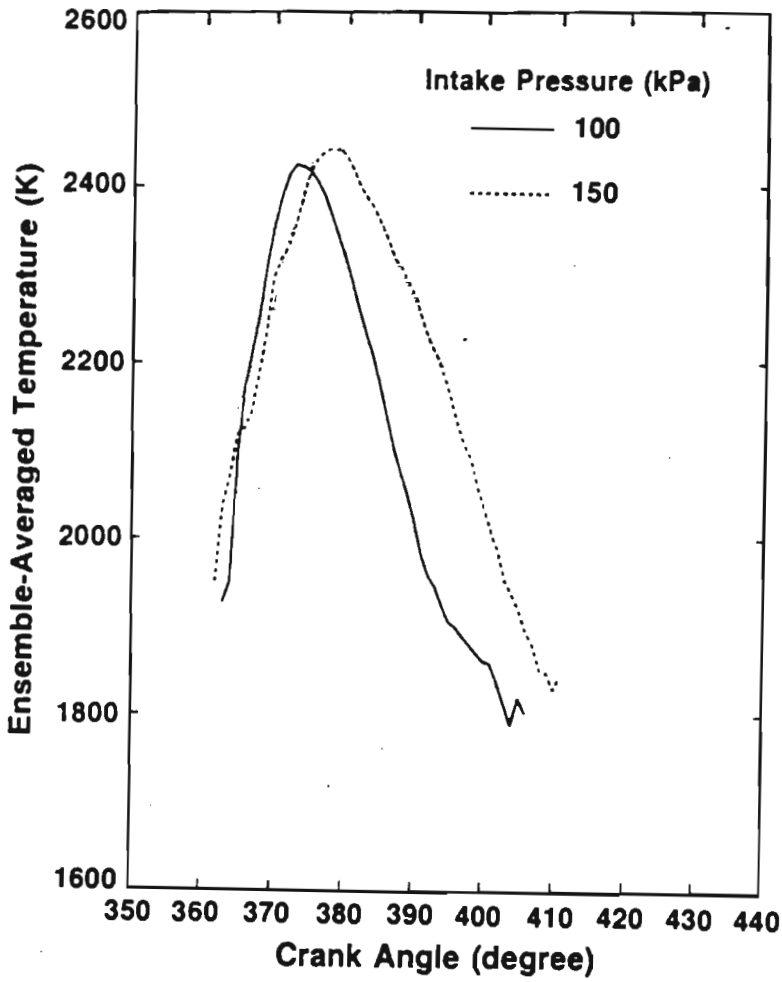

Figure 18 The variation of measured ensemble-averaged flame temperatures at the pre-chamber centre for two intake pressures (after Peterson and Wu, 1986).

In view of the advances in measuring techniques the magnitudes of radiant temperature obtained by Peterson and Wu (1986) and Wahiduzzaman (1987) were regarded as more accurate than those of Flynn et al. (1972). The suggested variation of radiant temperature put forward by Borman and Nishiwaki (1987) is in good agreement with their observations.

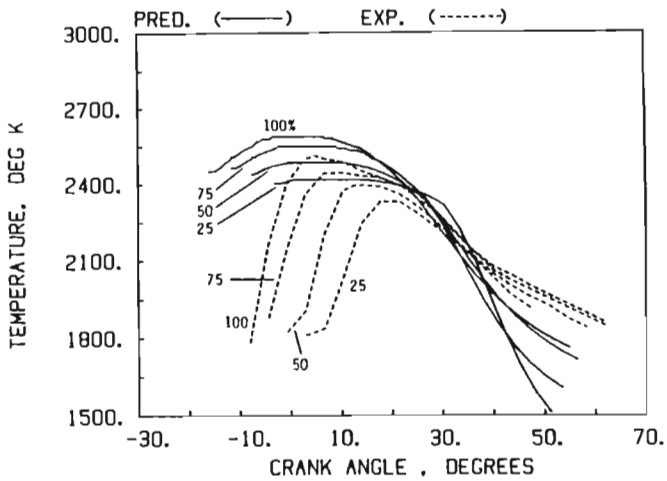

Figure 19 Predicted and measured radiation temperatures for four loads at 2100 r/min (Wahiduzzaman et al., 1987).

In the radiation heat transfer model of Morel and Keribar (1986) applied in a two zone combustion model the radiation temperature was linked to the average temperature of the burned zone T_b. At first this latter temperature gradually increased from its initial value at the start of combustion reaching a maximum shortly after TDC, and then decreased rapidly towards the end of combustion owing to rapid entrainment of air from the unburned zone and volume expansion. Up to the point of maximum temperature the radiation temperature was fixed at 90% of T_b to account for the preferential radiation heat transfer from the soot particles which were thus cooler than the surrounding burned gases.

After the burned zone temperature had been reached, the soot radiation temperature was obtained from an expression which included a weighting factor proportional to the square of the ratio of the burned mass to the total mass applied to the maximum temperature and to the burned zone temperature.

Morel and Keribar (1986) adopted this form of the radiation temperature in order to reflect the fact that, owing to the fourth power temperature dependence, the effective soot radiating temperature was dominated by the actively burning flame front.

The temperature of this front was higher than the average of the burned zone, which included actively burning species as well as burned-out products and which was being diluted by entrained air. In addition, since the soot was produced in the flame itself, its concentration was the highest in these hottest parts of the burned zone. Figure 19 shows the fairly good agreement with experimental data achieved by Wahiduzzaman et al. (1987) with this model. The use of a model of this form to compute radiation temperature was supported by Borman and Nishiwaki (1987) as mentioned earlier.

Representation of the emissivity in equation (12) varies from a constant value for the cycle to values which take into account both gas and soot radiation as functions of appropriate factors. The model of Annand (1963) made use of a constant which included the emissivity and the Stefan-Boltzmann constant. This model was revised subsequently by Annand and Ma (1970) with the separation of the Stefan-Boltzmann constant and the emissivity. Values for emissivity were presented according to engine speed and fuel/air ratio and an average value of 1,5 was calculated to represent all operating conditions. Morel and Keribar (1986) pointed out the reason for using a value greater than unity was to compensate for the use of mass averaged gas temperature as opposed to the much higher soot temperature.

The absorption of radiation in gas layers can be analysed by considering a beam of radiation of a certain intensity impinging on a gas layer of certain thickness. By applying Beer's law representing the exponential decay experienced by many types of radiation the gas emissivity can be obtained from the expression:

$$\epsilon_g = 1 - \exp(-KpL) \qquad \text{-----(13)}$$

where K = mean absorption coefficient
p = partial pressure of gas
L = mean beam length.

The mean beam length is a characteristic dimension for the geometry of the gas volume and represents a mean length of path along which radiant energy travels within the gas volume. From experimental data a satisfactory approximation for L for a specific geometry has been developed which is proportional to the ratio of the total volume of the gas to the total surface area.

The mean absorption coefficient and partial pressure in equation (13) are dependent on the particular gas species involved namely CO_2 and H_2O. Kamel and Watson (1979) fitted equations for the mean absorption coefficients to the curves of Abu-Romia and Tien (1967) which were solely dependent on temperature and independent of total gas pressure.

Soot emissivity was also represented as an exponential equation similar to equation (13) by Sitkei and Ramanaiah (1972), Kunitomo et al. (1975), Dent and Sulaiman (1977), Kamel and Watson (1979), Chang and Rhee (1983), Callahan et al. (1985) and Morel and Keribar (1986). Kamel and Watson (1979) calculated gas emissivities at atmospheric pressure and evaluated soot emissivity as a function of gas emissivity, excess air ratio and total pressure. Chang and Rhee (1983) calculated soot emissivity from an expression involving soot volumetric fraction which took into account complex optical constants for soot varying with wavelength and carbon to hydrogen ratio. Morel and Keribar (1986) followed on similar lines and proposed the expression:

$$\epsilon_s = 1 - \exp(-a.L) \qquad \text{-----(14)}$$

where L = radiation path length

a = soot absorption coefficient

and $a = 1575\ f_v.T_{rg}$

f_v = volume fraction of soot

T_{rg} = radiation temperature.

The volume fraction of soot depended on the soot concentration which was obtained from a soot model that tracked the

instantaneous rates of soot production and oxidation and integrated them with respect to time.

In terms of simplicity coupled with acceptable accuracy with reference to the relative contribution of radiation to the total heat transfer the procedure of Kamel and Watson (1979) for determining the emissivities can be regarded as appropriate. The same procedure was also used by Callahan et al. (1985) and by Szekely and Alkidas (1986) at the General Motors Research Laboratories, USA. The relative accuracy is reflected in the comparisons made by Kunitomo et al. (1975) of calculated values against experimental values from Oguri and Inaba (1972) and Sitkei and Ramanaiah (1972). Figure 20 shows the calculated radiation heat flux for various values of equivalence ratio as well as measured values and a curve obtained by applying Annand's radiation equation. As pointed out by Borman and Nishiwaki (1987) the model is quite sensitive to the value of the equivalence ratio.

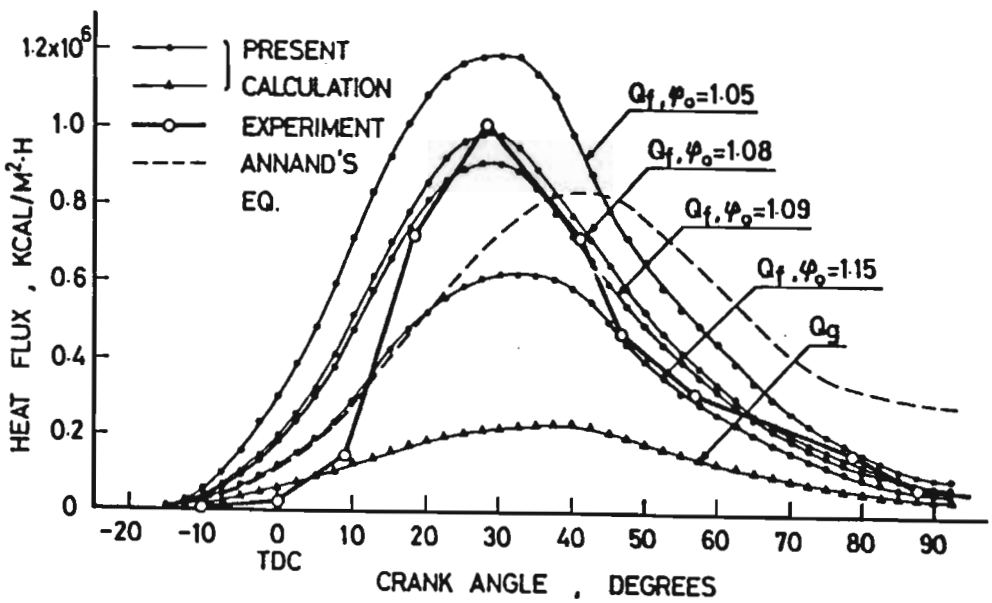

Figure 20 The variation of radiant heat flux with crank angle based on model calculations for different equivalence ratios and on Annand's equation compared to experimental data (Kunitomo et al., 1975).

2.2.4 Conduction

In the calculation of both convective and radiative heat transfer the temperature of the combustion chamber walls is required and is dependent on heat conduction from the surfaces. Wall temperatures supplied by researchers for these calculations vary from one constant value representing all the walls for all engine loads and speeds to values allocated to specific parts of the combustion chamber, which vary with load and speed. Callahan et al. (1985) approximated the wall temperature by using the temperature of the cooling water as it was easily measured and it represented a global temperature. In the heat release model of Alkidas (1986) the surface temperatures of the head, piston and liner were inputs to the model. The surface temperature of the head and piston were assumed to be the same and the liner temperature was arbitrarily set 10 K lower than the head temperature. The cylinder head surface temperature for the various engine test conditions was based on surface temperature measurements at one location in the cylinder head. Figure 21 shows the variation of cylinder head surface temperature with load for two engine speeds used by Alkidas (1987). Researchers such as Morel and Keribar (1985) have resorted to one-dimensional heat conduction models using a heat resistance network approach to improve surface temperature predictions.

It is necessary to put into perspective the relative influence of variations in wall surface temperature on heat transfer and on heat release computations. Lilly (1984) indicated that in practice the temperatures of the surfaces lining the combustion chamber had a small effect for two reasons. Firstly, with the fourth power law applied to radiation heat transfer, metal temperature had an insignificant effect. The relative contribution of metal temperature can be illustrated by considering measured variations of radiation temperature compared to maximum expected wall temperatures. Data from Peterson and Wu (1986) suggest variations of radiation temperature of 1800 - 2400 K while a survey of values published by Morel and Keribar

(1985) indicates an average wall temperature of 300°C as being close to maximum. Using the lowest radiation temperature of 1800 K the fourth power of the wall temperature represents approximately 1% of the fourth power of radiation temperature.

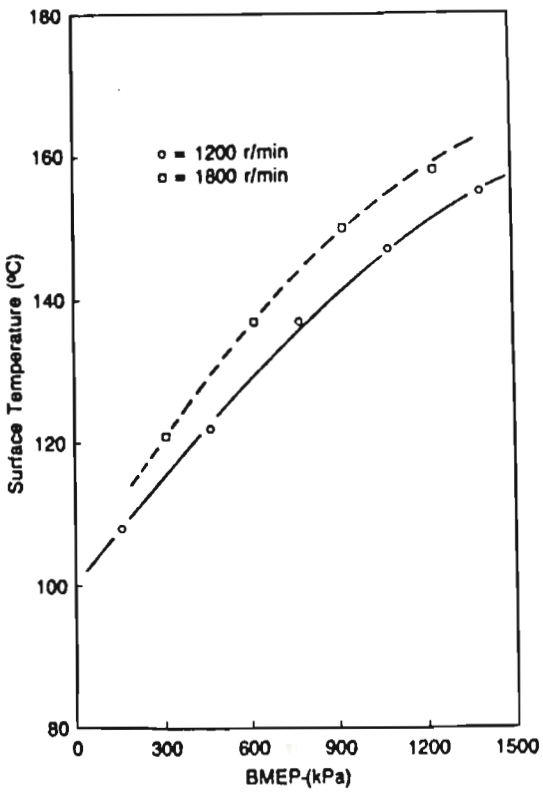

Figure 21 Cylinder-head surface temperature measurements versus load for two different speeds (Alkidas, 1987).

The second reason is that, although the effect of wall temperature on convective heat transfer is more significant than on radiation heat transfer as would be expected, convective heat is transferred from pockets of flame at temperatures much higher than the bulk gas temperature. The variations in heat flow are due to variation in the contact time of the pockets of flame with the wall rather than from variation in the temperature.

Hohenberg (1979) indicated that errors in wall temperature like errors in gas temperature, were insignificant at high loads but would result in considerable relative deviations in heat transfer at low loads. The relative deviations are illustrated in Figure 22 for no load and full load. The effect of varying chamber

surface temperature on rate of heat release and accumulated heat release was analysed by Martin and Ahmad (1986). The surface temperature was varied from a low value set equal to the cooling-water exit temperature to a high value near that of the exhaust manifold temperature. As shown in Figure 23 the effect on the rate of heat release was negligible while the differences in accumulated heat release were noticeable. Nevertheless, Martin and Ahmad (1986) showed that changes in heat transfer coefficient had a significant effect on both rates of heat release and accumulated heat release as illustrated in Figure 24. These graphs highlight the importance of computing accurate heat transfer coefficients.

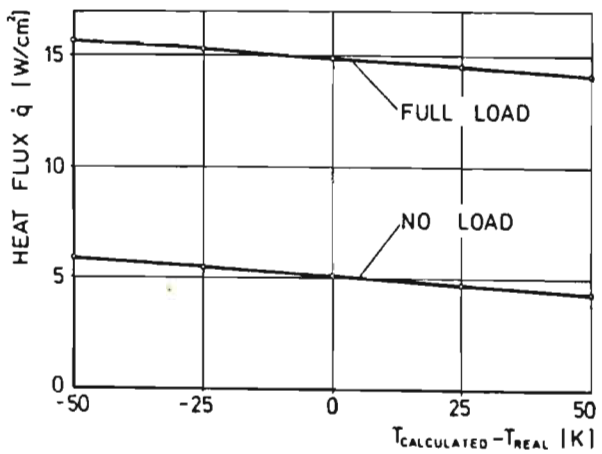

Figure 22 Calculated heat flux versus difference of calculated and real surface temperature at 1000 r/min (Hohenberg, 1979).

Owing to the cyclic variation of combustion, heat conduction through the chamber walls is the combination of a steady state and a transient component. The transient component consists of concentrated bursts of high heat flux during combustion followed by relatively long periods of low heat flux rates. This pattern produces temperature transients in thin layers of metal adjacent to the chamber wall surfaces. Morel, Wahiduzzaman and Fort (1988) suggested variations in the surface temperature of 20 - 40 K for most of the metal surfaces in the chamber. For the purposes of calculating heat transfer to be used in the computation of heat release this relatively small transient wall

surface temperature variation will have a negligible effect and therefore only steady state conduction need be considered.

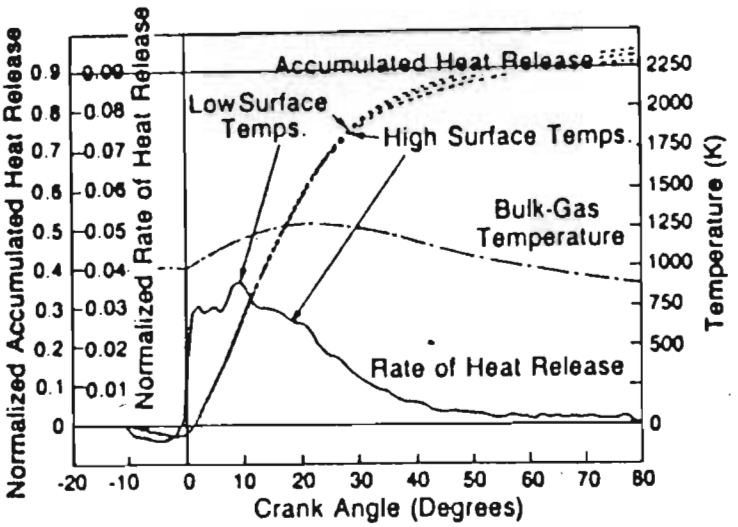

Figure 23 The influence of surface temperature on heat release characteristics in a DI diesel engine (Martin and Ahmad, 1986).

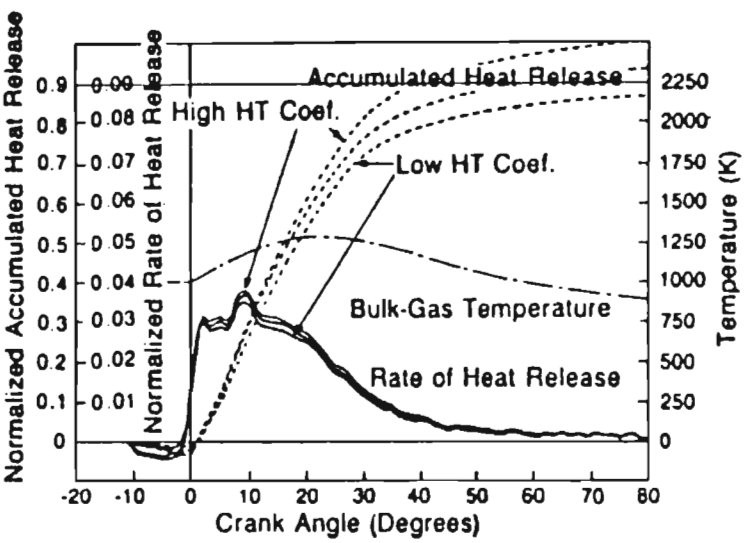

Figure 24 The influence of the heat transfer coefficient on heat release characteristics (Martin and Ahmad, 1986).

In the case of water-cooled engines the coolant circulates through the engine to control the temperature of the components in the vicinity of the combustion chamber by heat conduction. In addition the lubricating oil assists in cooling the underside of the piston. According to the analysis by Morel, Fort and

Blumberg (1985) on a turbocharged DI Cummins diesel engine the heat transfer was divided between the piston at 49%, head at 32% and liner at 19%. Establishing a heat conduction model for these components with appropriate boundary conditions is difficult especially when they are integrated and the effect of piston movement is included.

An accurate and complete solution of heat conduction from the combustion chamber necessitates a three-dimensional representation of the structure and the solving of Laplace's equation using finite differences or finite elements. Such a solution may be required when studying thermal loading and stress problems. However, Borman and Nishiwaki (1987) indicated that, for analyses that required only trends in metal temperatures with engine load and speed, simple one-dimensional conduction models could be used. Such models are therefore adequate for heat release analysis.

In one-dimensional analyses of heat conduction, heat transfer rate, q may be determined by applying Fouriers' law:

$$q = - \frac{k.A}{x} (T_2 - T_1) \qquad \text{-----(15)}$$

where k = thermal conductivity and is assumed constant
A = surface area
x = wall thickness
T_1, T_2 = wall surface temperatures.

For a multi-layer wall consisting of sections a, b and c the heat flow must be the same through all sections (Holman, 1986):

$$q = - \frac{k_a.A.(T_2 - T_1)}{x_a} = - \frac{k_b.A.(T_3 - T_2)}{x_b} = - \frac{k_c.A.(T_4 - T_3)}{x_c} \qquad \text{-----(16)}$$

Solving these equations:

$$q = \frac{T_1 - T_4}{x_a/k_a.A + x_b/k_b.A + x_c/k_c.A} \qquad \text{-----(17)}$$

The heat transfer rate in equation (17) may be considered as a flow and the combination of thermal conductivity, thickness of material, and area as a resistance to this flow thus providing a relationship similar to Ohm's law (Holman, 1986). This electrical analogy is used to solve complex problems such as those found in engine heat transfer.

Borman and Nishiwaki (1987) presented a typical procedure for obtaining steady-state wall surface temperatures. The first step was to carry out a detailed cycle simulation with appropriate assumptions for wall surface temperatures. Next, the time averaged bulk gas temperature, heat flux and heat transfer coefficient were obtained from calculated instantaneous values to yield a new surface temperature by the use of steady-state heat conduction correlations with a given coolant side temperature. For a typical DI diesel engine at full load the time-averaged heat transfer coefficient was 350 $W/m^2.K$ and the average bulk gas temperature was 1300 K.

Assanis and Heywood (1986) assumed approximate estimates for wall surface temperatures for use in their cycle simulation. Instantaneous convective and radiative heat transfer to the combustion chamber walls were calculated for the full cycle. At the end of the cycle a heat balance was performed between the cycle-averaged gas/wall heat transfer rate and the heat conducted through the walls of each component to compute new surface temperatures. These new temperatures were used in the next cycle iteration until the calculation converged. A similar procedure can be applied to cylinder pressure derived heat release analysis by also performing an energy balance between fuel input and calculated energy release.

2.3 Combustion Processes

The combustion in a diesel engine takes place as a result of a complex sequence of thermodynamic processes. These processes are influenced by such factors as combustion chamber geometry, fuel injection, air motion and heat transfer.

The rapidly expanding power of computers permits the development of more physically based models which provide spatial and temporal distributions of temperature, gas species and heat transfer. Verification of these models remains a problem owing to the difficulties in measuring temperatures, concentration of species and fluid motion in the combustion chamber during combustion, particularly in the case of direct injection diesel engines. Approaches to combustion modelling vary considerably in terms of complexity and emphasis. However, the models can be broadly categorised as zero-dimensional, quasi-dimensional and multi-dimensional (Heywood, 1980).

The zero-dimensional or thermodynamic models have no spatial resolution and therefore do not include any information on the fluid mechanics (Foster, 1985). These models are largely used for diagnostic and not predictive purposes. The majority of the models presently in use fall into this category.

Quasi-dimensional models predict the rate of burning of fuel from the fundamental physical and geometrical quantities involved. In these models a geometrical model describing some sort of link between the combustion process and engine design parameters is superimposed on the zero-dimensional model (Kumar, Edsell, Milkins and Watson, 1985).

Multi-dimensional models require equations for mass, species concentrations, momentum and energy conservation formulated in finite difference form. Simultaneous solutions of these equations necessitates the use of supercomputers to obtain

spatially and time resolved values of variables (Kumar et al., 1985).

Foster (1985) provided a comprehensive overview of zero-dimensional models covering single zone, two zone and three zone combustion. He stated that the foundation of all the models was the First Law of Thermodynamics with attention being focussed on the combustion process. His derivation of the necessary equations was based on that of Krieger and Borman (1966), one of the more widely applied First Law derivations in diesel engine research. The derivation of Foster (1985) is reviewed here as it is the foundation of the combustion model used in the present study.

Referring to a control volume in the combustion chamber as shown in Figure 25 it is assumed that at any instant in time the control volume is in thermodynamic equilibrium. Therefore the entire control volume contains a homogeneous equilibrium mixture of air and products of combustion. Phenomena such as temperature gradients, pressure waves, non-equilibrium compositions, fuel vaporisation and mixing are ignored. From these assumptions an energy balance in the form of a rate equation is given by:

$$\frac{d(mu)}{dt} = u.\frac{dm}{dt} + m.\frac{du}{dt} = - P.\frac{dV}{dt} + Q + h_f.\frac{dm}{dt} \qquad \text{-----(18)}$$

where

d(mu)/dt = rate of change of total internal energy, mu, of the control volume of mass, m

P.dV/dt = rate of mechanical work done on the piston

Q = rate of heat transfer into the control volume through the control volume boundary

h_f.dm/dt = rate of fuel energy released in the control volume determined from the mass burning rate, dm/dt, and the calorific value of the fuel, h_f.

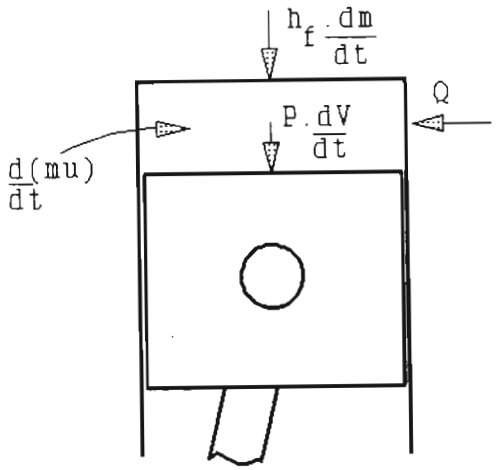

Figure 25 A schematic diagram of the combustion chamber showing the application of the First Law of Thermodynamics.

The solution of equation (18) requires additional relationships. Firstly the internal energy is a function of temperature, pressure and composition:

$$u = u(T,P,\phi)$$

Changing to a rate equation:

$$\frac{du}{dt} = \frac{\delta u}{\delta T}.\frac{dT}{dt} + \frac{\delta u}{\delta P}.\frac{dP}{dt} + \frac{\delta u}{\delta \phi}.\frac{d\phi}{dt} \qquad \text{-----(19)}$$

From the Ideal Gas Law, P.V = m.R.T, the rate equation becomes:

$$V.\frac{dP}{dt} + P.\frac{dV}{dt} = R.T.\frac{dm}{dt} + m.T.\frac{dR}{dt} + m.R.\frac{dT}{dt} \qquad \text{-----(20)}$$

Equation (20) can be used to eliminate dT/dt from equation (19). The fuel-air equivalence ratio, ϕ, in equation (19) is the value at any instant and was given by Krieger and Borman (1966) as:

$$\phi = \phi_o + \left(\frac{m}{m_o} - 1\right).\left(\frac{1 + f_o}{f_s}\right)$$

where ϕ_o = initial fuel-air equivalence ratio
m = instantaneous mass in the control volume
m_o = initial mass in the control volume
f_o = initial fuel-air ratio prior to fuel addition
f_s = stoichiometric fuel-air ratio.

changing to a rate equation:

$$\frac{d\phi}{dt} = \frac{1 + f_o}{f_s . m_o} \cdot \frac{dm}{dt} \qquad \text{-----(21)}$$

As the equilibrium composition of the control volume changes with time, the specific gas constant , R, is also changing and is a function of temperature, pressure and composition:

$$\frac{dR}{dt} = \frac{\delta R}{\delta T} \cdot \frac{dT}{dt} + \frac{\delta R}{\delta P} \cdot \frac{dP}{dt} + \frac{\delta R}{\delta \phi} \cdot \frac{d\phi}{dt} \qquad \text{-----(22)}$$

Equations (18) - (22) represent five equations and the seven unknowns, dm/dt, dT/dt, dP/dt, dφ/dt, dR/dt, du/dt and dV/dt. The partial derivatives of u and R with respect to T, P and φ can be obtained from a chemical equilibrium program. From equations (18) - (22) Krieger and Borman (1966) solved for the apparent mass burning rate:

$$\frac{1}{m} \cdot \frac{dm}{dt} = \frac{- \frac{R.T}{V} \cdot \frac{dV}{dt} - \frac{\delta u}{\delta P} \cdot \frac{dP}{dt} + \frac{1}{m} . Q - C.B}{u - h_f + \frac{\delta u}{\delta \phi} \cdot \frac{d\phi}{dt} - C \left(1 + \frac{1}{R} \cdot \frac{\delta R}{\delta \phi} \cdot \frac{d\phi}{dt}\right)} \qquad \text{----(23)}$$

where $B = \left(\frac{1}{P} \cdot \frac{dP}{dt} - \frac{1}{R} \cdot \frac{\delta R}{\delta P} \cdot \frac{dP}{dt} + \frac{1}{V} \cdot \frac{dV}{dt}\right)$,

$$C = \left(T \cdot \frac{\delta u}{\delta T}\right) / \left(1 + \frac{T}{R} \cdot \frac{\delta R}{\delta T}\right),$$

and dφ/dt is represented by equation (21).

Solution of equation (23) requires the following additional information:

a) a set of initial conditions such as a known composition at a known temperature, pressure and volume,
b) experimental pressure-time data for the cycle,
c) expressions for the internal energy, enthalpy and gas constant for the products and unburnt mixture,
d) a correlation for the heat transfer rate,
e) data which describe the geometry of the engine, and

f) the calorific value and C-H-O ratio of the fuel.

From the engine geometry and speed dV/dt can be calculated and the rate of change of pressure dP/dt is obtained from the experimental data. Foster (1985) described this type of model as a First Law model driven by the experimental pressure data thus making it diagnostic in nature. The model would have become predictive rather than diagnostic if an analytical expression had been used for generating cylinder pressure.

The thermodynamic properties of the mixture in the combustion chamber which define the internal energy, enthalpy and gas constant can be obtained from the instantaneous equilibrium composition of the mixture. The partial derivatives of internal energy and the specific gas constant with respect to temperature, pressure and equivalence ratio, which are required in equation (23), are usually expressed in terms of the mole fractions of the constituents in the mixture (Foster, 1985). Programs such as those of Olikara and Borman (1975), Way (1977) and Strehlow (1984) calculate the instantaneous equilibrium mole fractions. The program of Olikara and Borman (1975) also computes the partial derivatives of the mole fractions with respect to temperature, pressure and equivalence ratio for the products of combustion of any hydrocarbon fuel and air. In addition, one of the subroutines calculates the gas constant, enthalpy, internal energy and the partial derivatives of these with respect to temperature, pressure and equivalence ratio.

Faletti, Sorenson and Goering (1982) used an earlier version of the program developed by Strehlow (1984) for calculating the equilibrium composition of the mixture. The subroutine used the Weinberg technique and made it possible to take into account the effect of dissociation of the products of combustion. The mixture composition in conjunction with the pressure and temperature of the mixture were then fed into a subroutine developed by Savage (1982), cited by Faletti et al. (1982), which calculated the thermodynamic properties of the mixture. The

partial derivatives were calculated in a separate subroutine. This same model, which was used by Taylor (1987), forms the basis of the model developed in the present study.

Certain gas transport properties such as viscosity and thermal conductivity are normally required for heat transfer correlations such as that of Annand (1963). They may be determined from published equations fitted to experimental data such as those discussed by Strehlow (1984).

An estimate of the total mass which includes mass of air and fuel, is also required for solving equation (23). The air mass flow into the cylinder is measured and the exhaust residual can be estimated with the aid of a diesel engine simulation. The total mass during combustion is continuously augmented by the instantaneous mass of fuel burnt determined from the apparent mass burning rate.

As indicated by Foster (1985) and Taylor (1987) the results from solving equation (23) are extremely sensitive to the shape of the cylinder pressure data input. Slight oscillations in the pressure data are amplified considerably in the pressure derivative leading to wild oscillations in the calculated heat release. Foster (1985) stated that a 1% error in the pressure measurement could result in approximately a 50% error in the rate of heat release. Various researchers have highlighted the problems and errors associated with pressure measurement (Lancaster, Krieger and Lienesch, 1975; Callahan et al., 1985; Theobald and Alkidas, 1987; Timoney, 1987b). The major sources of possible error in cylinder pressure measurement listed by Timoney (1987b) were:

a) location of transducer and passage effects,
b) transducer/charge amplifier calibration,
c) determination of absolute pressure levels with piezo-electric transducers,
d) thermal effects on transducers,

e) accuracy and speed of analogue to digital conversion for data acquisition, and
f) non-uniformities of pressure across the cylinder.

A further factor affecting the accuracy of heat release rates derived from measurements on DI diesel engines was the instantaneous cylinder volume. The key problems indicated by Timoney (1987b) were:

a) location of TDC,
b) estimation of true (hot) geometric compression ratio and clearance volume, and
c) uncertain dynamic effects of crankshaft twist and oil film thickness.

A check on the overall accuracy of heat release analysis based on cylinder pressure measurement can be carried out by comparing the total heat released per cycle in energy units to the calorific value of the fuel mass injected per cycle. Timoney (1987b) referred to the ratio of these two quantities as the combustion efficiency. The presence of exhaust smoke indicates incomplete combustion and therefore less than 100% combustion efficiency. However, Timoney (1987b) indicated that even a very high smoke reading of six Bosch units represented a mass of carbon of the order of 0,5% of the mass of the fuel consumed. Hence, substantial deviations from a combustion efficiency of 100% would suggest either errors in the data acquisition or improperly calibrated constants in the heat transfer coefficients.

Van Gerpen, Huang and Borman (1985), in calculating heat release using the model of Krieger and Borman (1966), heat transfer from the model of Annand (1963) and thermodynamic properties of the gas mixture with the subroutines of Olikara and Borman (1975), arbitrarily multiplied the heat transfer rate by a constant so that the calculated amount of fuel burned by the time of EVO corresponded to the measured amount of fuel injected per cycle.

They pointed out that, although this procedure provided consistency in the calculations it did not correct for possible inaccuracy in the shape of the heat transfer curve. In addition they stated that the heat release model itself did not represent an accurate determination of the mass average internal energy, particularly during the earlier most heterogeneous stages of combustion. Therefore the heat release calculations from this model were to be used only for comparison purposes and general trends.

Taylor (1987) also compared the calculated fuel consumed to measured fuel consumed and found major differences which were attributed to errors in the measurement of pressure. His data were obtained from a three cylinder engine where it was assumed that fuel was distributed equally among the cylinders and that in the calculation of FMEP from IMEP and BMEP, each cylinder generated the same amount of work. Calibrations of fuel delivery on a test bench of the CAV rotary distributor fuel injection pump generally show significant scatter in the levels of fuel delivery among injectors. Therefore, there is a strong likelihood of unequal fuel deliveries to respective cylinders.

Owing to the heterogeneous form of the mixture and combustion in a diesel engine, formulation of two zone models has proved to be difficult with particular reference to the geometry of the zones. A combustion model representing a burned and an unburned zone is necessary in the case of spark-ignition engines where a definite flame front is propagated through the mixture. Morel and Keribar (1985) superimposed a quasi-dimensional burned-zone model on three flow regions in the combustion chamber of a direct injection diesel engine. The model corresponded to combustion behaviour observed in engine combustion motion pictures and to physical intuition and defined the location of the burned gases.

Morel and Keribar (1985) determined the mass of the burned gases and their temperature and composition at each time step from a thermodynamic cycle code and then calculated the fraction of the

total volume occupied by the burned gases. The burned zone shape and dimensions were defined on a geometrical basis according to the following constraints:

a) the burned zone was axisymmetric and located centrally,
b) the distances from the border of the burned zone to the cup bottom and to the head were equal,
c) the distances from the burned zone to cylinder liner and to cup side wall were such that the aspect ratios of the burned zones in the clearance volume and in the cup equalled the aspect ratios of the whole clearance volume and the whole cup respectively.

The resulting burned zone shapes for two piston positions is shown in Figure 26 superimposed on three flow regions as defined by Morel and Keribar (1985). These regions consisted of the cup, the region directly above the cup in the clearance volume and the remaining clearance volume above the piston crown. The intersections of the burned zone with the flow regions defined the ratios of burned volume and mass in each region, which were used to calculate the values of a number of variables for convective and radiative heat transfer computations. According to Morel and Keribar (1985) the zonal combustion model also provided for the representation of the following phenomena:

a) flow velocities generated by combustion with the expansion in one region driving the gases into another region,
b) different gas temperatures seen by surfaces in the three flow regions, and
c) the effect of burned zone location on radiation heat transfer.

This model was applied to a wide variety of engines by Morel and Keribar (1986), Morel et al. (1987), Wahiduzzaman et al. (1987) and Morel, Keribar and Blumberg (1988). Its predictions were found to be in good agreement with detailed data obtained in diesel engines.

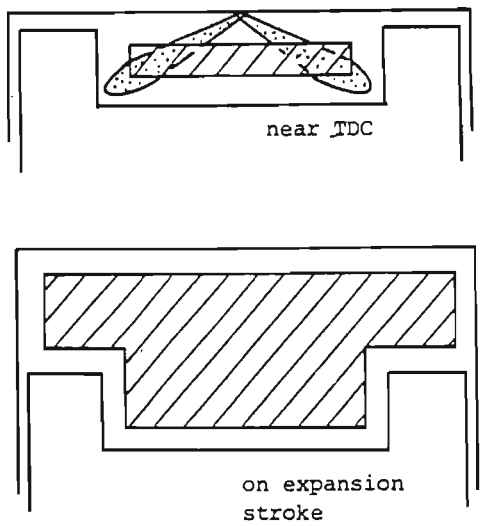

Figure 26 The burned and unburned gas zones for two piston positions super-imposed on the flow regions (Morel and Keribar, 1985).

The combustion model of Szekely and Alkidas (1986) was also in the form of a two zone system as described earlier in the heat transfer section. However, the combustion was also assumed to occur in two stages representing a high equivalence ratio or rich zone and a low equivalence ratio or a lean zone. Burnt volumes were determined from the thermodynamic cycle code and surface areas of each zone were determined with the aid of area-fraction values set equal to the volume fractions of the zone. Szekely and Alkidas (1986) concluded that the two stage model calculated much more realistic product temperatures than a single stage model, enabling elementary nitric oxide, soot kinetics and flame radiation models to be utilised.

Research efforts beyond the concept of burned and unburned zones in the combustion chamber have concentrated on finite difference and finite element models applied to the combustion chamber to solve the relatively complex differential equations governing the different processes (Gosman and Harvey,1982; Gunn,1987). A further line of approach that has been adopted is the modelling of the spray pattern as the fuel is injected into the engine and comes into contact with the wall. The effect of air motion is

superimposed on the spray. Models for air entrainment, fuel preparation and burning are also applied. Details of models of this type have been published by Kouremenos, Rakopoulos and Karvounis (1988) and Lipkea and DeJoode (1987).

Lipkea and De Joode (1987) from the John Deere Product Engineering Centre, Waterloo, Iowa, USA indicated that many features of diesel engine combustion systems had been successfully modelled using existing two-dimensional finite difference codes. However, the cost and specialised computer requirements of these types of models could preclude their use on a routine basis. As an intermediate step, quasi-dimensional or phenomenological modelling was widely and effectively used to model diesel engine combustion systems. The model developed by Lipkea and De Joode (1987) and applied by Lipkea, De Joode and Christenson (1987) and Tsai, Lipkea and De Joode (1987) generated a time dependent, quasi-dimensional analysis of the in-cylinder contents of a direct injection diesel engine. It required the input of engine geometry and operating conditions and was sensitive to fuel injection timing, fuel nozzle configuration, piston bowl diameter and air intake swirl level.

The fuel injected was divided into equal discrete mass elements, each one forming a zone which entrained air and moved. The concentration and movement of the small individual zones within the developing fuel spray were based on fully developed turbulent jet mixing correlations. The detailed zone division pattern took into account the internal recirculation within the fuel jet due to its unsteady nature and allowed the transition to a wall jet. The effect of swirling upon the free jet was also included. The zone division pattern provided the spatial framework for a step by step solution for the time dependent zone variables such as temperature, mass of unburned fuel, mass of entrained air and mass of nitric oxide. A developing jet is shown in Figure 27 in which the zone divisions are also indicated. All the air outside the jet zones was considered as one unburned zone. Only one jet was modelled and it was assumed to be independent of

other jets formed by additional holes in the injector nozzle. The results based on the modelled jet were increased by the number of holes in the nozzle.

Another approach to combustion modelling adopted by Durrett, Oren and Ferguson (1987) and Oren, Durrett, Ferguson, Timar, Tree and De Witt (1987) was to establish a multi-dimensional data set for diesel combustion model verification for use with a specially designed bomb which simulated diesel combustion. Time and space-resolved measurements of gas velocities, gas temperatures, wall temperatures and heat flux were carried out in addition to high speed photography of injection and combustion events. The object of this approach was to provide a multi-dimensional data set to be used for verifying a three-dimensional model which was close to completion.

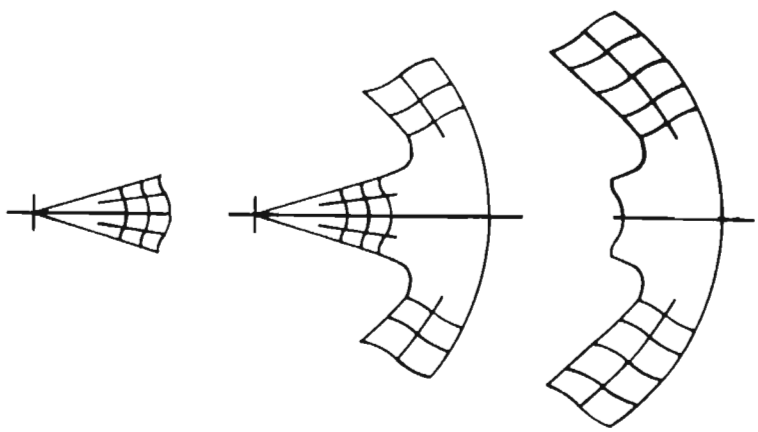

Figure 27 Developing free jet, wall jet and typical zones (Lipkea and De Joode, 1987).

Brehob and Kittelson (1988) highlighted the lack of experimental data that were required for validating models of combustion in compression-ignition engines, with particular reference to soot loading, chemical composition and temperature. They concluded that, in spite of the considerable amount of information available, the ultimate goal of obtaining the history of the conditions at a specific point in a realistic engine cylinder by a non-obtrusive diagnostic technique was not realisable.

It was concluded from this review of combustion models that the single zone model, although useful for basic comparisons in diagnostic work, had certain limitations, in particular the lack of spatial resolution, which precluded its successful use in thermal stress analysis, heat transfer and emissions modelling. At the other end of the scale the multi-dimensional models required computing power beyond the micro-computer and were not necessarily more accurate than simpler models. Therefore a model was required which was somewhere between the single zone and multi-dimensional models and which provided some degree of spatial as well as temporal resolution in terms of heat transfer and combustion temperatures. Such a model would then allow thermal stresses to be determined realistically in the combustion chamber and would represent combustion temperatures of the right order of magnitude for use in heat transfer calculations and the modelling of nitric oxide and soot formation. Models such as those of Morel and Keribar (1985) and Szekely and Alkidas (1986) were considered to be the closest in meeting these requirements.

The main objective in this project was to produce a combustion model with a less empirical grounding than existing zero-dimensional models. Hence the quasi-dimensional approach of Morel and Keribar (1985) was appropriate and, combined with other carefully selected sub-models, provided the guidelines for formulating the model in this project.

3. FORMULATION OF MODEL

The complete model in this study consisted of a number of sub-models representing in-cylinder gas flow processes, heat transfer and combustion. Each sub-model was developed such that its simplicity was determined by the importance of its relative contribution to the final output. Before discussing the formulation of the sub-models it is necessary to indicate the structure of the overall model and how the sub-models interact.

3.1 Basic Structure

A better understanding and appreciation of the relative complexity of the sub-models and their interaction can be gained by the use of flow charts. Figures 28 and 29 illustrate the structure of the model used to investigate motored engine and fired engine conditions respectively. For the modelling of in-cylinder gas flow the combustion chamber volume was divided into an inner cylindrical volume and an outer annular volume shown schematically in Figure 30. This approach was the same as applied by Borgnakke et al. (1981) and Murakami et al. (1988). Also shown in Figure 30 are the six discrete surfaces making up the total surface area of the combustion chamber as applied by Morel and Keribar (1985).

Referring to Figure 28, the mass of the cylinder contents at IVC is determined initially and the measured cylinder pressure is used via the Ideal Gas Law to calculate the bulk gas temperature. This temperature is applied in a number of subsequent calculations. It is used to determine the bulk gas properties which are required in the computation of swirl. The boundary layer or film temperature is obtained from the average of the bulk gas temperature and the respective wall temperature. The gas properties of the boundary layer which are required for computing the heat transfer coefficients at each wall are based on the film temperature.

At each crank angle between IVC and EVO the in-cylinder gas flow components of squish, swirl and turbulence are employed in the calculation of area-averaged resultant velocities at each of the designated surfaces in the combustion chamber. These velocities in conjunction with the gas properties of the boundary layer determine the convective heat transfer coefficients.

The temperatures of the walls are estimated from a steady state single-dimensional conduction model. The convective heat transfer is calculated from the input of the heat transfer coefficient, the wall area and the temperature differential between the wall and the bulk gas temperature.

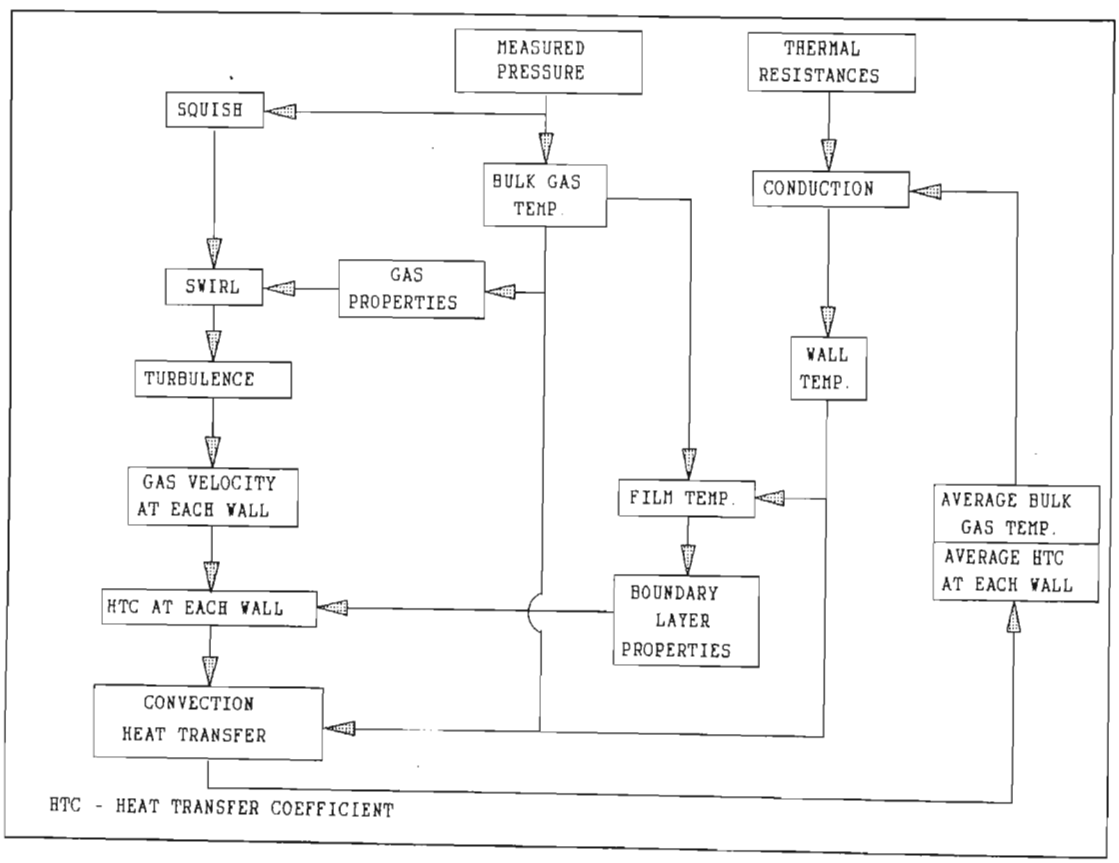

Figure 28 Block diagram showing structure of model for motored engine conditions.

After performing the gas velocity, heat transfer and gas temperature calculations at each crank angle from IVC to EVO,

an average bulk gas temperature and average heat transfer coefficients at each wall are computed for the full cycle and used to provide a better estimate of the wall temperatures. The calculation procedure is then repeated.

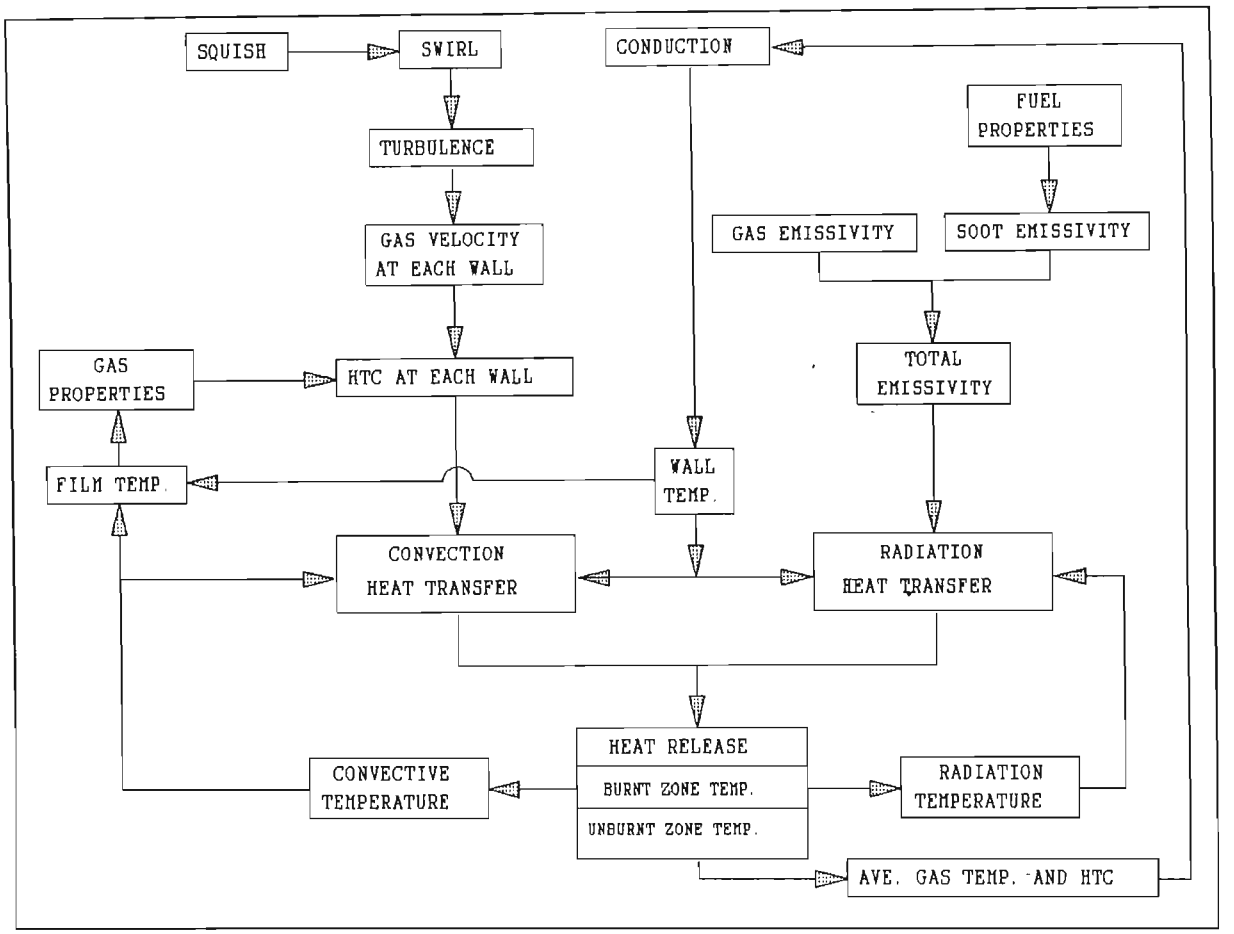

Figure 29 Block diagram showing structure of model for fired engine conditions.

With reference to the model structure shown in Figure 29 for fired engine conditions, the calculation procedure for the convection heat transfer is the same as for the motored engine case except for the input of a convective temperature based on the combustion process. A sub-model of radiation heat transfer is included which in turn requires the input of total emissivity, wall temperature and a radiation temperature which is also based on the combustion process. The total emissivity is made up of two components resulting from gas radiation and soot radiation respectively. The calculation of soot emissivity requires the

input of fuel properties. The computation of wall temperature is performed with the aid of a conduction model and an iterative procedure as for the motored engine case.

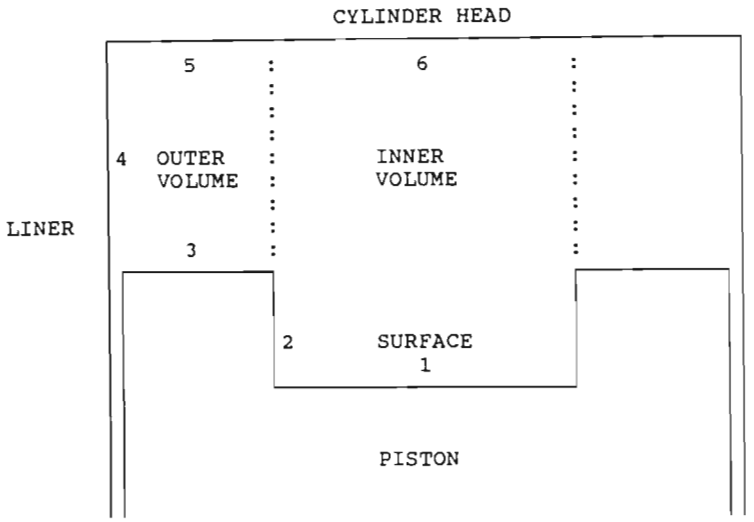

Figure 30 Division of combustion chamber volume into an inner and outer volume and of the chamber surface area into six discrete elements.

The heat release model into which the convection and radiation heat transfers were fed was adapted from an existing heat release model so that a burnt products zone and an unburnt zone were generated during the course of combustion. The temperatures of each zone were then used in the calculation of the convective and radiation temperatures. The measured pressure was required in the calculation of the bulk gas temperature and of the rate of heat release.

The computer programmes for executing each submodel were formulated in FORTRAN as the existing heat release model was in FORTRAN. Virtually all the model development was carried out on an IBM compatible PC XT computer fitted with a numeric coprocessor. The programme was divided into a number of subroutines to facilitate error checking and compilation.

3.2 In-cylinder Gas Flow

The gas flow characteristics in the combustion chamber of a DI diesel engine during the compression and expansion strokes is governed primarily by piston velocity, squish, swirl and turbulence intensity. The variation of squish and swirl during the cycle is determined by the conservation of mass and angular momentum. Turbulence intensity, which is more difficult to model accurately than squish or swirl, was computed from a model of turbulence with its roots in the Navier-Stokes equations. The area-averaged velocities were based on contributions from piston motion, squish, swirl and turbulence.

3.2.1 Squish flow

The calculation of squish flow was carried out by assuming that the combustion chamber was divided into two volumes as shown in Figure 30. Following on the approach of Murakami et al. (1988), if the gas density ρ_c is regarded as uniform in the combustion chamber, then it can be shown (See Appendix A) that the mass transportation dm_1 from volume 2 to volume 1 relative to the movement of the piston dl is given by :

$$dm_1 = \frac{R_1^2.(R_1^2 - R_2^2)}{(R_1^2.h + R_2^2.l)^2}.h.m_o.dl \qquad \text{-----(24)}$$

where

m_o = total mass of charge in chamber, kg
h = depth of bowl in piston, m
l = instantaneous distance between top of piston and head, m
R_1 = radius of bowl, m
R_2 = radius of cylinder, m

The ratio of mass to volume in the inner volume is given by the charge density and hence:

$$\frac{dm}{dt}_1 = \rho_c \cdot \frac{dV}{dt}_1 = \rho_c \cdot A_{12} \cdot \frac{dr}{dt} \qquad \text{-----(25)}$$

where A = area of interface between volumes 1 and 2, m^2

$= 2\pi R_1 . l$

dr/dt = radial or squish velocity, m/s

However,

$$\frac{dm}{dt}_1 = \frac{dm}{dl}_1 \cdot \frac{dl}{dt} \qquad \text{-----(26)}$$

where

dl/dt = piston velocity, m/s.

Hence by combining equations (25) and (26), the squish velocity is given by:

$$\frac{dr}{dt} = \frac{1}{2\pi \rho_c . R_1 . l} \cdot \frac{dm}{dl}_1 \cdot \frac{dl}{dt} \qquad \text{-----(27)}$$

Using equations (24) and (27), the squish and reverse squish velocities can be calculated at any crank angle during the compression and expansion strokes.

Axial flow into the cup resulting from the squish effect can be computed in a similar manner assuming a uniform air density. The chamber is divided into two volumes 3 and 4 as shown in Figure 31.

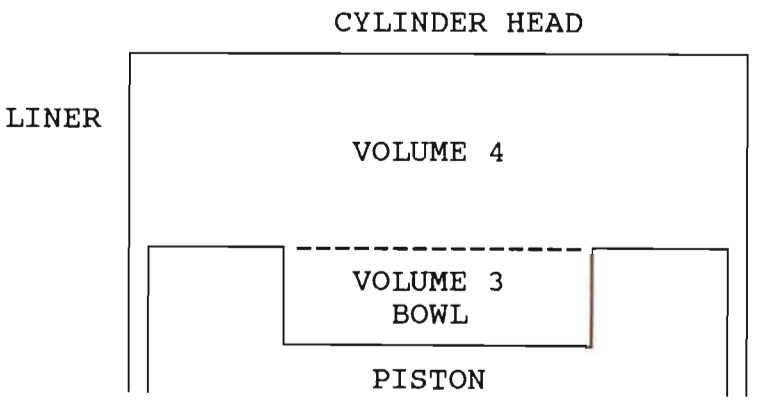

Figure 31 The division of the combustion chamber for calculation of the axial velocity into the piston bowl.

The mass transportation dm_4 from volume 3 to 4 relative to the movement of the piston dl is given by :

$$dm_4 = - \frac{R_1^2.R_2^2}{(R_2^2.l+R_1^2.h)^2}.h.m_o.dl$$

Applying the same approach as in equations (25) and (26) it then follows that the axial velocity into the bowl:

$$\frac{dx}{dt} = - \frac{R_2^2}{\pi\rho_c(R_2^2.l+R_1^2.h)^2}.h.m_o.\frac{dl}{dt} \qquad \text{-----(28)}$$

Both the squish velocity from equation (27) and the axial velocity from equation (28) are used as velocity components for computing the resultant velocity at each wall in the combustion chamber. Equations (25) and (27) are also required in the calculation of swirl velocities.

3.2.2 Swirl flow

The method selected for computing swirl flow is based on the model presented by Murakami *et al*. (1988). As for the squish flow calculation the combustion chamber is divided into an inner cylindrical volume 1 and an outer annular volume 2 by a virtual boundary radius equal to the bowl radius. The wall friction moment in each volume and the angular momentum exchange between the volumes provides the solution for the rotational speed of each volume ω_1 and ω_2.

According to Murakami *et al*. (1988) if the variation of the angular momentum in each volume with respect to time is equal to the summation of the angular momentum exchange between the volumes and the wall friction moment in each volume, then :

$$\frac{d(I_1\omega_1)}{dt} = T_{f1} + T_{f2} + T_{f6} + T_{v21} + T_{s21} \qquad \text{-----(29)}$$

$$\frac{d(I_2\omega_2)}{dt} = T_{f3} + T_{f4} + T_{f5} - T_{v21} - T_{s21} \qquad \text{-----(30)}$$

where I_1 = moment of inertia of inner volume

I_2 = moment of inertia of outer volume

T_{s21} = angular momentum flux transported from the inner volume to the outer volume by squish flow

T_{v21} = angular momentum flux transmitted from the inner volume to the outer volume by viscous shear

T_{f1} to T_{f6} = wall friction moments for each of the six surfaces designated in Figure 30.

During the compression stroke, $dm_1 \geq 0$ and the angular momentum transportation from the outer to the inner volume is given by:

$$T_{s21} = -\omega_2 \cdot \frac{dI}{dt}_2 = \frac{1}{2} \cdot \frac{R_2^4 - R_1^4}{R_2^2 - R_1^2} \cdot \omega_2 \cdot \frac{dm}{dt}_1$$

where $$I_2 = \frac{1}{2} \cdot \frac{R_2^4 - R_1^4}{R_2^2 - R_1^2} \cdot m_2$$

During the expansion stroke, $dm_1 < 0$ and the angular momentum is transported from the inner volume to the outer volume. Hence:

$$T_{s21} = \omega_1 \cdot \frac{dI}{dt}_1 = \frac{1}{2} \cdot R_1^2 \cdot \omega_1 \cdot \frac{dm}{dt}_1$$

where $$I_1 = \frac{1}{2} \cdot R_1^2 \cdot m_1$$

Angular momentum transmission by viscous shear between the inner and outer volumes was represented by the transmitted torque between two co-axial cylinders placed at the representative radii in each volume. These radii, R_{r1} and R_{r2} reflected the division of the inner and outer volumes into two equal volumes respectively as shown in Figure 32 (Murakami et al., 1988). On this basis:

$$T_{v21} = 4\pi\mu_e \cdot l \cdot \frac{R_{r2}^2 \cdot R_{r1}^2}{R_{r2}^2 - R_{r1}^2} \cdot (\omega_2 - \omega_1)$$

$$\mu_e = \nu_e \cdot \rho_c$$

$$\nu_e = k^{0,5} . l_m$$

$$l_m = 0,14\ R_2/2$$

$$k = 0,74\ c_m^2$$

where μ_e = effective turbulent viscosity, Pa.s
ν_e = effective turbulent kinematic viscosity, m^2/s
l_m = turbulence mixing length, m
k = turbulence kinetic energy, m^2/s^2
c_m = mean piston speed, m/s.

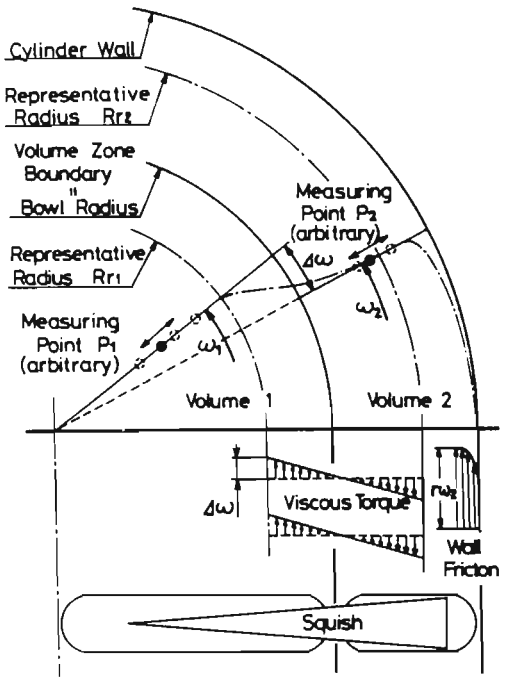

Figure 32 Schematic of the terms and representative radii in each volume used in the model (Murakami et al., 1988).

Murakami et al. (1988) pointed out the difficulty of obtaining wall friction directly in the combustion chamber with its complex boundaries. The wall friction at each surface was therefore estimated by assuming an infinite atmosphere adjacent to each surface and then multiplying by a corrective coefficient, ß. The

friction moments on the disc-like surfaces were given by von Kármán's approximate solution. Hence:

$$T_{f1} = T_{f6} = \beta.(-0,0365).\rho_c.\omega_1^2.R_1^5.\left(\frac{\nu}{\omega_1.R_2^2}\right)^{0,2}$$

$$T_{f3} = T_{f5} = \beta.(-0,0365).\rho_c.\omega_2^2.\left\{R_2^5\left(\frac{\nu}{\omega_2.R_2^2}\right)^{0,2} - R_1^5\left(\frac{\nu}{\omega_1.R_2^2}\right)^{0,2}\right\}$$

where ν = laminar kinematic viscosity, m^2/s.

The friction moments on the cylindrical surfaces were provided by the local friction coefficient for a flat plate, thus giving the following equations:

$$T_{f2} = \beta.(-0,0296).\left(\frac{2\nu}{\omega_1.R_1^2}\right)^{0,2}.\rho_c.(R_1.\omega_1)^2.2\pi R_1^2 h$$

$$T_{f4} = \beta.(-0,0296).\left(\frac{2\nu}{\omega_2.R_2^2}\right)^{0,2}.\rho_c.(R_2.\omega_2)^2.2\pi R_2^2 l$$

Equations (29) and (30) can then be represented as two ordinary differential equations of the form:

$$\frac{d\omega_1}{dt} = f(\omega_1,\omega_2)$$

$$\frac{d\omega_2}{dt} = f(\omega_1,\omega_2)$$

These equations were treated as simultaneous equations and were solved by iteration at each crank angle increment using the predictor-corrector method (McCracken and Dorn, 1964). The solution was started with the Runga-Kutta method. Variables that were computed with each increment of crank rotation, and used in the equations, included the distance between piston crown and head, the mass of gas in each volume, the gas density and the kinematic viscosity of the gas.

3.2.3 Turbulence intensity

The method adopted for calculating turbulence intensity was similar to that of Davis and Borgnakke (1982) from Ford Motor Company. The method relied on the classical k and ϵ turbulence approach. The model of Davis and Borgnakke (1982) was an extension of the work done by Launder and Spalding (1972) and followed on the model reported by Borgnakke et al. (1981). This model had subsequently demonstrated its reliability in applications by Belaire, Davis, Kent and Tabaczynski (1983), Davis, Tabaczynski and Belaire (1984) and Davis and Tabaczynski (1988). This record was regarded as sufficient justification for its use in this research.

To maintain simplicity in the model without sacrificing a practical level of accuracy the production of turbulence due to shear at the interface between the inner and outer demarcated volumes in the combustion chamber was ignored. In addition production of turbulence due to shear at the walls was disregarded. The graphs of angular momentum flux provided by Murakami et al. (1988) illustrated the relatively small contribution of these factors compared to squish, which, according to Fansler (1985) dominated as a producer of turbulence near TDC. The equation for production and dissipation of turbulent kinetic energy given by Davis and Tabaczynski (1988) in fact did not include terms for production due to shear within the gas flow and at the walls.

The production of turbulence due to compression was also included in the model as a number of researchers had indicated that it was significant (Wong and Hoult, 1979; Borgnakke et al., 1981; Morel and Keribar, 1985; Assanis and Heywood, 1986). The k - ϵ model consisted of two coupled differential equations describing the variation of turbulent kinetic energy and its dissipation rate:

$$\frac{dk}{dt} = P^{k}_{com} + P_{sq} - \rho_c \cdot \epsilon \qquad \text{-----(31)}$$

$$\frac{d\epsilon}{dt} = P^{\epsilon}_{com} + C_1 \cdot \frac{\epsilon}{k} \cdot P_{sq} + \rho_c \cdot \frac{k^2}{L^2} - C_2 \cdot \frac{\epsilon^2}{k} \qquad \text{-----(32)}$$

where k = turbulent kinetic energy, m^2/s^2
ϵ = dissipation rate of k, m^2/s^3
ρ_c = density of gas in cylinder, kg/m^3.

The P terms represent the volumetric production of k and ϵ due to compression and squish:

$$P^{k}_{com} = \frac{2}{3} \cdot k \cdot \frac{d\rho_c}{dt} \quad ,kg/m.s^3$$

$$P^{\epsilon}_{com} = \frac{4}{3} \cdot \epsilon \cdot \frac{d\rho_c}{dt} \quad ,kg/m.s^3$$

$$P_{sq} = C_3 \cdot \frac{d\rho_c}{dt} \cdot \frac{1}{2} \cdot V_r^2 \quad ,kg/m.s^3$$

where C_3 = constant
V_r = squish velocity at bowl lip, m/s

Also in equation (32) the constants C_1 and C_2 were 1,45 and 1,9 respectively as specified in the equations of Borgnakke et al. (1981) and provided originally by Launder and Spalding (1972). The term k^2/L^2 in equation (32) was not specified in any of the equations applied by Borgnakke et al. (1981), Davis and Borgnakke (1982), Belaire, Davis, Kent and Tabaczynski (1983), Davis, Tabaczynski and Belaire (1984) and Davis and Tabaczynski (1988). However, Morel and Keribar (1985) included it as an ad hoc representation of the boundary layer effects on the bulk dissipation rate. The value of L was set by Morel and Keribar (1985) at twice the minimum geometrical dimension of the region in the combustion chamber.

In the model for this study a global turbulence was determined for each of the two volumes previously defined for the calculation of swirl. Hence the instantaneous turbulent kinetic energy and its dissipation rate were computed for each region. The value of L in equation (32) was set equal to twice the

instantaneous piston-to-head clearance for the outer volume, and twice the sum of this same clearance and the depth of the bowl for the inner volume.

In the application of these equations it was assumed that a negative production of turbulence was impossible as in the cases of turbulence production from both compression and squish where $d\rho_c/dt$ was negative after TDC during the expansion stroke. For the compression term, $d\rho_c/dt$ was equated to zero after TDC. The production of turbulence from squish was treated as an inflow source of turbulence and therefore, for the inner volume, the squish production term was positive during the compression stroke and zero during expansion. For the outer volume the reverse was true with the production being initially zero and then positive for the reverse squish effect.

As indicated in an earlier chapter the model was formulated to include the period between IVC and EVO only and therefore turbulence production during the intake stroke was excluded. As a result it was necessary to provide a starting value for k and ϵ at IVC. Details of a procedure for calculating a starting value for k are provided in a later section. For the initial dissipation rate the following expression applied by Belaire et al. (1983) was used:

$$\epsilon = C_4 . k^{1,5}/l$$

where C_4 = adjustable constant
l = integral length scale set equal to the sum of the piston-to-head clearance at IVC and the depth of the bowl.

In the application of this model ordinary differential equations (31) and (32) were solved in the same way as the two coupled equations for the swirl velocities. The equations were therefore of the form:

$$\frac{dk}{dt} = f(k,\epsilon)$$

$$\frac{d\epsilon}{dt} = f(k,\epsilon)$$

Hence these equations were solved for each of the two volumes using the predictor-corrector method, the solution being initiated with the Runga-Kutta method. The resulting turbulence kinetic energies were then used in the calculation of a resultant velocity at each wall in the combustion chamber.

3.2.4 Combined flow

The equation for the resultant velocity at each of the six walls that were designated originally in Figure 30 was made up of two velocity components parallel to the relevant wall outside the boundary layer as applied by Morel and Keribar (1985) and a third component representing the contribution from turbulence. Assanis and Heywood (1986) calculated a resultant velocity for the whole chamber based on mean flow velocity, turbulence intensity and instantaneous piston speed. They mentioned that, although their equation for resultant velocity was speculative, it was constructed in such a way that increases in any of the three component velocities led to increases in the heat transfer rate, while at the same time errors due to over-estimating the contribution from any one component was minimised. Applying this same approach it was evident that the velocity components based on swirl and squish could be regarded as reliable. The contribution from turbulence was not as well defined. However, it did not dominate the calculation of the resultant or effective velocity. Published measurements of turbulence intensity indicated that its magnitude was generally less than 30% of the maximum tangential velocity.

For the purposes of the proposed model the same approach as that of Morel and Keribar (1985) was used for calculating the effective velocity:

$$U_{eff} = \sqrt{(U_x^2 + U_y^2 + 2k)}$$

where U_x, U_y = velocity components parallel to the surface in question outside the boundary layer

k = the kinetic energy of turbulence of the chamber volume adjacent to the surface of interest.

Referring to Figure 33 the velocity components that could be calculated or determined relatively easily were as follows:

a) swirl velocity in and directly above the bowl,

b) swirl velocity in the clearance volume above the piston crown,

c) squish or radial velocity towards cylinder axis at the bowl circumference,

d) reverse squish or radial velocity away from the cylinder axis at the bowl circumference,

e) axial velocity caused by piston movement,

f) axial velocity caused by flow into the bowl during the compression stroke, and

g) axial velocity caused by flow out of the bowl during the expansion stroke.

Representation of the average velocity components at each wall required some assumptions with respect to velocity distribution.

Using the same approach as Morel and Keribar (1985) the radial velocities were assumed to reach a maximum at the boundary between the inner and outer volumes, decaying linearly from there towards the liner and towards the cylinder axis where they became zero.

The assumption of a solid body type of rotation for the swirl component particularly near TDC was supported in general by a number of researchers who had carried out flow measurements or had used fairly complex well tested models (Arcoumanis et al., 1986; Arcoumanis et al., 1983). In addition, this assumption helped to simplify the computation without causing a significant loss of accuracy.

The axial velocity caused by piston movement was a linear function of piston speed increasing from zero at the head to the piston velocity at the piston face. The axial velocity from flow into the bowl was assumed to be maximum at the plane of entry into the bowl, decaying to zero at the bottom of the bowl.

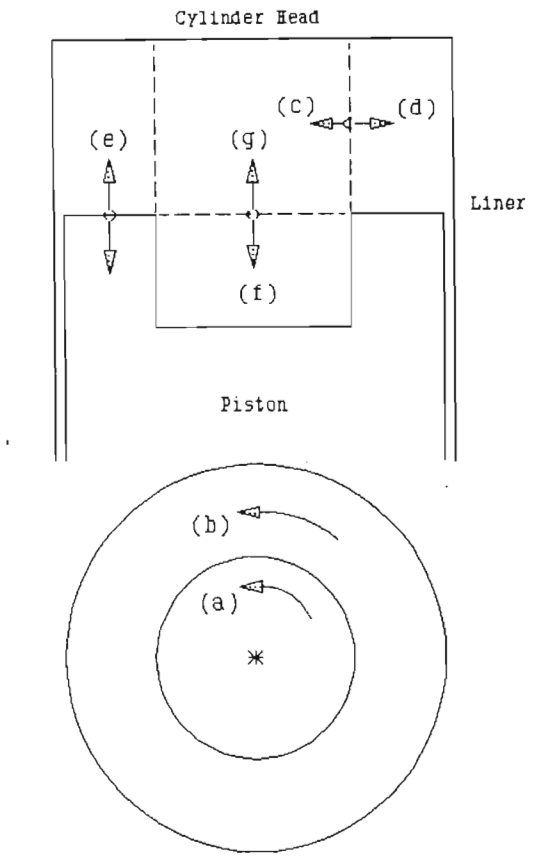

Figure 33 Schematic of the cylinder and piston showing the velocity components.

Taking into account measured flow distributions in the chamber published by researchers, representative velocity components at each of the six walls of the combustion chamber were formulated. For surface 1 at the bottom of the cup an average tangential velocity U_{s1} was obtained by calculating the radius at which equal inner and outer areas occurred and multiplying this radius by the angular swirl velocity. The radial velocity component was based on an area-averaged squish velocity, U_{r1} decaying from a maximum to zero at the cylinder axis. By equating the integrated velocities on either side of a radius, r as shown in Figure 34,

the average velocity could be determined. Measurements carried out by Brandl, Reverencic, Cartellieri and Dent (1979) showed that squish motion had little effect upon the flow in the lower part of the bowl. The measurements of Fansler (1985) indicated solid body rotation over the full radius of the lower part of the bowl during compression and expansion strokes. Referring to Figure 34:

$$U_{r1} = \frac{r}{R_1}.v_s \qquad \text{-----(33)}$$

$$\text{and} \quad V = \frac{2}{3}.\pi.R_1^2.v_s \qquad \text{-----(34)}$$

$$\text{Also } V_2 = \frac{2}{3}.\pi.\frac{r^3}{R_1}.v_s \qquad \text{-----(35)}$$

$$\text{But } V_2 = V_1 = V/2$$

Hence from equations (33), (34) and (35) it can be shown that the area-averaged radial velocity for surface 1 is:

$$U_{r1} = v_s/2^{0,333}$$

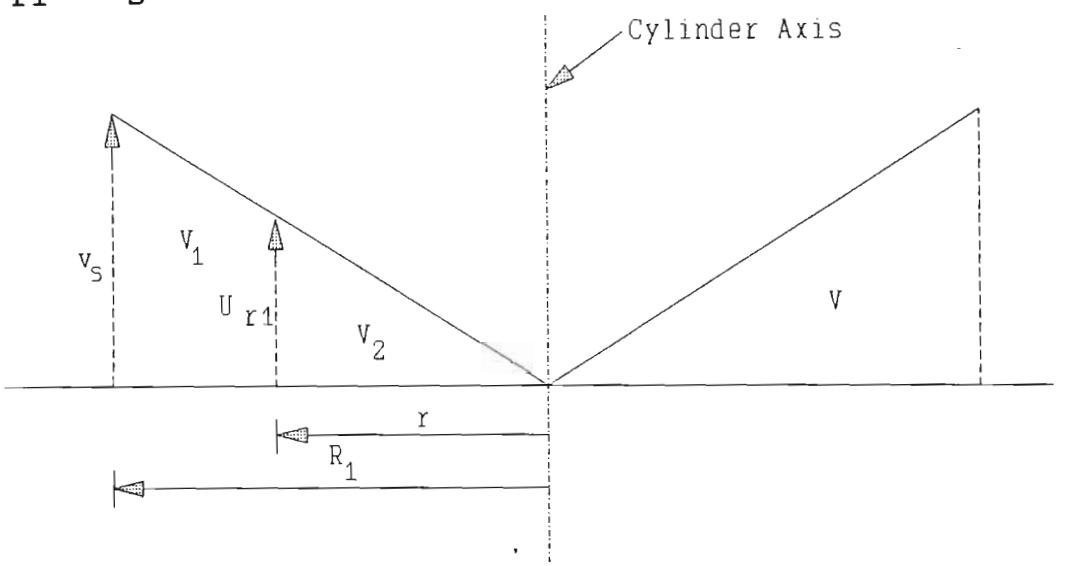

Figure 34 Schematic showing variables for calculating an area-averaged radial velocity for surface 1.

The average velocity components at the side of the bowl consisted of the swirl velocity calculated at the maximum bowl radius and of the radial and axial velocities added together and averaged

assuming they decayed linearly from a maximum at the tip of the bowl to zero at the bottom. This assumption was realistic when compared with published data (Arcoumanis et al., 1983; Fansler, 1985; Arcoumanis et al., 1986).

Surface 3 which represented the piston crown had swirl velocity and squish or radial velocity components. As for surface 1 an area averaged swirl velocity, U_{s3} could be determined. The calculation procedure of average radial velocity, U_{r3} was similar to that for surface 1, however, the final equation was not as simple requiring a procedure such as the Newton-Raphson method to solve the equation. Referring to Figure 35:

$$U_{r3} = \frac{R_2 - r}{R_2 - R_1} . v_s \qquad \text{for } R_1 \leq r \leq R_2 \qquad \text{-----(36)}$$

$$\text{Also} \quad V = \frac{\pi}{3}.(R_1^2 + R_1R_2 + R_2^2).v_s - \pi.R_1^2.v_s \qquad \text{-----(37)}$$

$$\text{and} \quad V_1 = \frac{\pi}{3}.\frac{R_2 - r}{R_2 - R_1}.(R_2^2 + R_2.r - 2r^2).v_s \qquad \text{-----(38)}$$

$$\text{But} \quad V_1 = V_2 = V/2$$

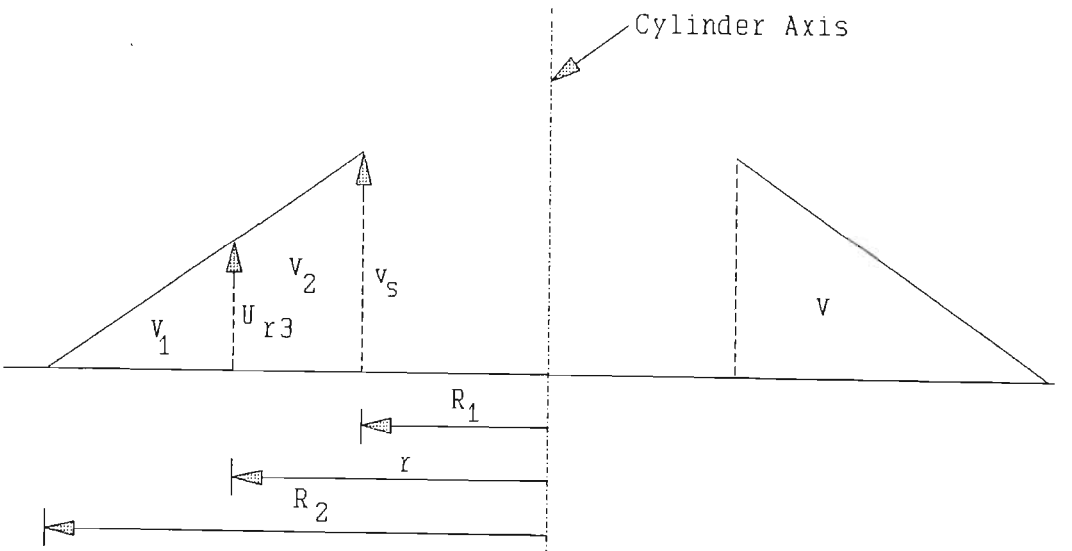

Figure 35 Schematic showing variables for calculating an area-averaged radial velocity for surface 2.

Therefore from equations (37) and (38) the following equation for r can be derived:

$$2r^3 - 6R_2.r^2 + (R_2^3 - 3R_1^2.R_2 + R_1^3) = 0$$

This was a cubic equation for r which was solved using the Newton-Raphson method. The area-averaged radial velocity for surface 3 could then be computed from equation (36).

The liner surface 4 was subjected to a tangential velocity from swirl and an axial velocity which was equal to half the piston velocity on that section of the head above the piston crown. Surfaces 5 and 6 had the same velocity components as the piston crown and the bottom of the cup respectively.

The resultant velocity at each of the six walls could therefore be calculated from the two orthogonal velocity components u_x and u_y determined by the swirl, squish and piston velocities and the turbulence kinetic energy of the volume adjoining the wall. This resultant velocity was then used in the calculation of a skin friction coefficient and the heat transfer coefficient which was used to determine the convective heat transfer rates at each of the six walls.

3.3 Heat Transfer

An important component of the combustion process in compression-ignition engines is the heat transfer which represents a loss of energy reducing the amount of work done on the piston. Heat transfer has to be controlled so as to not only maximise efficiency but also to limit the temperatures to which engine components are exposed. In engines heat losses from the combustion chamber gases are due both to convection and radiation with wall temperatures being governed by conduction.

3.3.1 Convection

The procedure used for determining the convective heat transfer was similar to that of Morel and Keribar (1985) based on a model representing the effects of gas flow. The starting point for this model was the instantaneous heat flux equation:

$$q_c(t,A) = h_c(t,A).[T_{cg}(t,A) - T_w(A)] \qquad \text{-----(39)}$$

where $q_c(t,A)$ = heat flux which varies as a function of time and chamber wall

$h_c(t,A)$ = heat transfer coefficient which varies as a function of time and chamber wall

$T_{cg}(t,A)$ = gas temperature outside the thermal boundary layer which varies as a function of time and chamber wall

$T_w(A)$ = wall temperature which varies as a function of chamber wall but which remains constant within each cycle, except for the liner temperature.

The convective heat exchange between the gases in the combustion chamber and the chamber walls was determined via Reynolds' analogy modified by Colburn. Reynolds first pointed out the similarity between the mechanism of fluid friction in the boundary layer attached to the wall and the transfer of heat by forced convection. The analogy linked the heat transfer across the thermal boundary layer to the flow velocity at the outer edge of the momentum boundary layer (Morel and Keribar, 1985). The analogy applied to a plane surface with laminar or turbulent flow and to turbulent flow in a pipe and was represented by the following relationship:

$$St.Pr^{2/3} = C_f/2 \quad \text{with } 0,5<Pr<100 \qquad \text{-----(40)}$$

where St = Stanton number

and $St = Nu/(Re.Pr) = h/(\rho.U.C_p)$ -----(41)

Nu = Nusselt number

Re = Reynolds' number

Pr = Prandtl's number

h = heat transfer coefficient

U = velocity at outer edge of boundary layer

C_p = specific heat

C_f = skin friction coefficient.

Substituting (41) into (40) and re-arranging:

$$h = (C_f/2).\rho.U.C_p.Pr^{-2/3} \qquad \text{-----(42)}$$

Prandtl's number generally has values in the range 0.6 to 0.8 for the gas in the combustion chamber. The velocity U was determined as the resultant velocity at each wall as detailed earlier in this chapter. The skin friction coefficient in equation (42) was modelled according to Blasius's equation applied to flat plate boundary layers and fully developed pipe flow:

$$C_f = a/Re^{1/4}$$

$$= a.(\rho.U.\delta/\mu)^{-1/4} \qquad \text{-----(43)}$$

where a = constant which has a value of 0.046 in flat plate boundary layers and 0.067 for fully developed turbulent flow in pipes. The mean of these two values was used (Morel and Keribar, 1985).

δ = boundary layer thickness

μ = dynamic viscosity of gas in boundary layer

Equations (42) and (43) required values of ρ,Cp,Pr and μ to be calculated from gas properties at the wall boundary layer temperature. Tables of the thermodynamic and transport properties of air in the CRC Handbook (1986) indicated negligible variation of these properties with pressure in the relevant temperature range. The boundary layer or film temperature was represented as the arithmetic mean between the bulk or free

stream temperature outside the boundary layer and the wall temperature. Regression equations were fitted to the relevant data in the CRC Handbook (1986) for the properties of air and these equations were then used in conjunction with the temperature to calculate the respective properties. It was thus assumed that the gas properties of the boundary layer approximated to those of air.

Morel and Keribar (1985) provided approximations for boundary layer thickness for each of the six walls which were related to geometrical dimensions of the combustion chamber. They stated that these approximations were expected to be adequate as the boundary layer thickness had a weak influence on the calculation of the friction coefficient. The same approximations were used in this model.

The effective or free stream temperature outside the boundary layer was determined with the aid of a two zone combustion model described later in this chapter. A procedure for estimating the wall temperatures via a conduction model is also detailed later in this chapter.

3.3.2 Radiation

The model for radiation was selected so that it would be sufficiently complex so as to take into account fuel properties and equivalence ratio but not so sophisticated as to require substantial computations. A similar model as applied by Callahan et al. (1985) was used. This model was based on work by Kunitomo et al. (1975) subsequently modified by Kamel and Watson (1979). The radiant heat flux was calculated from the well established equation:

$$q_r(t,A) = \epsilon_f(t).\sigma.\{[T_{rg}(t,A)]^4 - [T_w(A)]^4\} \qquad -----(44)$$

where $q_r(t,A)$ = radiation heat flux which varies as a function of crank angle and chamber wall

$\epsilon_f(t)$ = flame emissivity which varies as a function of crank angle

σ = Stefan-Boltzmann constant

$T_{rg}(t,A)$ = radiation temperature which varies as a function of crank angle and chamber wall

$T_w(A)$ = wall temperature as previously defined.

There are two main sources of radiation in the combustion chamber of a diesel engine, soot and certain gases. The flame emissivity represents a combination of these two components. By assuming that the total absorption coefficient was the sum of the absorption coefficients of the gas and soot, Chang and Rhee (1983) derived the equation:

$$\epsilon_f = 1 - (1 - \epsilon_s).(1 - \epsilon_g) \qquad \text{-----(45)}$$

Non-luminous radiation from the combustion gases is mainly due to emission contributions from the tri-atomic molecules of carbon dioxide and water vapour. The total gas emissivity can be calculated from the following approximation:

$$\epsilon_g = 1 - (1 - \epsilon_{CO_2}).(1 - \epsilon_{H_2O}) \qquad \text{-----(46)}$$

Callahan <u>et al</u>. (1985) applied the equations put forward by Kamel and Watson (1979) for evaluating the gas emissivities. For a particular gas i:

$$\epsilon_i = 1 - \exp(-K_i.p_i.L) \qquad \text{-----(47)}$$

where ϵ_i = emissivity of gas i

K_i = mean absorption coefficient of gas i

p_i = partial pressure of gas i

L = mean radiation length.

The mean absorption coefficients for CO_2 and H_2O were calculated using equations from Kamel and Watson (1979) which represented curve fits to graphs presented by Abu-Romia and Tien (1967). Callahan et al. (1985) stated that these equations were only valid for gas temperatures between 800 K and 1950 K:

$$K_{CO_2} = 1,02 - 1,11\left(\frac{T_g}{1000}\right) + 0,422\left(\frac{T_g}{1000}\right)^2 - 0,05368\left(\frac{T_g}{1000}\right)^3$$

$$K_{H_2O} = 0,52 - 0,888\left(\frac{T_g}{1000}\right) + 0,5266\left(\frac{T_g}{1000}\right)^2 - 0,1043\left(\frac{T_g}{1000}\right)^3$$

The partial pressures of the gases at each crank angle increment, $p_i(\theta)$ were computed from the mass fraction of fuel burned, $X(\theta)$, the molar fraction of the respective gas, $y_i(\theta)$ and the total gas pressure $P(\theta)$:

$$p_i(\theta) = X(\theta).y_i(\theta).P(\theta)$$

Callahan et al. (1985) approximated the mean radiation length using the definition proposed by Kunitomo et al. (1975):

$$L = 3,5\ \frac{V(\theta)}{A(\theta)}$$

where $V(\theta)$ = instantaneous volume
$A(\theta)$ = instantaneous surface area of combustion chamber

The procedure used to calculate soot emissivity was the same as developed by Kunitomo et al. (1975) and applied by Callahan et al. (1985). Soot emissivity at atmospheric pressure was related to gas emissivity at atmospheric pressure which was obtained from the following equations of Kamel and Watson (1979):

$$\epsilon_{CO_2} = 0,711(p_{CO_2}.L/100)^{0.333}/(T_g/100)^{0,5} \qquad \text{-----(48)}$$

$$\epsilon_{H_2O} = 0,707(p_{H_2O}.L/100)^{0,6}.(p_{H_2O}/100)^{0,2}/(T_g/100) \qquad \text{-----(49)}$$

where p_{CO_2} and p_{H_2O} = partial pressures, kPa
L = mean radiation length, m
T_g = bulk gas temperature, K.

Callahan et al. (1985) also used the same equations from Kamel and Watson (1979). However, in modifying the constants at the beginning of the two equations to take into account the change in units of the partial pressures from bars, specified by Kamel and Watson (1979), to kPa they made the error of multiplying instead of dividing the existing constant in the first equation by $100^{0,333}$ and the existing constant in the second equation by $(100^{0,6})(100^{0,2})$. This error caused the gas emissivities to be much greater than they should have been.

The total gas emissivity at atmospheric pressure ϵ_{ga} was calculated from equation (46). The soot emissivity at room temperature was obtained from an empirical equation developed by Kunitomo et al. (1975):

$$\epsilon_{sa} = \epsilon_{ga} \cdot \left(\frac{0,09}{\phi_o^2 - \tau^2 + 0,35\tau - 0,38} + 6.8\tau - 5.95 \right) \quad --(50)$$

where τ = specific gravity of the fuel

ϕ_o = effective excess air ratio.

Callahan et al. (1985) provided a graph of the effective excess air ratio versus specific gravity. They indicated that a significant amount of data showed that the effective excess air ratio was fairly insensitive to specific gravity and that more data were required to verify the relationship at higher specific gravities.

The soot emissivity at room temperature in equation (50) was used to calculate a mean absorption coefficient:

$$K_{sa} = -\frac{1}{L} . \log(1 - \epsilon_{sa})$$

Kunitomo et al. (1975) provided an empirical equation for determining the mean absorption coefficient at a given pressure:

$$K_s = K_{sa} \cdot \left(\frac{P}{100}\right)^m$$

where P = total cylinder pressure, kPa

$m = 4{,}95/(\phi_o + 1{,}5) - 0{,}25.$

The soot emissivity at the given pressure was finally determined from the equation:

$$\epsilon_s = 1 - \exp(-K_s L)$$

The flame emissivity in equation (45) could therefore be calculated from the gas and soot emissivities and substituted into equation (44) for computing the heat flux.

The radiation temperature in equation (44) has been represented by researchers with values varying from the adiabatic flame temperature to the bulk gas temperature. The procedure used for this work was based on the model applied by Morel and Keribar (1986) in which the radiation temperature T_{rg} was linked to the average temperature of the burned zone T_b. After the start of combustion up to the point of maximum temperature in the burned zone, $T_{rg} = 0{,}9\ T_b$. This was done by Morel and Keribar (1986) to account for the preferential radiant heat transfer from the soot particles which were thus cooler than the surrounding burned gases. After the point of maximum temperature the radiation temperature was determined from an equation similar to that used by Morel and Keribar (1986):

$$T_{rg} = 0{,}9[T_{b,max} + (T_b - T_{b,max})(\theta - \theta_{max})/(\theta_{EVO} - \theta_{max})] \quad (51)$$

where $T_{b,max}$ = maximum burnt temperature

θ = instantaneous crank angle

θ_{max} = crank angle at $T_{b,max}$

θ_{EVO} = crank angle at EVO

This form of equation was adopted by Morel and Keribar (1986) to account for the fact that due to the fourth power temperature dependence of radiation the effective soot radiating temperature was dominated by the activity burning flame front, the temperature of which was higher than the average of the burned zone. Temperature of the burned zone was affected by the presence of burned-out products and by air entrainment.

Equation (51) causes the radiation temperature to decrease almost linearly from the maximum value to a value close to the bulk gas temperature in accordance with the variations in temperature predicted by Borman and Nishiwaki (1987). This relationship was chosen over that of Morel and Keribar (1986) as the latter relied on a factor which was proportional to the square of the ratio of burnt mass to total mass. In the present model the ratio of burnt mass to total mass does not reach a value of one thus causing the radiation temperature at the tail end of combustion to be higher than the bulk gas temperature. Nevertheless the calculation of T_{rg} in equation (51) is still linked to the variation of T_b.

The same wall temperature values as for the convective heat transfer calculation were applied in equation (44). Hence the radiative heat transfer combined with the convective heat transfer provided the total heat transfer to be used in the calculation of fuel energy release rates. However, it was necessary to provide representative wall temperatures in the final calculation of both these heat transfer mechanisms with the aid of a heat conduction model.

3.3.3 Conduction

The objective in formulating a conduction model was to provide temperatures at each of the six designated surfaces in the combustion chamber that were of the right order of magnitude and that were linked to the operating conditions. The latter conditions included engine speed, load, coolant and oil

temperatures. However, it was also important to provide a relatively simple model generating an output with acceptable accuracy.

Holman (1986) indicated that, even though the thermal conductivities of materials varied with temperature, over a range of 100 to 200°C the variation was not great, being of the order of 5 to 10%, and there was justification in assuming constant values to simplify problem solutions. However, determination of accurate convective heat transfer coefficients particularly in an engine for use in determining combustion chamber surface temperatures can pose a problem. These coefficients play an important role in the calculations particularly in the case of the gas-to-wall coefficient.

After studying published results of temperature distributions in the combustion chamber components certain guidelines were established for preparing a conduction model. First of all the combustion chamber was divided into the three main components of piston, liner and cylinder head. The inlet and exhaust valves were treated as being part of the head and the conditions in the head were adjusted to account for temperature differences that would be caused by the valves and ports, particularly the exhaust valve which is generally at a somewhat higher temperature than the cylinder head. The heat transfer through each of the three components was assumed to be one-dimensional and steady state and was represented by resistance networks as shown in Figure 36. The resistance network at each one of the six surfaces consisted of two thermal resistances representing the gas-to-wall convection resistance in the combustion chamber and the combined conduction and convection resistance from the wall through to either the coolant in the case of the liner and head or the oil in the case of the piston.

Morel and Keribar (1985) adopted the heat resistance network approach but divided the components into a number of smaller elements as shown in Figure 37. Eleven individual surfaces in

the cylinder were specified. Figure 38 shows the variation in temperatures at each of these surfaces for four different swirl and piston bowl combinations ENG1, ENG2, ENG3 and ENG4 in the same engine. The temperatures of the head surfaces for the baseline engine ENG2 with a high swirl and a bowl diameter to bore diameter ratio of 0,67 tended to be very similar in magnitude to the piston temperatures while the liner temperatures were approximately 100 K lower.

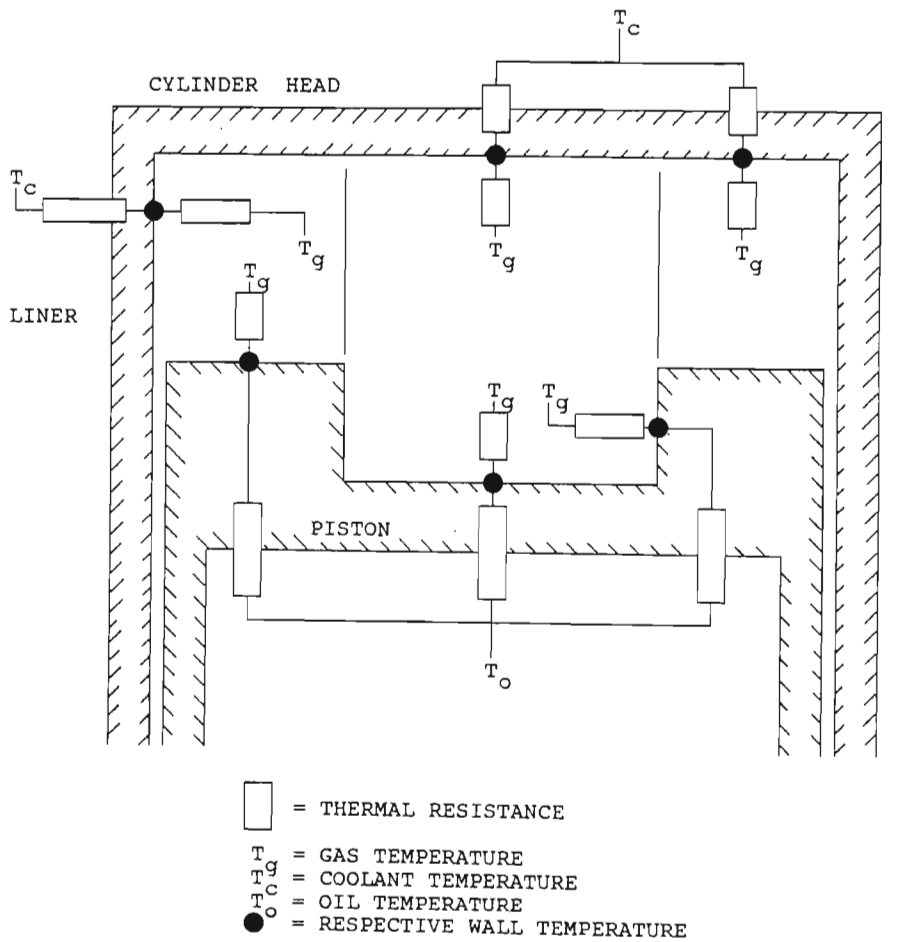

Figure 36 Schematic of the one-dimensional steady state heat conduction model with resistance networks.

Calculation of the wall temperatures from the thermal resistance network in Figure 36 was governed by the average bulk gas temperature, the average gas-to-wall heat transfer coefficient at each wall, a thermal resistance characterised for each wall and influenced by material properties and dimensions, and finally

the coolant or oil temperature. It was possible to measure the coolant and oil temperatures on the engine. The average bulk gas temperature and average gas-to-wall heat transfer coefficient were calculated via an iterative process from the complete model. The thermal resistance for each wall was the most difficult variable to specify with an acceptable level of accuracy. These variables were eventually established after studying temperature distributions for similar engine configurations published by Woschni (1979), Woschni and Fieger (1979), Haddad and Watson (1984), Morel et al. (1985) and Morel and Keribar (1985). In addition the measurements of surface temperature that were carried out in this project provided a further guideline.

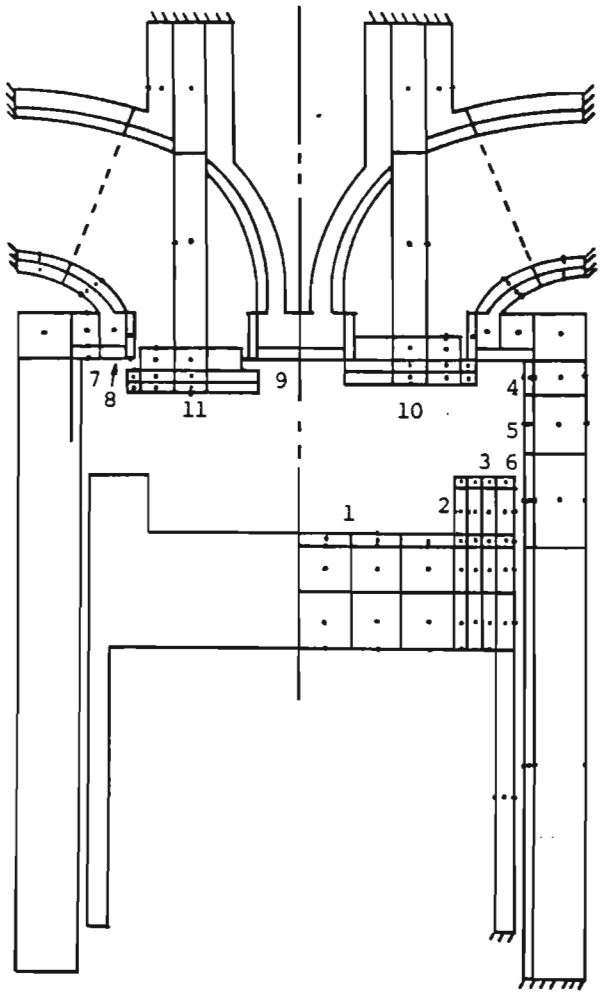

Figure 37 Schematic of heat conduction network elements for a bowl-in-piston geometry with chamber surfaces numbered (Morel and Keribar, 1985).

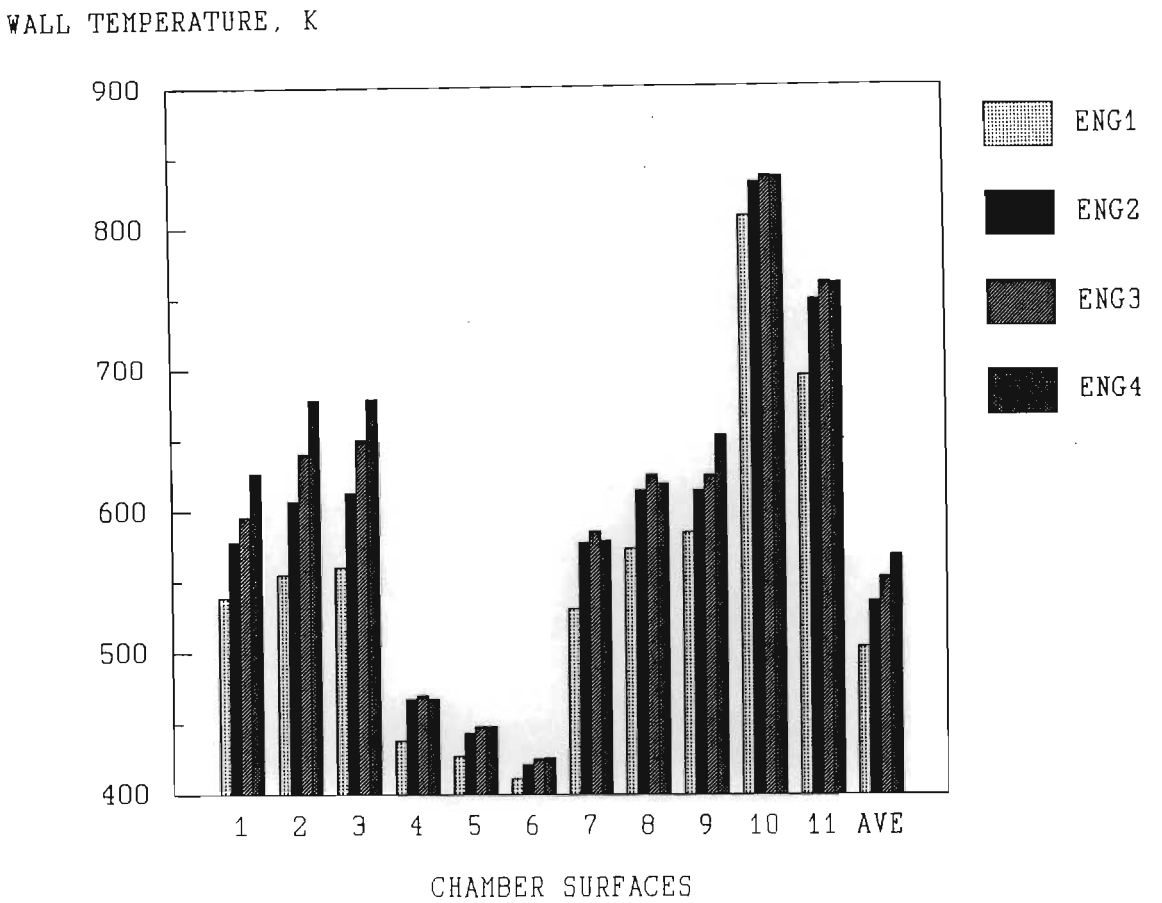

Figure 38 Variation of the wall temperature at each of the 11 walls demarcated by Morel and Keribar (1985) for four different swirl and piston bowl combinations in the same engine.

The liner wall temperature could not be assumed to be the same for any piston position as the temperature could be expected to decrease from a maximum at the head side where maximum combustion temperatures occurred to approximately the coolant temperature at BDC. Adopting a similar approach to Taylor et al. (1989) thermal loading data from Haddad and Watson (1984) providing the variation of the gas-to-wall heat transfer coefficient and gas temperature with piston to head clearance were used to determine a regression equation for the variation of wall temperature with piston-to-head clearance based on the maximum wall temperature and coolant temperature. It was assumed that the wall temperature at BDC was equal to the coolant temperature. The

maximum wall temperature was determined from the average gas temperature and gas-to-wall heat transfer coefficient assuming one-dimensional steady state heat conduction through the liner.

The regression equation for the wall temperature, T_w was:

$$\frac{T_w - T_c}{T_{wm} - T_c}.100 = 98{,}08408 - 5{,}79013\ C + 0{,}155267\ C^2 - 0{,}00176\ C^3 + 0{,}00000\ C^4$$

where C = percentage of maximum piston to head clearance.

T_c = coolant temperature, K

T_{wm} = wall temperature at the top of the liner, K.

Figure 39 shows the resulting variation of wall temperature with piston to head clearance. The shape of the curve was in good agreement with temperature distributions presented by Woschni (1979) and Yoshimitsu, Toyama, Sato and Yamaguchi (1984). To calculate the average temperature of the wall exposed to the chamber from the head to a point level with the piston at any point in the cycle, the wall temperature was integrated over that length and then divided by that length.

The typical procedure that was presented by Borman and Nishiwaki (1987) for obtaining steady-state wall surface temperatures was adopted for this work. For the engine run under motored conditions, the first step was to calculate a time averaged bulk gas temperature using the Ideal Gas Law for the whole cycle. It was assumed that the gas temperature outside of the period when both valves were closed was equal to the inlet temperature at IVC. An appropriate assumption was then made for a starting value for the global time-averaged heat transfer coefficient. From the average gas temperature and heat transfer coefficient in addition to a suitable thermal resistance it was possible to provide initial estimates of the six wall temperatures by using the thermal resistance networks in Figure 36.

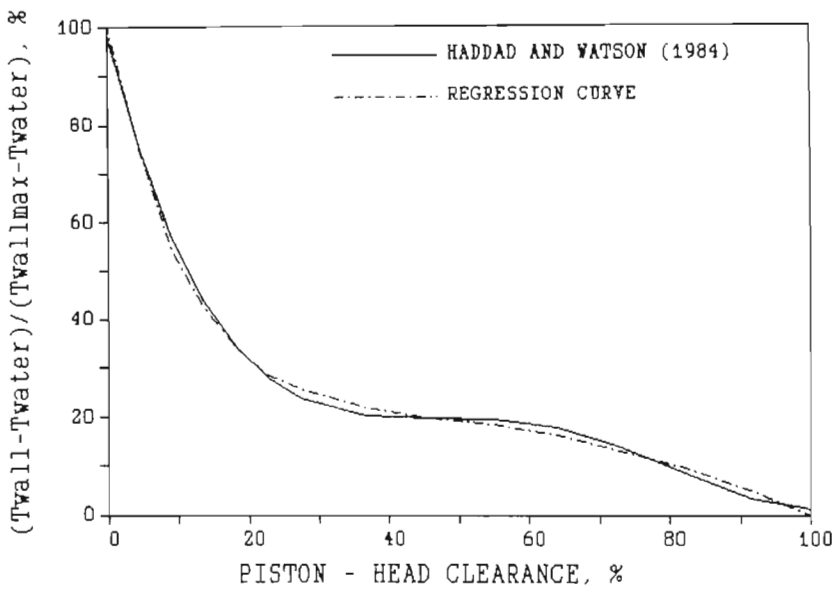

Figure 39 Percentage change in liner wall temperature relative to the wall temperature at the top of the liner and coolant temperature versus percentage of maximum piston-to-head clearance.

With these wall temperatures the full simulation including the calculation of convective heat transfer from the gas flow characteristics was executed. The time averaged heat transfer coefficients for each wall were then determined in addition to an average bulk gas temperature which took into account heat transfer. Again the heat transfer coefficient at IVC was assumed to apply over the cycle excluding the period from IVC to EVO.

The wall temperatures were re-calculated with the revised and more realistic gas temperature and heat transfer coefficients and the model was re-executed. It was generally found that one iteration was sufficient to achieve an acceptable level of accuracy.

A similar procedure to the above was adopted for the fired engine tests. Appropriate starting values for the wall temperatures were provided and the heat transfer coefficients for each wall surface were calculated between IVC and EVO. The remainder of

the cycle was represented by the heat transfer coefficient at IVC. Hence average heat transfer coefficients could be calculated. As the contribution to the average heat transfer coefficient from the radiative component was relatively small it was not included in the calculations. Hence only the convective heat transfer coefficient was taken into account. The inlet temperature at IVC was used to indicate the chamber temperature from TDC at valve overlap through to IVC and exhaust temperature was assumed from EVO to TDC at valve overlap. An average gas temperature could then be determined for the complete cycle. These values in conjunction with coolant and oil temperatures provided a first estimate of wall temperature. The model was then re-executed and the wall temperatures calculated a second time. It was generally found that no further iterations were necessary.

3.4 Two-Zone Combustion Model

A quasi-dimensional burnt zone model based on the model formulated by Morel and Keribar (1985) was developed for this analysis. An existing single zone model founded on the Krieger-Borman equation that had been applied by Faletti et al. (1982) and Taylor (1987) was modified to generate a burnt zone volume and to take into account the flow-based convective heat transfer and radiation heat transfer. The thermodynamic cycle code in this model supplied the mass of the burned gases and the bulk gas temperature. Then from the ideal gas law:

$$P_b.V_b = m_b.R_b.T_b \qquad \text{-----(52)}$$

$$P_u.V_u = m_u.R_u.T_u \qquad \text{-----(53)}$$

$$P_t.V_t = m_t.R_t.T_t \qquad \text{-----(54)}$$

where P = pressure, kPa
V = volume, m^3
m = mass, kg
R = gas constant, kJ/kg.K

T = temperature, K

subscript b = burnt zone

u = unburnt zone

t = total cylinder contents

Pressure and the gas constant were assumed to be the same throughout the cylinder. Hence $R_b = R_u = R_t$ -----(55)

and $P_b = P_u = P_t$ -----(56)

Also $m_b + m_u = m_t$

and $V_b + V_u = V_t$

From equations (52), (53) and (54) it can be shown that:

$$T_t = \frac{P_t \cdot V_t}{m_t \cdot R_t} = P_t \cdot \left(\frac{V_u + V_b}{m_t \cdot R_t}\right)$$

$$= P_t \cdot \left(\frac{m_u \cdot R_u \cdot T_u / P_u + m_b \cdot R_b \cdot T_b / P_b}{m_t \cdot R_t}\right)$$

Simplifying with equations (55) and (56):

$$T_t = (m_u \cdot T_u + m_b \cdot T_b)/m_t$$

Hence $T_b = (m_t \cdot T_t - m_u \cdot T_u)/m_b$

Substituting for m_u and re-arranging:

$$T_b = T_u + (T_t - T_u)/(m_b/m_t) \qquad \text{-----(57)}$$

The bulk gas temperature T_t in equation (57) was obtained from the thermodynamic cycle code. The temperature of the unburnt zone T_u was generated from a sub-model relying on the First Law of Thermodynamics and taking into account heat transfer from the burnt zone to the unburnt zone. The ratio of the instantaneous burnt mass of gas to the total mass of gas in the cylinder , m_b/m_t was determined by tracking the production of CO_2 specified as one of the species in the gas mixture and comparing it to the total mass of CO_2 that would have been generated under stoichiometric conditions. The derivation of the final equation

used for the mass ratio is supplied in Appendix B. The burnt volume V_b could then be determined from equation (52). The derivations of the equations that were necessary to determine the geometry of the burnt zone from a given burnt volume are provided in Appendix C. The resulting third order equations were solved by the Newton-Raphson method.

The fixed geometry of the burnt volume permitted the calculation of the surface area at the interface between the burnt and unburnt zones. This surface area, the temperature difference between the two zones and an adjustable constant representing a gas-to-gas heat transfer coefficient were used in the calculation of heat transfer from the burnt to the unburnt zone. The constant was adjusted so that the peak temperature of the burnt zone did not exceed the adiabatic flame temperature.

The temperatures and masses of the burnt and unburnt zones as well as the geometry of the burnt zone were used in the calculation of the convective and radiation heat transfer components. Following a similar procedure to that of Morel and Keribar (1985) a convective temperature, T_{cg} was calculated for each of the regions shown in Figure 31 from the following equation:

$$T_{cg} = T_u.(1 - m_b/m_t) + T_b.m_b/m_t$$

Assuming uniform density in the burnt and unburnt zones, volume can be substituted for mass. Then,

$$T_{cg} = T_u.(1 - V_b/V_t) + T_b.V_b/V_t$$

The instantaneous burnt and unburnt volumes for each of the two piston positions shown earlier in Figure 27 could be determined once the geometrical shape of the total burnt volume had been fixed. For the first case where the burnt volume was confined to the cup and the space directly above the cup, the temperature in the clearance volume above the piston crown coincided with the

unburnt temperature as would be expected. Therefore for surfaces 1,2 and 6:

$$\frac{m_{b1}}{m_{t1}} = \frac{V_{b1}}{V_{t1}}$$

where subscript b1 = burnt zone in region 1
t1 = total zone in region 1

For surfaces 3,4 and 5:

$$m_b = 0 \text{ and hence } V_b = 0$$

Therefore $T_{cg} = T_u$.

When the burnt volume expanded into the clearance volume above the piston crown the convective temperature for surfaces 3, 4 and 5 was no longer the unburnt temperature but was determined by the volume of the burnt zone which extended into region 2.

For surfaces 3, 4 and 5:

$$\frac{m_{b2}}{m_{t2}} = \frac{V_{b2}}{V_{t2}}$$

where subscript b2 = burnt zone in region 2
t2 = total zone in region 2.

For surfaces 1, 2 and 6:

$$\frac{m_{b1}}{m_{t1}} = \frac{V_{b1}}{V_{t1}}$$

and $V_{b1} = V_b - V_{b2}$.

These volume ratios could therefore be used with the burnt and unburnt temperatures to calculate the convective temperatures for regions 1 and 2.

The radiation temperature, T_{rg} as indicated earlier was calculated from an equation involving the maximum and instantaneous temperatures of the burnt zone, T_b and $T_{b,max}$ and a ratio varying from 0 to 1 based on the variation of crank angle.

Within the combustion model a number of iterations were performed to achieve acceptable accuracy in the computation of T_u at each crank angle. Hence all the variables that were dependent on the calculation of T_u had to be recalculated after each iteration until convergence was reached.

After linking all the sub-models and checking that each model output was of the right order of magnitude, the next and final steps that remained were the calibration and verification of the model.

4. CALIBRATION AND VERIFICATION

One of the most difficult aspects in developing a combustion model made up of several sub-models was the verification of the output from the model. A number of assumptions were made either to simplify the model or because presently there was insufficient knowledge to provide less empirically based relationships for different events occurring in the complex combustion process.

In order to establish a model which is able to generate reliable and consistent results it is imperative that each of the sub-models, particularly those incorporating empirical constants, be examined critically and calibrated with experimental data. The combined effect of these sub-models must also be analysed in detail before a researcher can apply the model with confidence knowing its limitations.

The output from certain parts of the model, namely the gas flow sections in this project was compared to published data. However, the actual heat transfer calculations were compared with data collected during the project. In addition, an energy balance of energy input computed from the heat released against the energy input from the measured fuel delivery was applied to verify the complete model.

4.1 In - Cylinder Gas Velocities and Heat Transfer

The heat transfer characteristics in the model relied heavily on the gas flow regime and therefore as a starting point it was necessary to check the validity of the swirl and squish velocities and the turbulence intensity and calibrate empirical constants where necessary.

Three sets of published data were selected for these purposes. As the swirl and squish flow model was the same as applied by Murakami et al. (1988) their data were used to check for errors that may have been made in implementing the relevant equations.

The other sets of data used were those of Johnston et al.(1979) and Morel and Keribar (1985). Once again, because a similar procedure to Morel and Keribar (1985) was applied which often made use of the same equations, it was appropriate to compare model outputs where possible. The data of Johnston et al.(1979) were used for verification of the model in the same way as Morel and Keribar (1985).

4.1.1 Swirl and squish flow

Murakami et al. (1988) presented graphs of angular momentum contributions from wall friction, from viscous shear between volumes and from squish flow between volumes. As indicated earlier they divided the chamber into two volumes consisting of an inner cylindrical volume of radius equal to the cup and an outer volume making up the remaining portion above the piston crown. The curves were generated for a standard piston configuration with a compression ratio of 13:1 and for an engine speed of 1000 r/min. By adopting the same engine configuration and equations governing the flow characteristics good agreement with the angular momentum flux curves of Murakami et al. (1988) was obtained except in the case of the viscous torque. The resulting differences in the computation of the swirl ratios are illustrated in Figure 40 for both volumes. It was found that by doubling the angular momentum transmission by viscous shear, excellent agreement with the swirl ratios of Murakami et al. (1988) was obtained as shown in Figure 41.

The initial discrepancy in viscous torque had a significant effect on swirl ratio for both volumes in the middle sections of the compression and expansion strokes as indicated in Figure 40. The reduced viscous shear resulted in the swirl velocity of the inner volume not being reduced as much as it should have been by the lower swirl velocity of the outer volume. Similarly the swirl velocity of the outer volume was less than it should have been as its rotational speed had not been increased by its viscous link with the faster rotating inner volume.

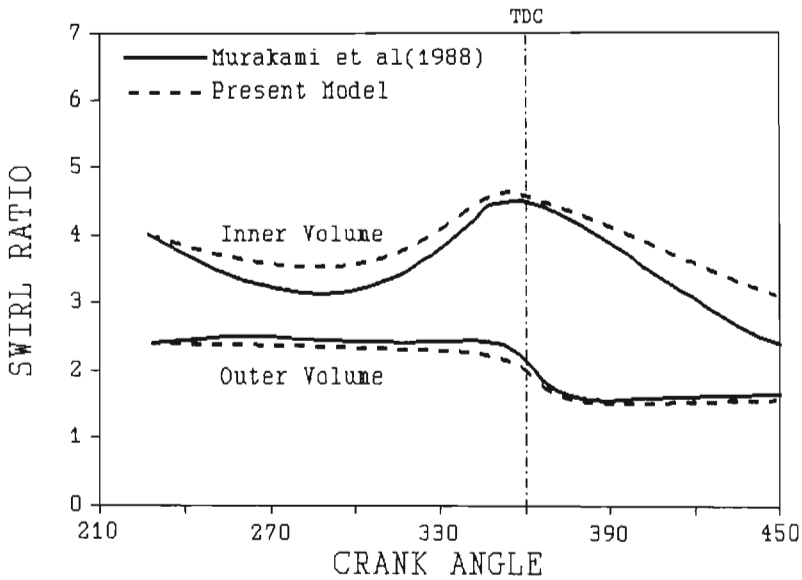

Figure 40 The variation of swirl ratios with crank angle for the inner and outer volumes compared to the swirl ratios obtained by Murakami et al. (1988) at 1000 r/min.

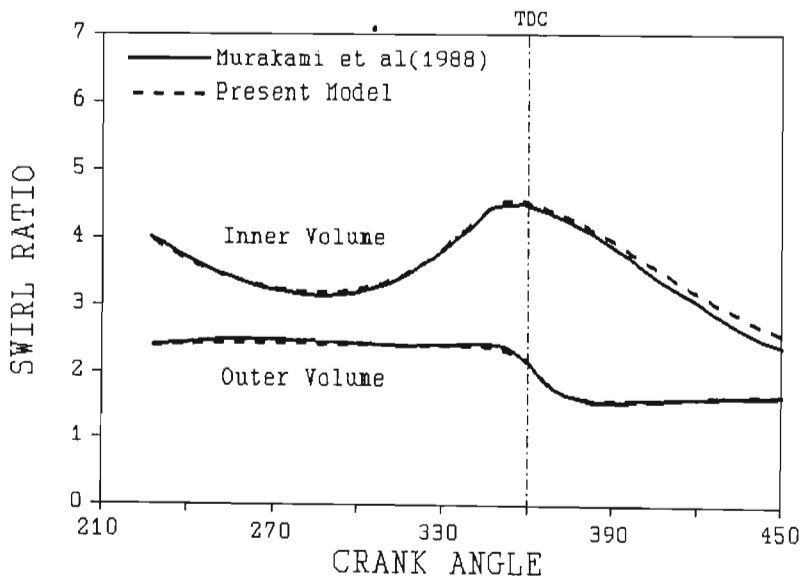

Figure 41 The variation of swirl ratios with crank angle for the inner and outer volumes with the viscous torque doubled as compared to the swirl ratios obtained by Murakami et al. (1988) at 1000 r/min.

The remaining small differences between curves in Figure 41 can be attributed to differences in assumed temperature and pressure conditions which affect the density and viscosity of the air in the chamber. As specified by Murakami et al. (1988) the corrective coefficient ß detailed earlier representing an adjustable friction factor was set equal to two for both the inner and outer volumes in generating the swirl ratios in Figures 40 and 41.

Having obtained good agreement with the results of Murakami et al. (1988) the results of Morel and Keribar (1985) were used as an independent check. The swirl equation applied by Morel and Keribar (1985) also involved angular momentum changes but applied to three volumes instead of two. The inner volume specified by Murakami et al. (1988) was divided further by Morel and Keribar (1983) into a volume corresponding to the bowl and the volume above the bowl. The equations also took into account squish effects and viscous friction as well as intake and exhaust flux of angular momentum thus accounting for events during the intake and exhaust strokes in addition to compression and expansion.

Morel and Keribar (1985) provided sets of graphs for one particular engine configuration and operating condition which was established as the baseline case. The engine modelled was a turbo - charged direct injection unit with a displacement of 2 L/cylinder operating at 1800 r/min and 1517 kPa IMEP. The combustion chamber had a compression ratio of 14,8, bore/stroke ratio of 0,92 and piston cup diameter/bore ratio of 0,67. The cup contained 88% of the chamber volume at TDC.

Because of the difficulty of simulating the actual combustion and the resulting pressure development, comparisons were made with the data of Morel and Keribar (1985) using data generated under motored conditions. The turbocharger on the baseline engine produced a bulk gas temperature, T_2 at IVC of 485 K. Assuming atmospheric air temperature, T_1 = 25°C, barometric

pressure P_1 = 100 kPa and compressor efficiency e_c = 60% and applying the following equation from Goering (1986):

$$T_2/T_1 = 1 + [(P_1/P_2)^{0,286} - 1]/e_c,$$

the resulting inlet manifold pressure P_2 was approximately 300 kPa giving a pressure ratio of three. Bulk gas temperature was adjusted to be the same as the unburned zone temperature given by Morel and Keribar (1985) in one of their graphs. All subsequent comparisons with the model of Morel and Keribar (1985) were based on these values.

Apart from a small relative increase in cylinder mass from the injected fuel and changes in the viscosity of the chamber contents with the increased bulk gas temperatures from combustion, the gas velocity characteristics generated from the two models were expected to be comparable. Figure 42 shows the swirl ratios for the inner and outer volumes respectively for the two models. Regions II and III specified by Morel and Keribar (1985) had similar swirl ratios as would be expected. For simplifying comparisons with the flow model of Murakami et al. (1988) the swirl ratios for the two regions were averaged to represent the inner volume.

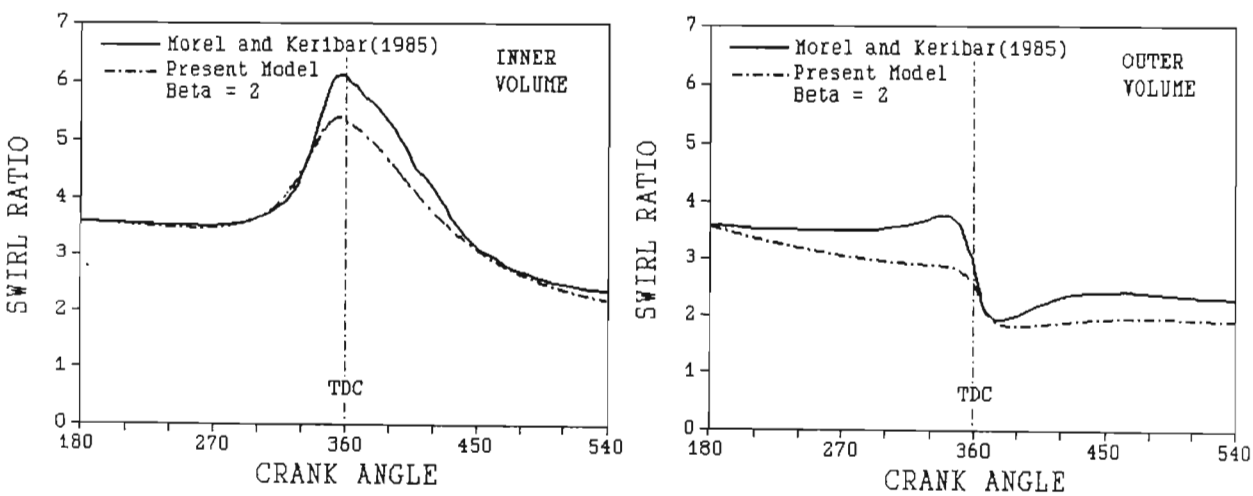

Figure 42 The variation of swirl ratios with crank angle from the present model compared to the swirl ratios obtained by Morel and Keribar (1985) at 1800 r/min.

The swirl ratios for the inner volume in Figure 42 compare very favourably. The deviation close to TDC can be attributed to injection and combustion in the curve of Morel and Keribar (1988). The fuel injected before TDC increases the density of the chamber contents and hence the angular momentum transportation from the outer volume to the inner volume. This change increases the swirl velocity of the inner volume.

The swirl ratios for the outer volume in Figure 42 differ substantially with the curve of the present model decaying at a marked rate. The increase in speed from 1000 r/min for the engine of Murakami et al. (1988) to 1800 r/min for the engine of Morel and Keribar (1985) was then examined as a possible factor contributing to the difference. However, Figure 43 shows that an increase in speed from 1000 r/min to 1800 r/min increases the swirl ratio only slightly.

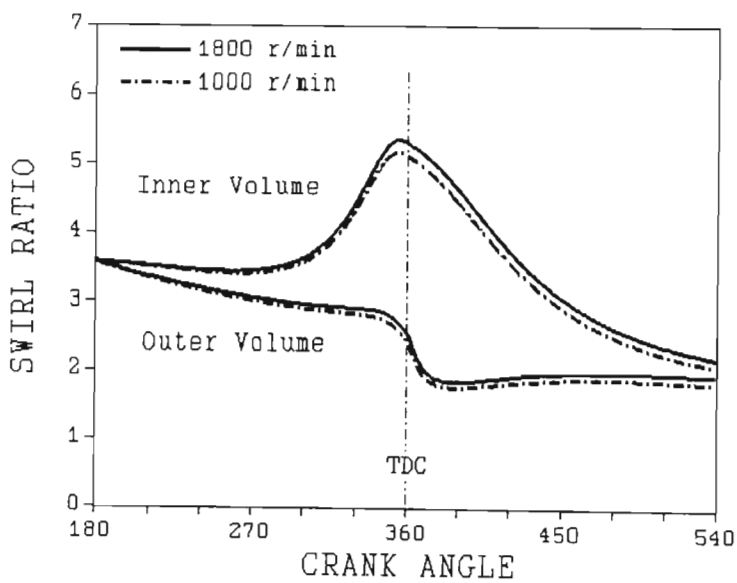

Figure 43 The variation of swirl ratio in the inner and outer volumes for two different speeds applied to the baseline engine of Morel and Keribar (1985).

The discrepancies in Figure 42 suggested that a different corrective coefficient for each volume should be examined. In order to determine a suitable ß for the outer volume, the

validation procedure used by Morel and Keribar (1985) was adopted. They selected a set of measured data from Johnston et al. (1979) obtained from an engine with pancake combustion chamber geometry and compression ratio of 5,4. The swirl ratio at 160°BTDC was extremely high being 18,25 because of the tangential intake valve used. Morel and Keribar (1985) stated that, because of the high initial swirl value, the percentage swirl decay during compression and expansion caused by wall friction would also be high, thus providing an ideal situation for model testing.

Morel and Keribar (1985) computed the maximum tangential swirl velocity at the wall to represent the maximum velocity measured by Johnston et al. (1979). This value provided approximately equal initial momentum for the calculation and for the experiment. Figure 44 shows the swirl ratios generated by Morel and Keribar (1985) compared to the experimental data of Johnston et al. (1979). In applying the present model to the same engine it was necessary to decide how to specify the inner and outer volumes for the flat piston arrangement. Murakami et al. (1988) found that, from the tangential velocity distribution obtained experimentally from a flat piston geometry, a boundary between the volumes could be drawn on the radii of 60% to 70% of cylinder radius. They subsequently used 65% for the flat piston arrangement in their work. Morel and Keribar (1985) did not specify the boundary directly although for this particular verification they mentioned the assumption of a linear velocity profile increasing from zero at the centreline to a maximum at the wall.

In keeping with the recommendations of Murakami et al. (1988) a boundary at 65% of cylinder radius was used to generate the swirl velocity in the present model for the engine of Johnston et al. (1979). Figure 45 shows the curve published by Morel and Keribar (1985) and the curves generated by the present model. The corrective coefficient ß was initially set equal to two and then decreased to one to reduce the viscous torque. The latter

setting provided results which corresponded fairly closely to the curve of Morel and Keribar (1985) and hence to the measured data of Johnston et al. (1979).

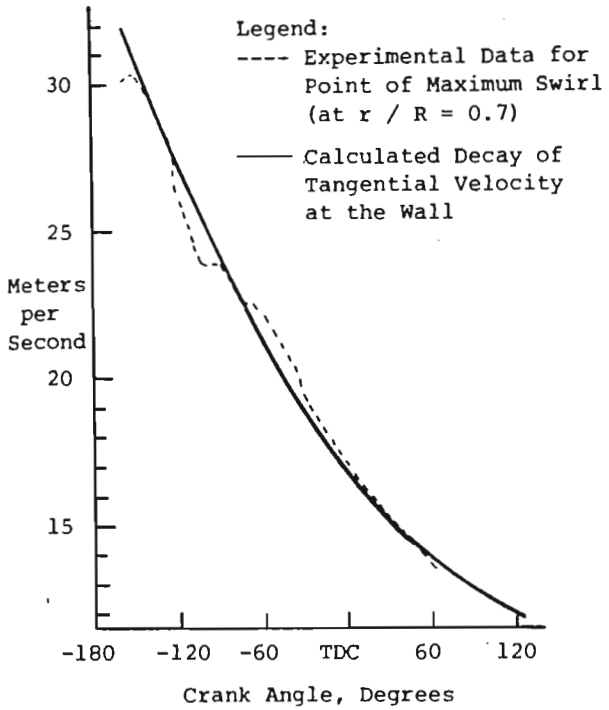

Figure 44 The variation of swirl ratio measured by Johnston et al. (1979) for a pancake combustion chamber compared to the model output of Morel and Keribar (1985).

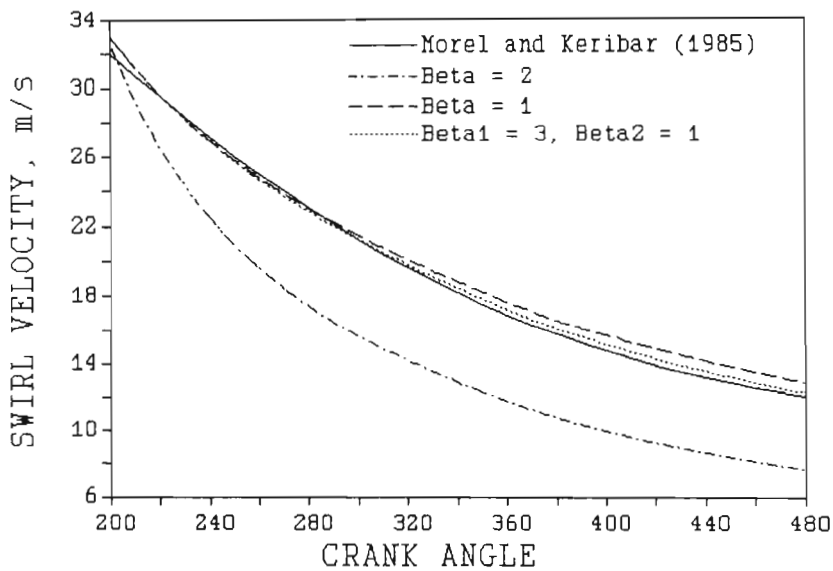

Figure 45 The swirl ratios from the present model with different convective coefficients applied to the engine of Johnston et al. (1979) compared to the model output of Morel and Keribar (1985).

Murakami et al. (1988) had achieved good agreement between their model and experimental data using ß = 2. Decreasing ß to one resulted in a substantial increase in swirl ratio for both volumes because of the effective decrease in wall friction as shown in Figure 46. A comparison with the curves of Morel and Keribar (1985) using ß = 1 showed much better agreement with the outer volume angular velocity but poor agreement with the inner volume. The effect of using different corrective coefficients for each volume was then investigated. Murakami et al. (1988) concluded that for the inner volume, the value of ß lay between 0 and 1 while for the outer volume the range was 2 to 4. This latter range specification contradicted the measured swirl values of Johnston et al. (1979). It also appeared that, in order to offset the higher swirl ratio of the inner volume a larger ß was required implying a greater wall friction. Figure 47 shows the effect of specifying $ß_1 = 3$ for the inner volume and $ß_2 = 1$ for the outer volume. Apart from a slightly higher swirl ratio at the peak for the inner volume the curves follow very closely.

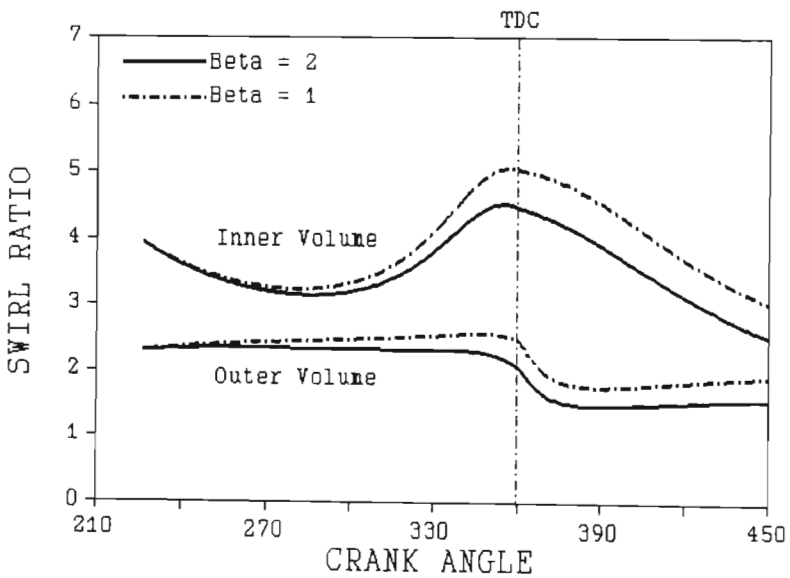

Figure 46 The swirl ratios with two different corrective coefficients for the standard engine of Murakami et al. (1988).

In the case of the outer volume there is some deviation over most of the compression and expansion strokes. The deviation is a maximum close to TDC, however, Murakami et al. (1988) were not able to record data close to TDC to validate this section of the model. A direct comparison of this new curve with the experimental data suggests reasonable agreement.

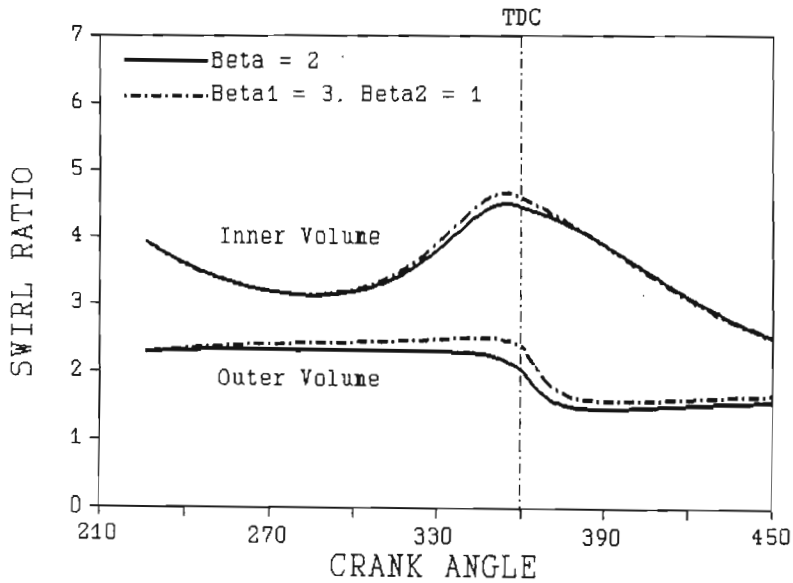

Figure 47 The swirl ratios with different corrective coefficients for the inner and outer volumes for the standard engine of Murakami et al. (1988).

Application of the same values of β_1 and β_2 to the flat piston engine of Johnston et al. (1988) provided a curve in much closer agreement with the curve of Morel et al. (1985) as shown earlier in Figure 45. Applying $\beta_1 = 3$ and $\beta_2 = 1$ to the engine of Morel and Keribar (1985) yielded the curves shown in Figure 48. Once again fairly good agreement was achieved and it was concluded that the values of $\beta_1 = 3$ for the inner volume and $\beta_2 = 1$ for the outer volume should be used for further applications.

On the basis of the good agreement obtained between the present model and the experimental data from the two very different engines of Johnston et al. (1979) and Murakami et al. (1988) as well as the output from the relatively sophisticated model of Morel and Keribar (1985), it was concluded that the swirl ratios

that were being generated by the present model were sufficiently accurate to provide a reliable foundation for the calculation of convective heat transfer. This model also provided a useful tool for investigating the effects of varying combustion chamber geometry on the gas flow processes.

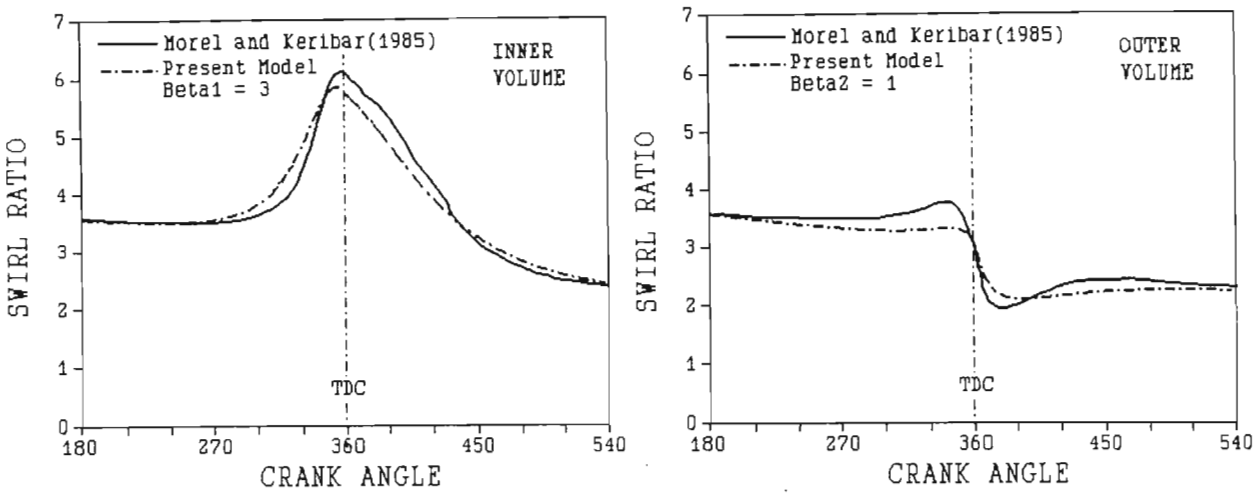

Figure 48 The swirl ratios with corrective coefficients $\beta_1 = 3$ and $\beta_2 = 1$ as compared to the model output of Morel and Keribar (1985).

4.1.2 Turbulence intensity

The achievement of an absolute indication of turbulence intensity via modelling is impossible without extensive measurements in the engine on both a spatial and temporal basis to verify the model. However, for this work it was important that acceptable trends and orders of magnitude were reflected in the output of the model rather than the attainment of accurate turbulence intensities.

If the turbulence intensities in the vicinity of each of the six walls was examined in conjunction with the mean velocities generated by swirl and squish and piston velocities at these walls, certain expected trends could be predicted as the piston approached TDC. The flow effects close to TDC were of particular concern as these had a significant bearing on the peak heat transfer rate. The model of Morel and Keribar (1985) produced

a prominent peak in turbulence intensity within the bowl at TDC due to kinetic energy of injection and of squish motion leaving the clearance space between the piston crown and head (see Figure 9). The turbulence in this latter space was first reduced by increased viscous dissipation caused by the small clearance and then increased with the reversed squish. Turbulence generation due to compression caused the rise in turbulence intensity during the compression stroke. The predictions of Assanis and Heywood (1986) also showed this increase, however, there was no second peak close to TDC reflecting the increased turbulence in the cup from squish (see Figure 49).

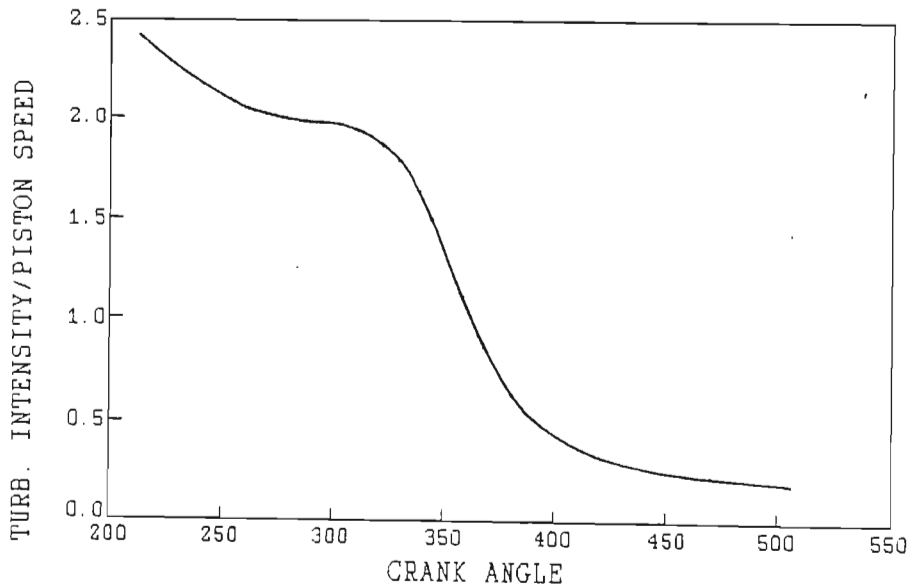

Figure 49 Predictions of the variation of non-dimensional turbulent intensity over the duration of the compression and expansion processes (after Assanis and Heywood, 1986).

The measurements by Fansler (1985) of turbulence indicated that as the squish and swirl flows reached their maximum velocities, the rms fluctuations representing turbulence at the radii close to the side of the cup showed a sharp peak. Nearer the centre of the cup this peak was considerably less pronounced but still present. Moving axially from the cup entrance to the bottom of the cup Fansler (1985) measured a decrease in turbulence close to TDC (see Figure 50).

Further examination of Figure 50 shows no evidence of the increase in turbulence due to compression which Morel and Keribar (1985) generated with their models in the range of 280 - 350°CA. Rao and Bardon (1985) mentioned that measurements by different investigators did not consistently support this phenomenon.

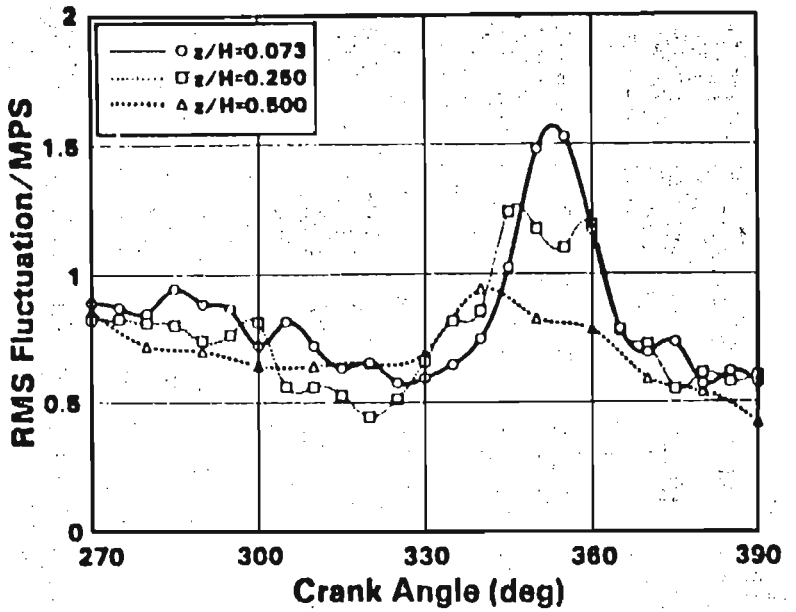

Figure 50 Ensemble-averaged rms velocity fluctuations/mean piston speed measured at distances of 7,3%, 25% and 50% of the bowl depth from the cylinder head and at a radius equal to 80% of the bowl radius. Engine speed = 600 r/min (Fansler, 1985)

With reference to the problem of providing a starting value for turbulence at IVC, Hayder et al. (1985) cited the expressions used by Grasso and Bracco (1983) which related the initial values of turbulence kinetic energy and its dissipation rate to the engine speed in r/min and volumetric efficiency, e_v:

$$k = A.e_v^2.(rpm)^2$$

$$\epsilon = B.e_v^3.(rpm)^3$$

where A and B = dimensional empirical constants.

Hayder et al. (1985) modified these expressions by assuming that the initial turbulence intensity was proportional to a characteristic intake velocity and introduced an explicit initial

reference length scale based on the maximum open intake area. The final equations also included chamber cross-sectional area, crank angle of intake opening and mean piston speed.

It was evident from these approaches to determining initial turbulence values that mean engine speed and a parameter reflecting the average intake air velocity should be considered in formulating a suitable equation for turbulence at IVC. In order to obtain an indication of the range of turbulence intensities that could be expected at IVC in practice a study of published, measured and modelled values was carried out. The results are assembled in Table 1. As can be seen both flat pistons and bowl-in-piston configurations were examined as, at IVC, the bowl has very little effect on the generation of turbulence.

Turbulence models such as those of Morel and Keribar (1985) and Davis and Tabaczynski (1988) determined turbulence kinetic energy during the intake stroke based on port and valve geometry and lift, flow rates and discharge coefficient. These same factors are used to determine swirl ratio at IVC. It is therefore proposed that turbulence intensity should be a function of swirl ratio at IVC and mean piston speed. The swirl ratio is governed by the intake characteristics while the mean piston speed combines engine stroke and speed.

After an examination of the turbulence intensity values and their variation with other variables the following dimensionally correct expression was formulated for turbulence intensity, TI:

$$TI = \frac{\sqrt{(MPS.TV)}}{2} \quad , \text{ m/s} \qquad \text{-----(58)}$$

where MPS = mean piston speed, m/s

TV = tangential velocity in the cylinder at bore diameter and at IVC, m/s.

From Table 1 it can be seen that equation (58) provides values of the right order of magnitude in most cases although the value predicted for the engine of Morel and Keribar (1985) is approximately half their modelled value. However, Morel and Keribar (1985) did not verify their modelled values directly with measurements.

In spite of the differences obtained between equation (58) and the actual values in Table 1 it was concluded that this equation provided credible values for turbulence intensity at IVC. In addition the portion of the engine cycle of greatest importance was close to TDC with both valves closed. For this period it had been shown that the generation of turbulence was largely independent of the starting value at IVC being primarily determined by engine geometry (Hayder et al., 1985; Arcoumanis and Whitelaw, 1987).

Table 1 Modelled and measured turbulence intensities for different engines and conditions

Ref.	Measured/ Modeled	Piston Type	Stroke (m)	Bore (m)	Comp. Ratio	Engine Speed (r/min)	MPS (m/s)	Swirl Ratio	ITV (m/s)	MTV (m/s)	ITI (m/s)	ETI (m/s)	MTI (m/s)
1	Model	Flat	0.0794	0.096	9	1500	3.97	1.5	11.3	11.5*	3.8	3.35	2.62
1	Model	Flat	0.0794	0.096	9	1500	3.97	1.9	14.3	14.4*	2.5	3.76	2.15
2	Meas.	Flat	0.083	0.076	5.4	460	1.273	18.25	33.4	33.4*	1.97	3.26	0.7
3	Model	BIP	0.144	0.133	14.8	1800	8.64	3.6	45.1	77**	20.2	9.88	29.5
4	Meas.	BIP	0.11	0.125	16	1000	3.67	3.4	22.2	24.4**	2.9	4.5	5.1
4	Meas.	BIP	0.11	0.125	16	1000	3.67	2.1	13.7	13.3**	2.9	3.54	3
5	Meas.	BIP	0.108	0.0984	11	600	2.16	1.41	20.4	16.3**	1.81	3.32	3.79
5	Meas.	BIP	0.108	0.0984	11	300	1.08	2.81	10.2	8.15**	1.31	1.65	1.23

BIP = bowl-in-piston
MPS = mean piston speed
ITV = tangential gas velocity calculated at bore diameter and at IVC
MTV = maximum tangential velocity in the cylinder after IVC
* - Tangential velocity calculated at bore diameter
** - tangential velocity calculated at bowl diameter
ITI = turbulence intensity at IVC
ETI = turbulence intensity at IVC estimated from equation (58)
MTI = maximum turbulence intensity in the cylinder after IVC
Ref. 1 - Davis and Tabaczynski (1988)
2 - Johnston et al.(1979)
3 - Morel and Keribar (1985)
4 - Saito, Daisho, Ushida and Ikeya (1986)
5 - Fansler (1985)

The selection of published data to verify the turbulence model was very limited. Researchers such as Fansler (1985) and Saito, Daisho, Uchida and Ikeya (1986) had published experimental data for turbulence within the bowl. However, owing to the problem of the confined space at TDC no measurements in the zone above the piston crown had been performed.

While the model applied in this present study was based on the models of Borgnakke et al. (1981), Davis and Borgnakke (1982), Belaire et al. (1983), Davis et al. (1984) and Davis and Tabaczynski (1988), none of these researchers provided suitable results for calibrating or validating the present model. Hence the results of Morel and Keribar (1985) were used as they had provided curves representing turbulence in the region above the piston crown as well as the bowl. While their curves were generated from a model, the general trends and relative magnitudes of turbulence were representative of what was expected in practice.

The present model required the adjustment of the two constants, C_3 and C_4 governing the magnitude of turbulence production from squish and the initial dissipation rate. Using the same baseline engine of Morel and Keribar (1985) that was discussed earlier in this section the two constants were adjusted until reasonable agreement was achieved in terms of trends and relative magnitudes. The starting value for turbulence intensity used in this comparison was calculated from equation (58) and therefore was somewhat lower than the value obtained by Morel and Keribar (1985). However, it was not clear from the contents of their paper as to how they calculated the turbulence intensity from the turbulent kinetic energy. For the purpose of the present study the turbulent kinetic energy was determined from the turbulence intensity using the relationship $k = 3(TI)^2/2$ representing three dimensional kinetic energy.

To circumvent this discrepancy in starting values, the turbulence intensity output from the present model was multiplied by a

constant which then provided identical starting values for turbulence intensity. Figure 51 shows the output from the model against the curves of Morel and Keribar (1985). The constant C_4 was given a value of three which resulted in fairly close agreement between the curves during the early stages of the compression stroke.

For turbulence generation in the inner volume of the cylinder constant C_3 was set equal to one. Figure 51 shows that the turbulence intensity starts to rise earlier than the curve of Morel and Keribar (1985) as TDC is approached. The peak value of turbulence is also lower than that of Morel and Keribar (1985) and the subsequent rate of decay in turbulence is less. However, the model of Morel and Keribar (1985) was applied to a fired engine and included a term for production of turbulence from injection. Some of the terms were also influenced by gas properties. These factors would cause greater turbulence just after TDC as illustrated by the position of peak turbulence in Figure 51.

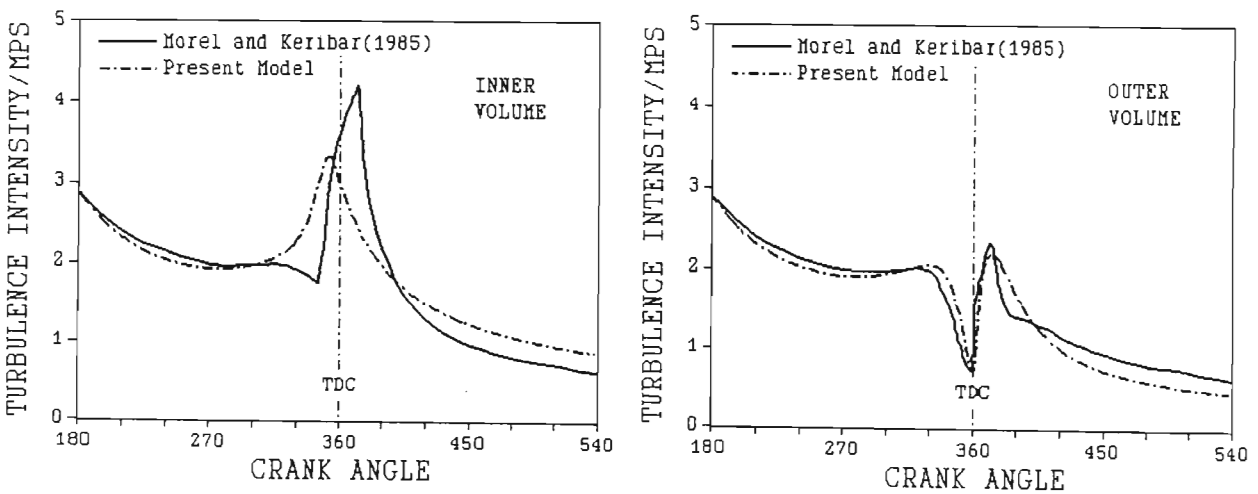

Figure 51 The variation of non-dimensional turbulence intensity for the present model compared to the model output of Morel and Keribar (1985).

In the case of the volume above the piston crown, setting C_3 equal to one resulted in the turbulence after TDC being somewhat lower than obtained by Morel and Keribar (1985). As this region is largely unaffected by turbulence from injection it was decided that C_3 should be increased to achieve better agreement between the two curves. It was found that a value of three provided approximately the same peak of turbulence from reverse squish as illustrated in Figure 51.

It was noticed in the implementation of the model that the term k^2/L^2 in equation (32) for the dissipation rate that was originally applied by Morel and Keribar, was largely responsible for the significant drop in turbulence in the piston crown region as TDC was approached. In Figure 51 the small rise in turbulence during the compression stroke for the outer volume is the result of turbulence production from compression. This effect cannot be seen in Figure 51 for the inner volume as the turbulence production from squish starts to dominate from a point earlier on in the compression stroke. This dominance of turbulence from squish induced velocity fluctuations is in agreement with the measurements of Fansler (1985) and Saito et al. (1986).

From the results obtained and illustrated in Figure 51 it was concluded that the model of turbulence was generating turbulence levels with acceptable trends and magnitudes. It was also necessary to take into account the difficulties of measuring turbulence intensity accurately and with adequate spatial resolution when using published data for verification purposes. From Table 1 it can be seen that the maximum turbulence intensity is generally less than 40% of the maximum tangential velocity. In the case of the measured intensities for the bowl-in-piston engines the maximum turbulence intensity was of the order of 1/4 of the maximum tangential velocity measured at the bowl lip. Hence it was concluded that, while the contribution of turbulence was significant in relation to the other velocity components, it did not dominate the resultant velocities.

4.1.3 Resultant velocities

Having achieved an acceptable level of accuracy for the squish and swirl velocities and having generated turbulence intensities of the right order of magnitude and with the correct trends, the next step was to combine the velocity components to obtain a resultant at each of the six walls in the combustion chamber demarcated previously in Figure 30. The velocities at each wall were examined to assess the validity of their trends and relative magnitudes. In addition these resultant velocities were compared directly with those that were generated from the model of Morel and Keribar (1985). Figure 52 shows the radial and tangential velocities, turbulence intensity and resultant velocity adjacent to each wall, again for the baseline engine used by Morel and Keribar (1985). From these graphs it can be seen that the swirl velocity plays the dominant role for all the walls with squish and turbulence contributing to a small but significant extent. Figure 53 shows the resultant velocities at the walls in contact with the inner volume of the chamber and the outer volume respectively.

All three curves for the inner volume in Figure 53 exhibit the prominent peak close to TDC indicating the strong influence of the swirl velocity which is at a maximum on the side of the bowl. The double peak for walls 2 and 6 is caused by the squish velocity. The effect of squish is more pronounced for wall 6 as the squish velocities are more intense in the vicinity of the head while experimental data indicate that the squish flow does not penetrate all the way down the side of the bowl (Brandl et al., 1979; Fansler, 1985). Hence the resultant velocity in the bottom of the bowl is unaffected by squish.

For the walls surrounding the outer volume, namely, the piston crown, liner and cylinder head, the velocity profiles are also dominated by the swirl velocity. As expected the squish and reverse squish velocities affect the resultant velocity for the

piston crown and the cylinder head, and the swirl velocity at the liner is greater than that for the piston crown and head.

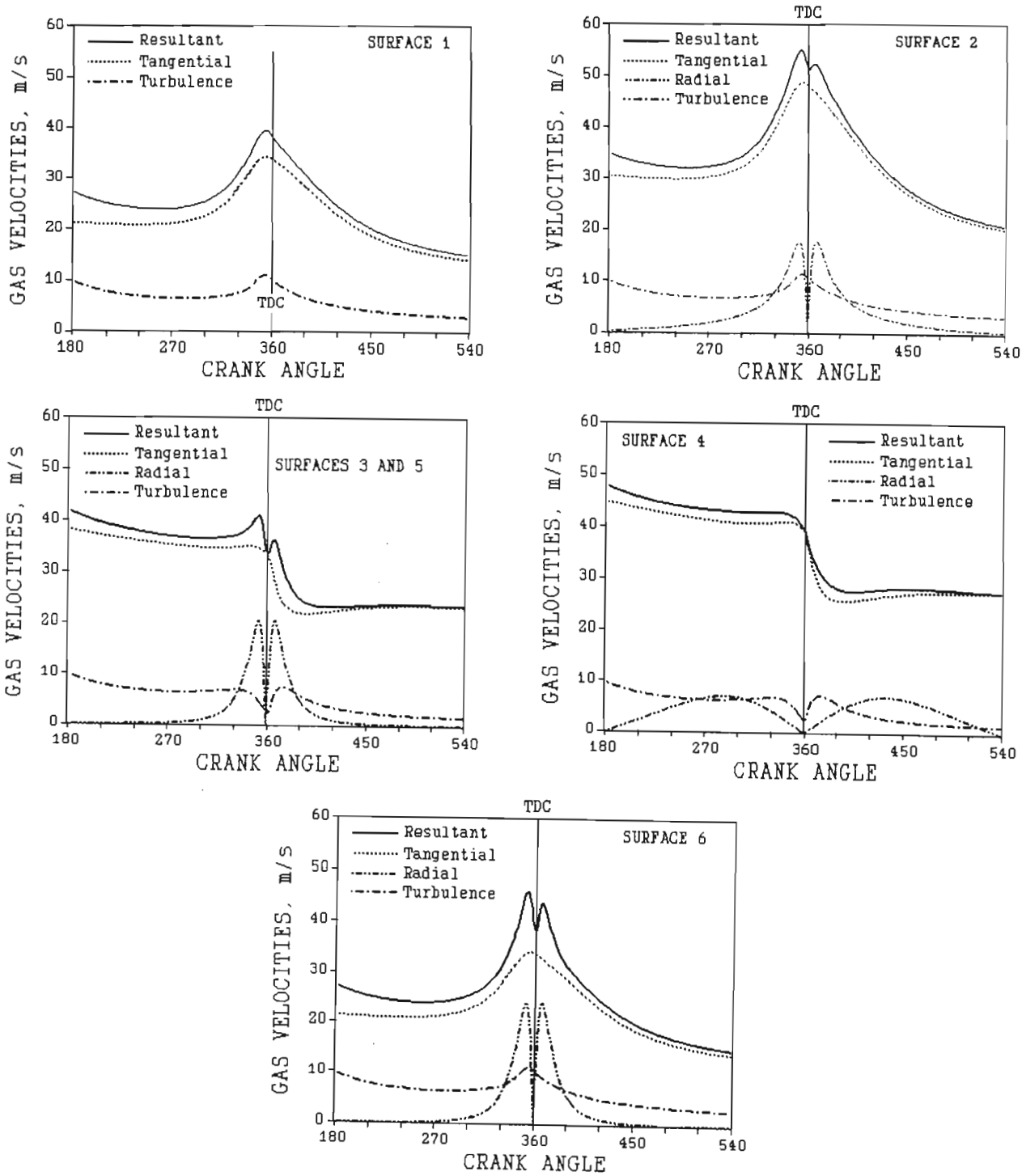

Figure 52 The area-averaged tangential velocities, turbulence intensity and resultant gas velocity adjacent to the six surfaces.

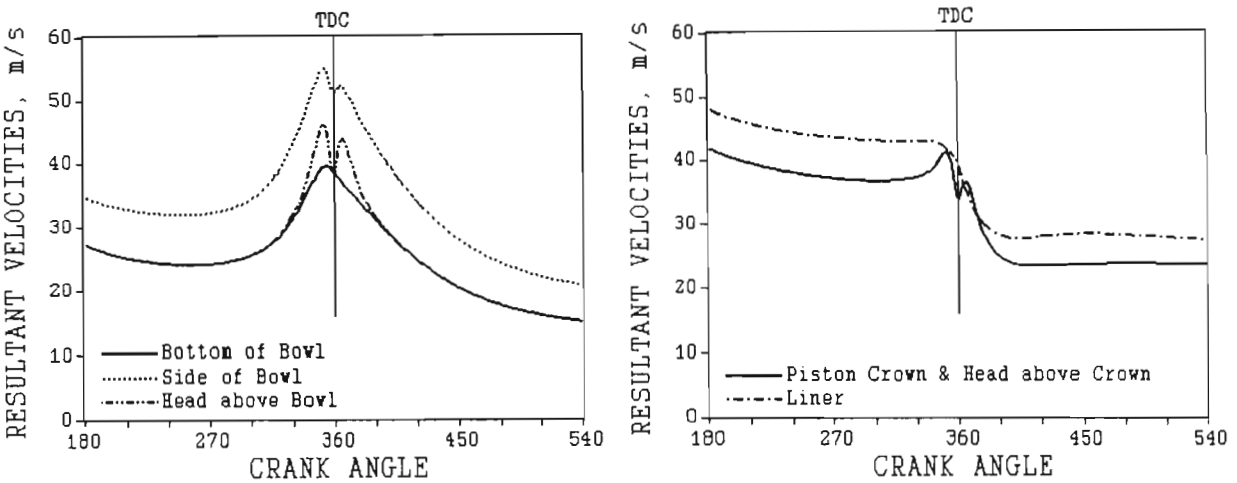

Figure 53 The resultant velocities adjacent to the chamber surfaces surrounding the inner and outer volumes

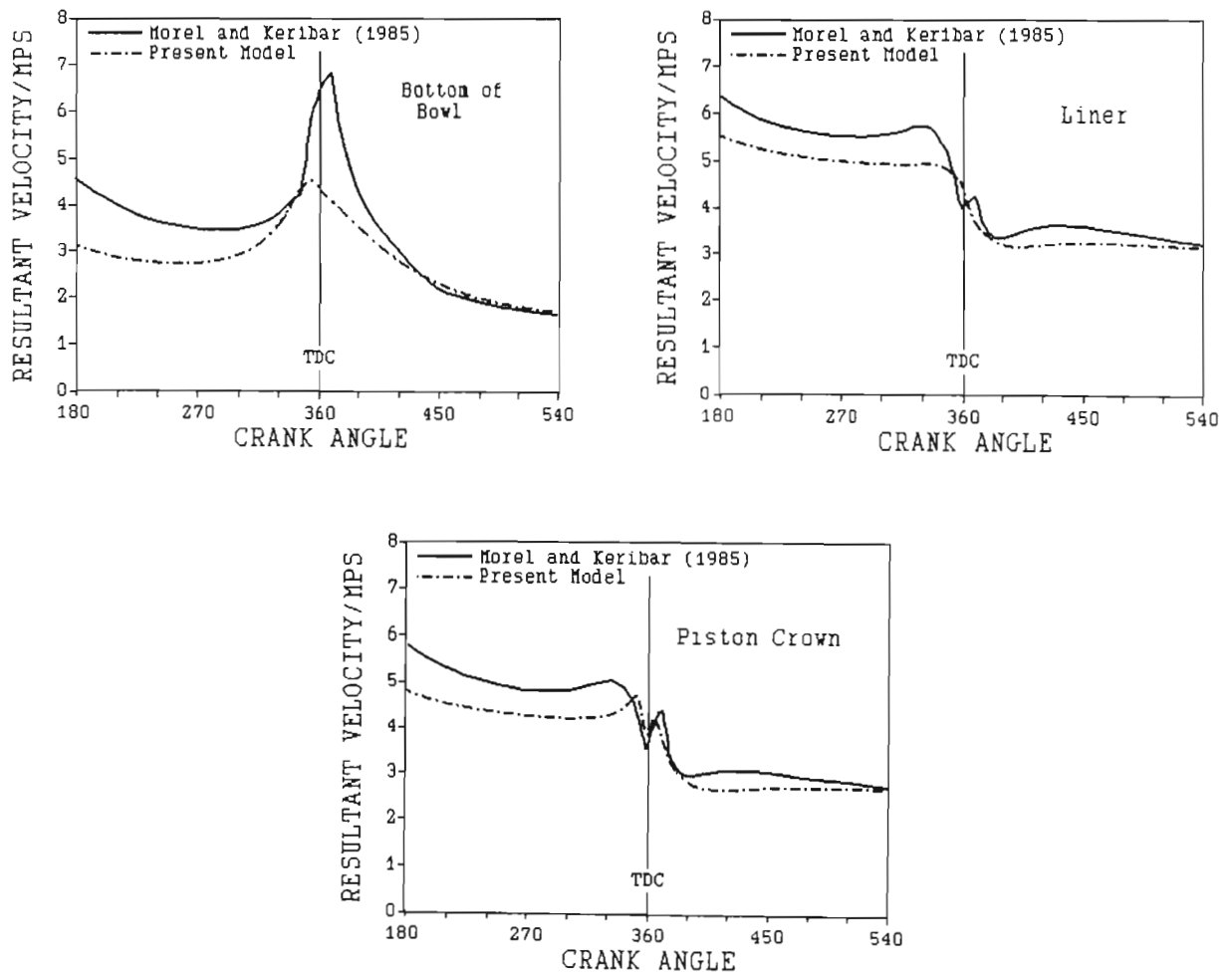

Figure 54 The area-averaged resultant velocity at the bottom of the bowl, piston crown and liner compared to the model output of Morel and Keribar (1985).

Comparisons with the model output of Morel and Keribar (1985) show some significant differences as illustrated in Figure 54 for the bottom of the piston bowl, the piston crown and the liner. The main reason for these differences is a lower turbulence intensity from the present model. The graph of Morel and Keribar (1985) for the bottom of the bowl shows a much more substantial peak close to TDC owing to a greater contribution to the resultant velocity from turbulence. However, the model of Morel and Keribar (1985) takes into account the effects of injection and combustion which have not been included in the present model. In addition the turbulence intensity at IVC in the model of Morel and Keribar (1985) is greater thus causing the discrepancy shown in all three figures during the compression stroke.

As TDC is approached in the graphs for the piston crown and the liner in Figure 54 there is fairly good agreement between the curves. The resultant velocity at the liner given by Morel and Keribar (1985) suggests a small contribution from turbulence as a result of reversed squish. From the velocities illustrated in Figure 52 for surface 4 it can be seen that if the magnitude of turbulence was amplified it would begin to affect the resultant velocity. However, on the basis of the published results from actual measurements of turbulence shown in an earlier section the magnitude of turbulence intensity shown in Figure 52 for surface 4 is realistic.

4.1.4 Friction and heat transfer coefficients

The convective heat transfer coefficient is a function of the skin friction coefficient, resultant gas velocity and gas properties in the boundary layer as indicated in the formulation of the model. The friction coeficient in turn is a function of Reynolds number and therefore is also determined by the resultant velocity as well as a boundary layer thickness and gas properties in the boundary layer. Values for the friction coefficient were published only by Morel and Keribar (1985) as no other

researchers appeared to have used the Colburn analogy for heat transfer. Therefore comparisons of the present model output were made with the modelled results of Morel and Keribar (1985).

As the calculation of the friction coefficient and the heat transfer coefficient relied on the evaluation of gas properties in the boundary layer it was necessary to predict the film temperature in the layer based on the average difference between the wall temperature and the gas temperature. This comparison was carried out assuming motored conditions once again. Representative values for wall temperatures were applied in the calculation of film temperature.

In calculating the gas properties as functions of temperature it was particularly important to determine a correct gas density as this variable in conjunction with the resultant velocity had considerable influence on both the friction coefficient and on the heat transfer coefficient. Figure 55 for the friction coefficient at the bottom of the cup, piston crown and liner respectively shows the curves of Morel and Keribar (1985) and the output from the present model. As can be seen good agreement between the curves was achieved particularly in the case of the piston crown. The differences can be attributed to an initial difference in resultant velocities during the compression stroke and then changes in gas properties due to combustion as well as differences in resultant velocities. It can be concluded from these graphs that both the magnitudes and the trends in the friction coefficient are acceptable.

The convective heat transfer coefficient was then determined for the engine of Morel and Keribar (1985). Figure 56 shows the variation of the area-averaged heat transfer coefficient with crank angle for the present model and for that of Morel and Keribar (1985). Good agreement between the curves was achieved for the compression stroke, the discrepancy in the expansion stroke being the result of combustion.

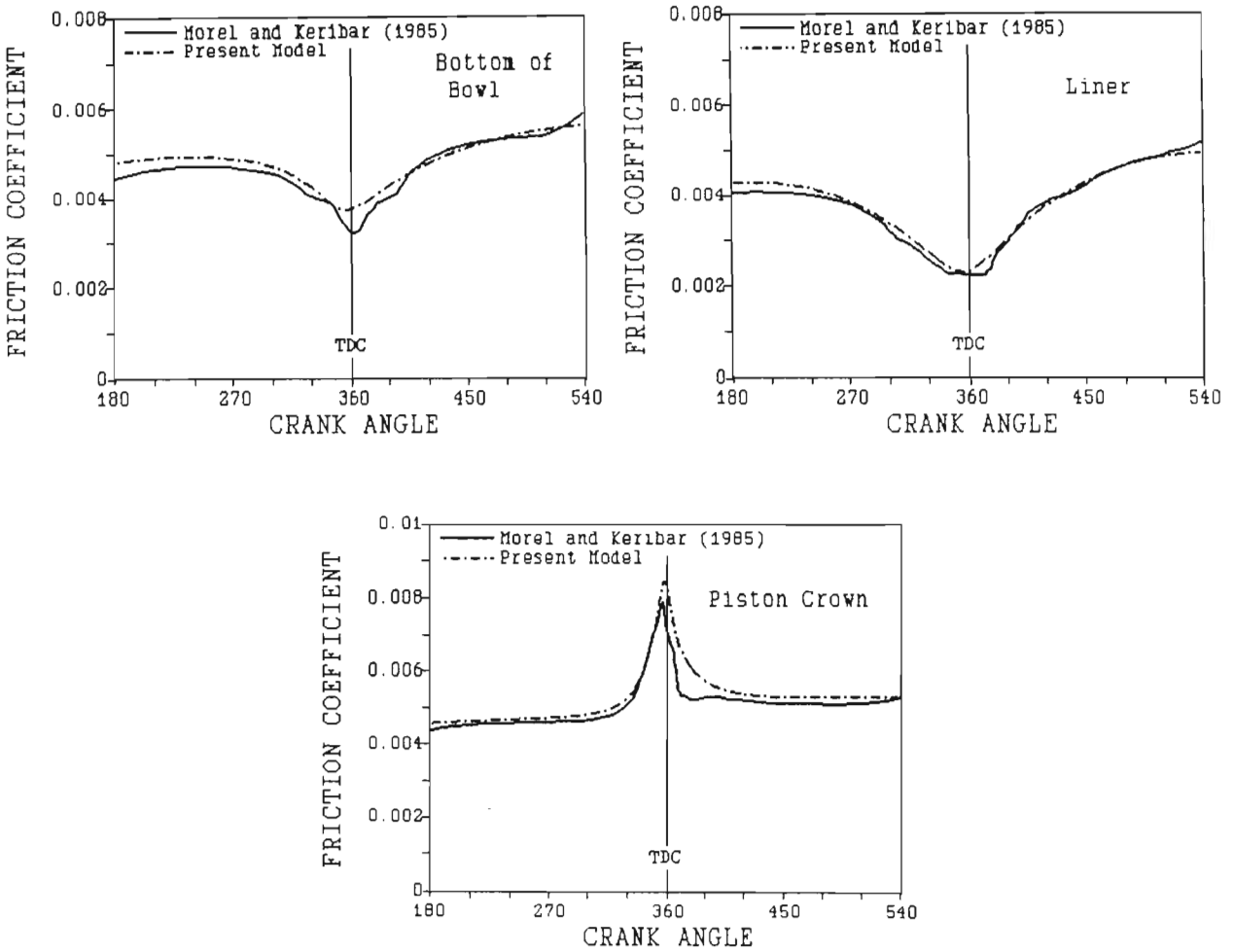

Figure 55 The friction coefficient for the bottom of the bowl, piston crown and liner compared to the model output of Morel and Keribar (1985).

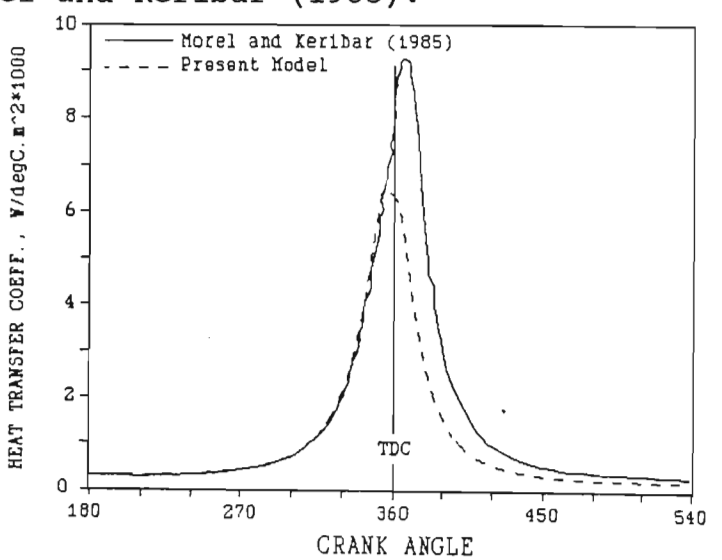

Figure 56 The area-averaged convective heat transfer coefficient compared to the model output of Morel and Keribar (1985).

4.2 Engine Tests

Verification of the model necessitated the use of published data and the collection of new heat transfer data. Published data were used primarily to compare with the gas flow predictions from the model. As the model was diagnostic in nature it was difficult to rely on published data to verify the heat transfer predictions without being able to generate the actual combustion pressure conditions in the cylinder. Apart from measurements of cylinder pressure, a heat flux probe was used to monitor variations in surface temperature which were then converted into heat flux. The probe and the data processing techniques were developed by Taylor et al. (1989) and for this work remained the same except where indicated in the text. The engine test facility that was used in this project was developed within the Department of Agricultural Engineering at the University of Natal, Pietermaritzburg and was housed in the laboratories of the Department. The instrumentation and equipment were reliable and accurate, having been checked, calibrated and used in many projects in the Department.

4.2.1 Equipment and instrumentation

The data were obtained from a four-cylinder naturally aspirated ADE 236 engine with specifications and geometry listed in Table 2. All the dimensions including the piston crown-to-head clearance at TDC and the compression ratio were based on actual measurements in the engine. The engine was mounted on a test bed with a conventional cooling system and was loaded by an AW dynamometer which provided the measurement of torque. Fuel consumption was determined from a batch fuel flow system and air flow rate into the engine was measured accurately with the aid of a parabolic orifice at the air inlet in conjunction with a surge chamber to eliminate pulsations. Steady state temperatures that were measured on the engine included oil temperature, coolant temperature, exhaust temperature and inlet air temperature, which was monitored close to the inlet valve.

Table 2 Specifications and geometry of the ADE 236 engine

Engine	ADE 236 Naturally aspirated Direct injection
Number of cylinders	4
Compression ratio	16,41:1
Bore (m)	0,0985
Stroke (m)	0,127
Connecting rod length (m)	0,224
Piston bowl diameter (m)	0,061
Average piston bowl depth (m)	0,0188
Piston crown - head clearance (m)	0,0008

The number one cylinder of the engine was instrumented with a Kistler 6121 pressure transducer mounted flush with the cylinder head and situated just inside the piston bowl area as shown in Figure 57. The heat flux probe was designed and developed by Taylor et al. (1989) so that it could be installed in the engine in place of the pressure transducer. The second thermocouple incorporated in the probe was situated 2,3 mm back from the exposed surface of the probe as illustrated in Figure 58 and therefore provided temperature measurements for calculating heat flux at that point in the combustion chamber.

Injection timing was determined from the signal of a needle lift transducer of the inductive type and crank rotation was monitored with an optical shaft encoder providing a TDC reference and pulses at each half degree crank angle increment. These pulses were used to trigger the data acquisition system. Engine speed was determined from the frequency of the TDC pulses.

A multi-channel data acquisition system described by Hansen, Taylor, Lyne and Meiring (1989) was used to monitor and record the signals emanating from the range of transducers. The system provided a means of recording both high speed and steady state variables as well as displaying, processing and storing data.

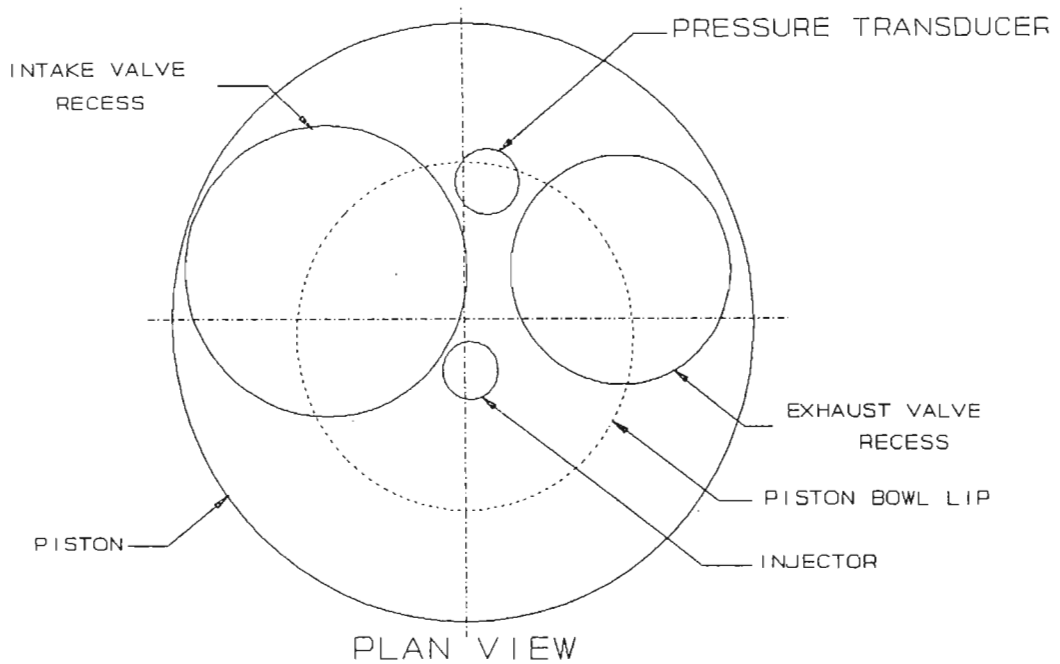

Figure 57 A plan view of the position of the pressure transducer in relation to the cylinder head, valves and piston bowl.

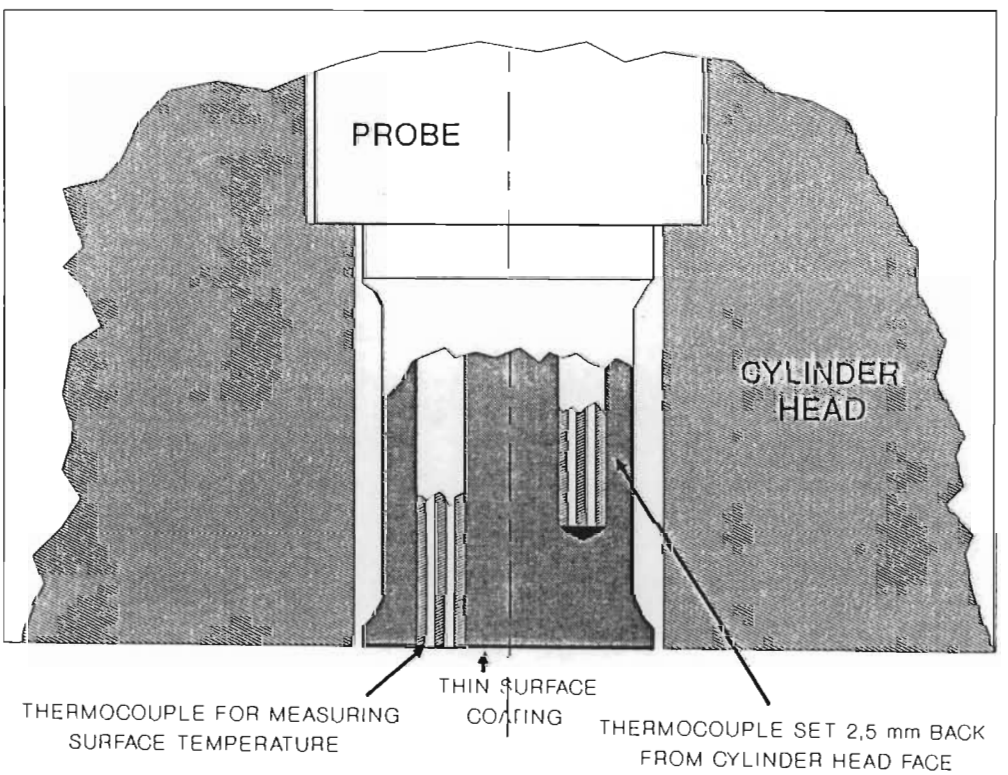

Figure 58 A cross-section of the surface temperature and heat flux probe (Taylor et al., 1989).

When motoring the engine, the high pressure pipe to the fuel injector of the instrumented cylinder was disconnected and the engine was driven by the other three cylinders in a similar manner to that reported by Lawton (1987). Initially it was found that the engine tended to run erratically as a result of uneven fuel distribution to the cylinders. The disconnected pipe was re-routed away from the engine to facilitate the fitting of a dummy injector which then balanced the fuel distribution and stabilised the engine speed.

4.2.2 Test procedure

A rigorous calibration procedure was performed before the test to ensure that the measurements were accurate. Calibration checks were also carried out after the test to isolate any change in the response of the instrumentation. The engine was warmed up until the thermostat for regulating the flow of the coolant had opened. The fuel used in all the tests was a commercially marketed crude oil-derived diesel fuel with a cetane number of 51.

After noting ambient pressure and temperature, steady state and high speed data were recorded systematically at a number of points within the torque-speed range of the engine. Initially the cylinder fitted with the pressure transducer was motored and the speed was varied from 1400 r/min to 2200 r/min in steps of 200 r/min. Thereafter under firing conditions, data were recorded initially at the rated speed of 2200 r/min with the torque varying from zero to 200 Nm in steps of 50 Nm. The load was then maintained at 200 Nm and the speed was reduced from 2200 r/min to 1400 r/min again in steps of 200 r/min. By using this test pattern the model could be checked for conditions of both varying load and constant speed, and varying speed and constant load. At each one of these test points a total of 90 consecutive cycles of high speed data were captured and averaged in addition to the steady state data. Using the window facility of the data

acquisition system, the high speed data were captured only during the compression and expansion strokes.

The same test procedure was then repeated with the heat flux probe installed. However, a total of 90 full cycles, each consisting of two engine revolutions, were captured and averaged at each engine setting along with the steady state data. The engine was also motored after the tests under fired conditions and data were recorded at the same speeds as for the motored tests at the beginning.

As the pressure transducer was piezo-electric it did not provide an absolute base-line of pressure and therefore it was necessary to select a particular point in the cycle where a pressure value could be established from measured variables. The following equation based on the Ideal Gas Law was applied:

$$P_{IVC} = \eta_v \cdot P_a \cdot T_{in} / T_a$$

where P_{IVC} = cylinder pressure at IVC, kPa
η_v = volumetric efficiency
P_a = atmospheric pressure, kPa
T_a = atmospheric temperature, K
T_{in} = inlet temperature measured at inlet valve, K.

All the pressure data were then corrected according to the pressure at IVC.

4.3 Results and Discussion of Motored Engine Tests

As a further step in the model verification process it was necessary to compute convective heat transfer via the model using cylinder pressure data obtained from a motored engine. The calculated heat transfer was then compared to the heat transfer determined from the heat flux probe output.

Before the convective heat transfer model could be applied to the ADE 236 engine under motored conditions, prediction of the gas flow characteristics during the compression and expansion strokes required a starting value for the swirl ratio at IVC. Results of tests carried out by Atlantis Diesel Engines (Pty) Ltd. on an ADE 236 master cylinder head fitted to a steady flow rig were used to arrive at a swirl ratio at IVC of 2,24. The Ricardo Momentum Summation method was applied in predicting this value as detailed in Appendix D. This estimate was made assuming a volumetric efficiency of 100%. The lower volumetric efficiency that occurs in practice in naturally aspirated engines is the result of reduced mass flow rate into the cylinders thus leading to a lower angular momentum flux generated by the inlet port over the induction period. From the derivation of the equation for the Ricardo swirl ratio supplied by Lilly (1984) it could be deduced that the swirl ratio was reduced in direct proportion to the volumetric efficiency. Hence the swirl ratio at IVC of 2,24 was adjusted for varying speeds by multiplying it by the volumetric efficiency measured at these speeds.

The motoring pressure data that were captured at speeds varying from 1400 r/min to 2200 r/min tended to follow the variation in volumetric efficiency with reference to the peak pressure values as illustrated in Figure 59. The volumetric efficiency increased from 80% at 1400 r/min to a peak value somewhere between 1600 and 1800 r/min of approximately 87% and then decreased to 78% at 2200 r/min. Referring to Figure 59 the peak pressures increase as the speed is increased from 1400 r/min with the pressures at 1600 and 1800 r/min being identical. Thereafter they decrease in accordance with the volumetric efficiencies. Although the volumetric efficiency at 2200 r/min is lower than that for 1400 r/min the peak pressure was higher and this can be attributed to the net heat loss being directly proportional to time resulting in a net increase in cylinder pressure and temperature with increasing engine speed. It was concluded from the close correlation of peak motoring pressure with volumetric efficiency

that the instrumentation was responding precisely to conditions in the engine.

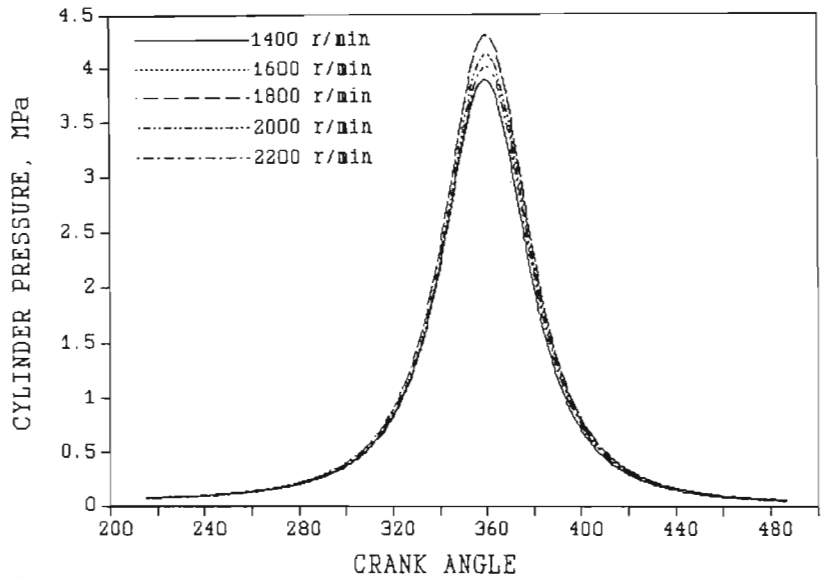

Figure 59 Variation of motoring cylinder pressure with crank angle for different engine speeds.

The motored engine tests provided a means of verifying the convective heat transfer component of the model and excluded the complexities of the combustion process. The convective heat transfer rates were also driven primarily by the gas flow characteristics and therefore comparisons of predictions with the values determined from the heat flux probe provided further verification of the gas flow models. Comparisons of motored engine tests before and after fired engine tests indicated that soot deposition had a significant effect on heat flux and therefore required investigation.

4.3.1 Convection

The instantaneous convective heat transfer rates which were determined from the measurements of temperature via the heat flux probe were derived from the same experimental techniques as Taylor et al. (1989). The temperature measurements were converted into heat flux using Fourier analysis taking into

account both the steady and unsteady components. The steady component was based on the temperature difference between the surface thermocouple and a second thermocouple within the probe situated 2,3 mm away from the surface. Hence one-dimensional heat conduction was assumed. As stated by Van Gerpen et al. (1985) the unsteady flux penetration was very small being of the order of 1 mm and the unsteady flux was very large compared to the steady component. Hence deviation from one dimensional heat conduction would not have a significant effect on the trends in the data. The probe used in this project had been specially designed by Taylor et al. (1989) to promote one-dimensional heat conduction.

Accurate determination of the thermo-physical properties of the probe proved to be difficult because of the design of the probe and the different materials and interfaces involved. Nevertheless, Taylor et al. (1989) were able to determine these properties with sufficient accuracy by using regression analysis and an energy balance. Full details of the experimental technique were provided by Taylor et al. (1989) and therefore have not been included in this section.

The temperature measurements from a clean probe for engine speeds varying from 1400 to 2200 r/min which represented the operating range of the engine from the lowest speed to rated speed, were processed via the procedures established by Taylor et al. (1989) to give heat flux. Figure 60 illustrates the instantaneous heat fluxes at the five speeds. It is evident that the curves are asymmetrical with respect to TDC with a steeper slope in the earlier part of the expansion stroke. This characteristic was observed by Dao, Uyehara and Myers (1973) and by Morel et al. (1987). Morel et al. (1987) attributed it to decreasing intensity of in-cylinder gas motions caused by wall friction and turbulence decay.

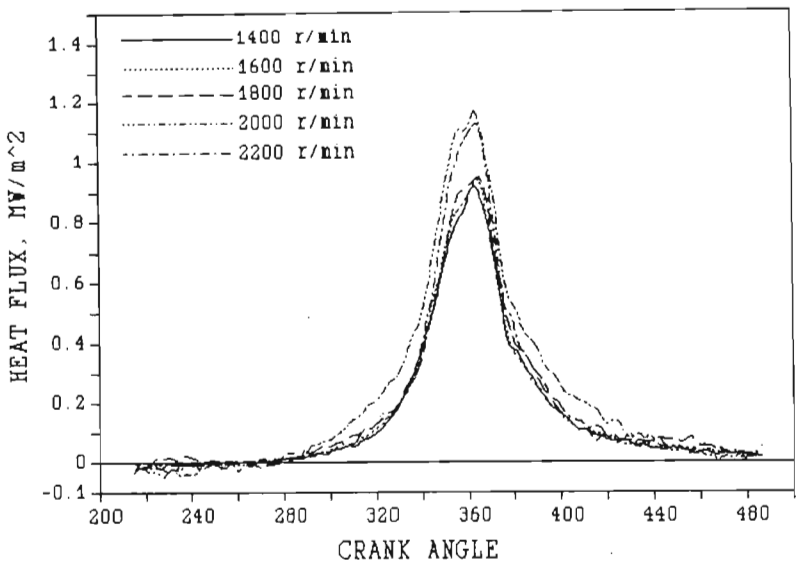

Figure 60 Variation of measured heat flux with crank angle under motored conditions for five different engine speeds.

The curve in Figure 60 for 2000 r/min is situated above the rest and shows abnormal variations when the piston is closer to BDC. This phenomenon was also observed with motored engine data captured after the fired engine tests. It appeared that, at this speed, gas flow instabilities were generated causing considerable fluctuations in the surface temperature which could not be eliminated by averaging 90 cycles. The peak value of heat flux at 2200 r/min also stood out from the lower speeds in spite of a low volumetric efficiency and hence a low starting swirl ratio. The unsteady flow characteristics at 2000 r/min could indicate a transition point in gas flow dynamics across the face of the probe leading to greater gas velocities at higher engine speeds and therefore greater heat fluxes.

Predictions of heat flux via the motored engine model were first carried out for the engine speed of 2200 r/min. The calculations of heat flux were arranged so that average values for designated surfaces were obtained. Hence a first step was to compare the predicted heat flux for the surface directly above the bowl with the measured flux as the probe was situated largely within the bowl perimeter. However, it was more appropriate to determine

a representative velocity at the probe position based on squish and swirl velocities and turbulence kinetic energy that could be expected close to the bowl lip. The resultant velocity was then computed from the inner swirl velocity at the bowl radius, the squish velocity at the bowl radius and the turbulence kinetic energy for the inner volume. The density and boundary layer thickness were assumed to be the same as for the surface of the head above the bowl. The average surface temperature measured at the probe was used to calculate the heat flux. Figure 61 illustrates the resulting heat flux from the latter assumptions as well as the average heat flux predicted for the head surface above the bowl and the heat flux determined from the probe.

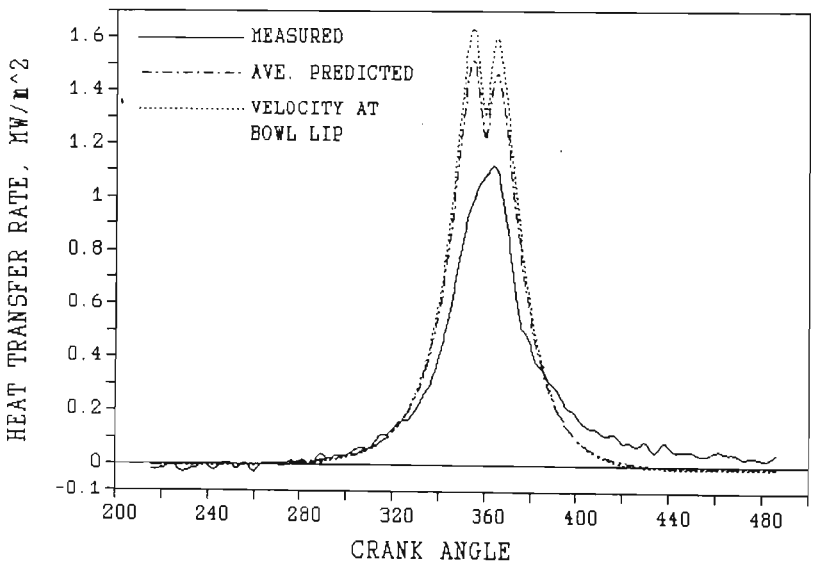

Figure 61 Heat flux measured at the probe compared to average predicted heat flux and heat flux predicted with a resultant velocity for the bowl lip at 2200 r/min.

It can be seen from Figure 61 that the predicted heat fluxes are significantly higher than the measured heat flux suggesting that the resultant velocities at the probe should be lower than initially assumed. Measurements of heat flux at points varying in distance from the bowl centre by Dao et al. (1973) showed a peak heat flux at approximately 85% of the bowl radius. The peak heat flux then decreased to a minimum as the bowl lip was approached. The location of the probe in the present study was

approximately 90-95% of the bowl radius from the centre of the bowl and therefore was situated in a region of transition from the inner swirl velocity to the outer swirl velocity. As shown earlier in Figure 1 these two velocities differ substantially. The same transition occurs with respect to turbulence. Hence it was decided that the resultant gas velocity at the probe should be computed from the average of the swirl velocities and of the turbulence kinetic energies and from the squish velocity at the lip. Figure 62 shows the result of this approach to the measured flux. It can be seen that the squish and reverse squish continue to dominate the predicted flux and provide the main cause of deviation from the measured flux.

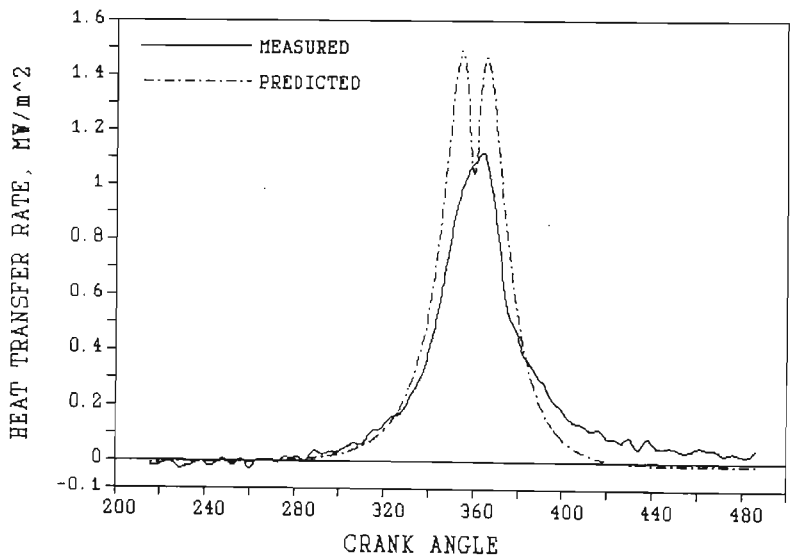

Figure 62 Heat flux measured at the probe compared to heat flux predicted with an average swirl velocity and average turbulence at 2200 r/min.

The clearance between the piston crown and head has a significant effect on squish velocities as indicated earlier. A decrease in clearance from 1 mm to 0,8 mm in the ADE 236 engine causes a 19% increase in peak squish velocity. Taylor et al. (1989) took special care in measuring this clearance with the head in situ and then included an adjustment determined from finite element modelling of the piston to take into account the expansion of the

piston under normal working conditions. They arrived at the value of 0,8 mm for the clearance.

Further examination of Figure 62 shows that there is some degree of reverse squish affecting the measured flux, but significantly less than predicted with the 0,8 mm piston crown-to-head clearance. The reason for this discrepancy was attributed to the proximity of the valve recesses to the probe leading to shorter flow paths for the gases being squeezed into the bowl. The result was an attenuation of the squish velocity in the vicinity of the probe. A more accurate prediction of squish velocity at the probe demanded complex computations that were beyond the scope of this work that had concentrated on a quasi-dimensional approach.

To circumvent this problem the squish velocity component included in the calculation of the resultant gas velocity at the probe was adjusted by a constant so that better agreement with the measured flux was achieved. Figure 63 shows the result with the squish velocity reduced to exactly half its value. There is excellent agreement with the reverse squish confirming that the peak on the measured heat flux was in fact due to reverse squish. However, it is evident that there is close on zero squish before TDC. The third curve shown in Figure 63 was generated by assuming zero squish before TDC. The result is very close agreement of the predicted flux with the measured flux.

The presence of zero squish at the probe during compression could be the result of not only the proximity of the valves but also almost zero penetration of the remaining squish into the solid body swirl rotation in the bowl. Hence the swirl component dominates at the probe during the compression stroke. In the early part of the expansion stroke reverse squish is not dominated by swirl and gas initially flows back from the bowl into the expanding space between the head and piston crown.

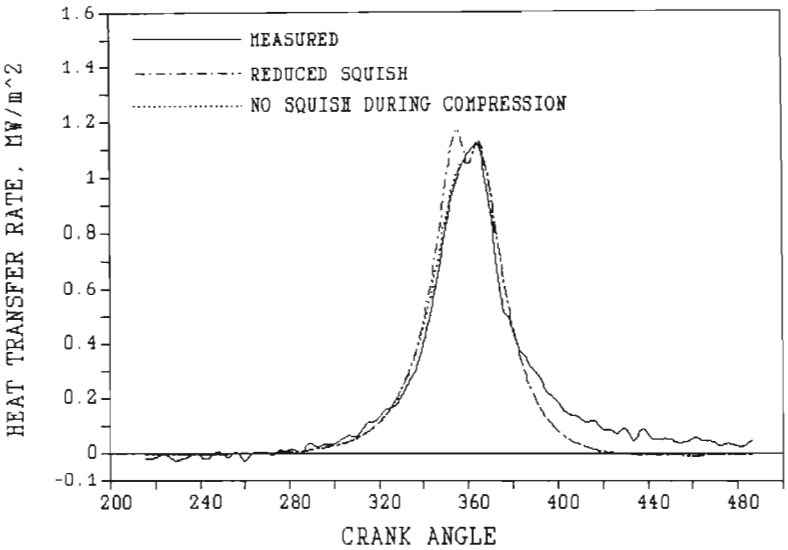

Figure 63 Heat flux measured at the probe compared to heat flux predicted with a reduced squish velocity.

Further verification of these adjustments to the resultant velocity at the probe was obtained by comparing model predictions to measured flux for the other four engine speeds. Figure 64 illustrates the two curves in each case. Apart from the fluxes at 1400 and 2000 r/min very close agreement was again evident. The close correspondence of the curves over the compression and expansion strokes confirms that the initial calibrations performed on the gas flow model were precise and applicable to the ADE 236 engine. The wall friction in particular that was determined in the model matched the actual conditions very closely as judged by the gradients of the two curves in the earlier part of the expansion stroke.

The curves in Figure 64 show that in spite of the net heat loss being proportional to time which should cause a decrease in net heat transfer with increasing engine speed, the in-cylinder gas velocities also increase in proportion to speed subject to the volumetric efficiency. The heat transfer across the boundary therefore also increases. The overall result is an increase in heat transfer rate with speed which is in agreement with the results of Morel et al. (1987).

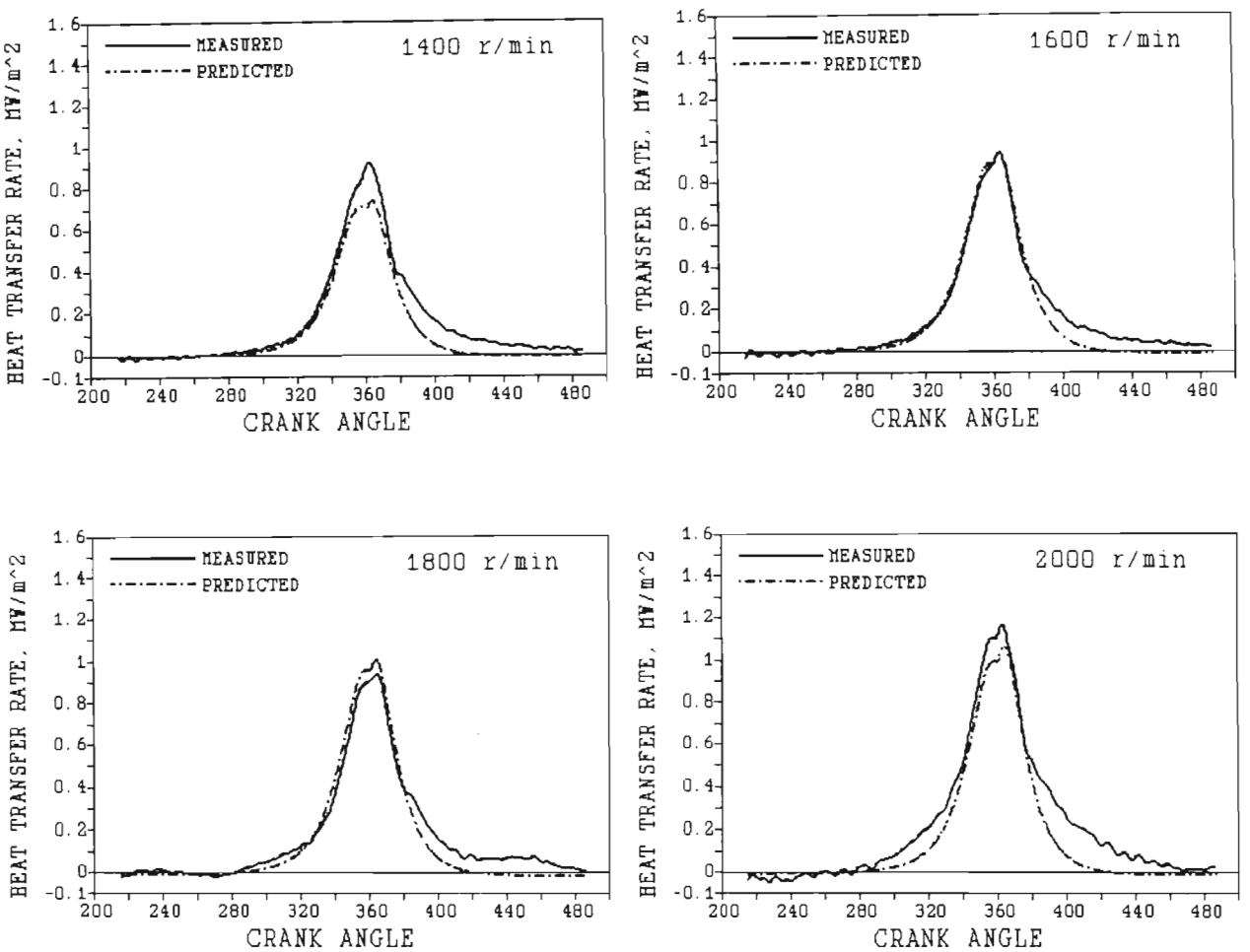

Figure 64 Comparison of predicted and measured heat fluxes at the probe for the motored engine at different speeds.

At all five speeds it can be seen that after approximately 375 - 380°CA the measured flux does not decrease at the same rate as the predicted flux. No definite reason for this deviation could be found. However, it was possible that as the exhaust valve and recess were upstream of the probe in terms of swirl, at a particular point in the cycle some additional turbulence was being generated in combination with the relatively hot valve. This turbulence and the heating effect of the valve resulted in a higher gas velocity across the face of the probe and hotter gases, thus causing a higher heat flux.

As indicated earlier the heat flux measured at 2000 r/min showed some unusual trends. Nevertheless, the shapes of the two peaks corresponded very closely. At 1400 r/min the predicted and measured curves did not correspond as well as at the other speeds. However, in terms of overall accuracy the prediction was regarded as acceptable.

It was concluded from these motored engine tests that the gas flow models had been formulated and calibrated precisely. Hence the predicted convective heat transfer rates which were largely driven by the gas flow characteristics were also sufficiently accurate. Such precision was very important as under fired engine conditions the convective heat transfer component dominated the overall heat transfer.

Although heat flux was measured at only one point in the combustion chamber, this was adequate for the verification of the gas flow model and the convective heat transfer model under motored conditions. Under fired engine conditions, the introduction of combustion and therefore radiative heat transfer in addition to convective heat transfer provided some additional variables that were difficult to account for as precisely as for the motored engine tests. A further variable which resulted from the combustion was soot deposition on the probe.

4.3.2 Influence of deposits on probe

Motored engine tests were performed before and after the fired engine tests with the objective of determining whether soot deposition on the probe affected the heat flux. Taylor et al. (1989) investigated the effect of soot on heat transfer with the same probe used in this project and concluded that the rate of heat transfer reached an equilibrium state within minutes of the engine being started. As shown in a subsequent section, the results obtained in this project are in agreement with the observations of Taylor et al. (1989).

A comparison of the heat flux measured at the probe before and after the engine was fired for approximately one hour indicated a significant attenuation of the signal as a result of insulation from the soot. Figure 65 illustrates this attenuation for 1400, 1800 and 2200 r/min. Morel, Wahiduzzaman and Fort (1988) stated that soot deposit on the surface of the heat flux gauge was a source of a systematic error as it reduced the surface temperature swing and thus the peak heat flux. They observed both a signal attenuation and phase lag in their engine tests. A phase lag can also be seen in Figure 65 where the peak heat flux for the dirty probe is slightly retarded relative to the clean probe causing the heat fluxes for the clean and dirty probe to merge during the expansion stroke.

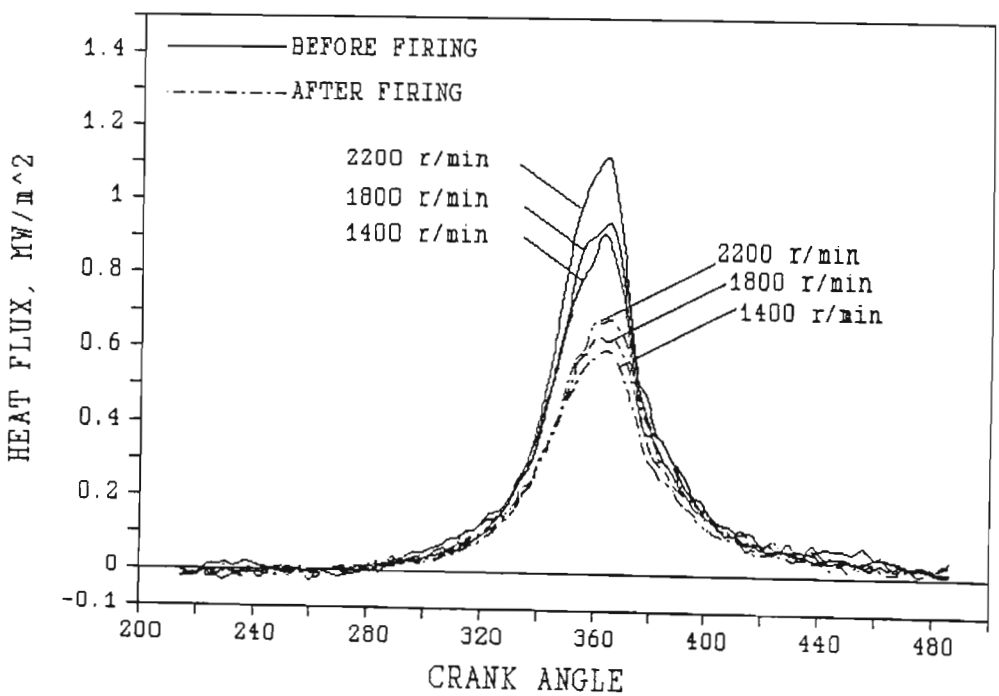

Figure 65 Attenuation of the heat flux measured at the probe for the motored engine as a result of soot deposits for different engine speeds.

Morel, Wahiduzzaman and Fort (1988) indicated that estimation of the magnitude of the error was difficult because of the absence of reliable data on properties of diesel soot deposits.

While it was difficult to compensate for the phase lag in this project a reliable estimate of the attenuation caused by the deposit could be established from the differences between the peak heat fluxes for the clean and dirty probe. In the case of the fired engine tests discussed later in this chapter the method used to account for the attenuation of the heat flux was to amplify the measured heat flux so that close agreement was achieved with the predicted heat transfer before the start of combustion in the compression stroke. Verification of the predicted convective heat transfer during the compression stroke was covered in the previous section.

The measurements of heat flux under motored engine conditions provided very useful information concerning not only the magnitudes and shape of the heat flux during the compression and expansion strokes but also the influence of soot deposits. These measurements established a very necessary basis from which to proceed to the analysis and interpretation of the fired engine results.

4.4 Results and Discussion of Fired Engine Tests

The aspects of importance that were investigated in detail for the engine under fired conditions were the sections of the model responsible for generating the two zones of combustion and the resulting convective, radiative and conductive heat transfers. The heat flux probe measurements were employed to verify the combined convective and radiative heat transfer rates using the resultant velocity specification applied in the motored engine tests. An adjustment to the heat flux measurements was made to account for the insulatory effects of soot deposits. The overall model was verified by performing an energy balance of energy input to energy release and heat transfer. The results of the fired engine tests are summarised in Appendix E.

4.4.1 Two-zone combustion

In the generation of the burnt and unburnt zones particular attention was paid to the burnt volume, the surface area of the burnt zone and the temperatures of each zone. Figure 66 illustrates the expansion of the burnt volume relative to the total volume for load settings varying from 50 to 200 Nm at an engine speed of 2200 r/min. The zero load setting was excluded from the analyses as significant cycle to cycle variations in combustion were observed during data capture including cycles with no combustion taking place at all. Averaging of 90 of the cycles at this setting generated a pressure curve which was not representative of the actual combustion events. This observation was confirmed during the energy balance checks where only 71% of the fuel was accounted for at zero load. Irregular fuel injection at zero load was a major contributor to the erratic combustion. In addition, because of the relatively retarded injection timing at low loads fuel was being injected in the earlier part of the expansion stroke when gas temperatures were already decreasing significantly in the cylinder thus inhibiting combustion. Figure 66 shows the start of combustion advancing with increasing load as expected for the CAV DPA rotary distributor pump.

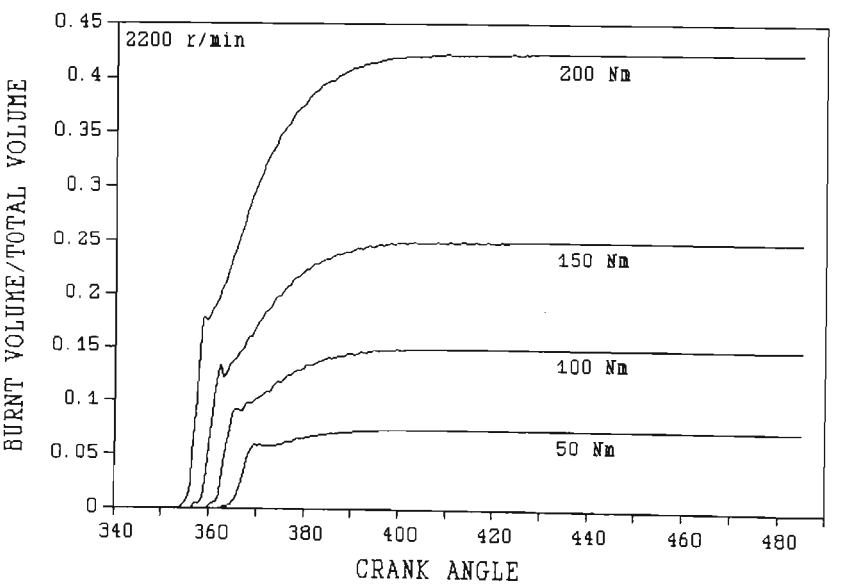

Figure 66 Variation of the ratio of burnt volume to total volume relative to crank angle for different load settings.

For each load there is an initial sharp rise in burnt volume coinciding with the premixed phase of combustion. Thereafter the burnt volume continues to increase at a slower rate depending on the proportion of fuel left to burn by diffusion. In all four cases the burnt volume to total volume ratio reaches a constant value by 400 - 420°CA. Hence for the remainder of the expansion stroke the burnt volume continues to expand as the total cylinder volume increases.

The surface area of the burnt zone increased as the burnt volume increased. The geometrical constraints imposed on the burnt zone while confined to the bowl initially yielded a uniform increase in surface area as shown in Figure 67. The rate of increase then reduced as the combustion moved into the diffusion phase. However, as the point was reached where the burnt volume expanded into the clearance volume, a discontinuity in the surface area occurred as illustrated in Figure 67 for the load of 200 Nm. This step was caused by the reshaping of the burnt volume as it was allowed to extend into the clearance volume. To circumvent the problem the following equation for the radius of the burnt zone R_b in the clearance volume was applied:

$$R_b = R_1 + (R_2 - R_1).(V - V_\delta)/(V_{EVO} - V_\delta) - \delta$$

where R_1 = radius of bowl

R_2 = radius of bore

V = instantaneous volume

V_δ = volume at the point in the cycle where the burnt zone expands into clearance volume

V_{EVO} = volume at EVO

δ = clearance between the burnt zone and the bottom of the bowl.

Figure 67 shows the result of using this equation for the load setting of 200 Nm. The importance of maintaining a uniform surface area lies in the fact that the computation of heat transfer from the burnt zone to the unburnt zone makes use of

this surface area. Hence any discontinuity in surface area would cause an abnormal discontinuity in heat transfer. Morel and Keribar (1985) who used the same geometrical constraints as described in this work made no mention of measures to avoid this discontinuity. Figure 67 includes the curves for the loads of 50, 100 and 150 Nm. Similar trends are evident in these curves with the gradients decreasing as the load is reduced.

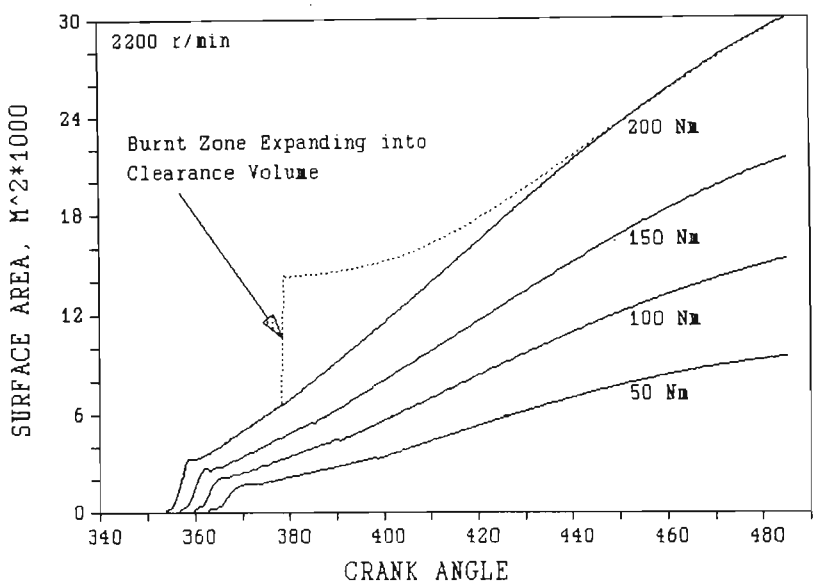

Figure 67 Variation of the surface area of the burnt zone with crank angle for different load settings.

The next step in the calibration and verification of the model after checking the surface area calculations for the burnt zone was to adjust the gas-to-gas heat transfer coefficient so that the peak burnt zone temperature did not exceed the adiabatic flame temperature. A formula presented by Gülder (1986) for calculating adiabatic flame temperatures was used. This formula took into account the effect of pressure, temperature, equivalence ratio and hydrogen to carbon atomic ratio of the fuel. As the first appearance of a flame was likely to occur under stoichiometric conditions for all loads, the adiabatic flame temperature was determined for an equivalence ratio of one. Choice of suitable temperatures and pressures and the measured hydrogen to carbon atomic ratio for the fuel led to a flame temperature of 2700 K. The effect of expected variations in

pressure and temperature with load on this value were not significant and therefore this value was used as a guideline for all the test points.

In order to set the gas-to-gas heat transfer coefficient, all the pressure data were processed through the model and the coefficient was adjusted so that none of the maximum burnt temperatures predicted at each load and speed exceeded 2700 K. A value of 0,02 for the coefficient was eventually selected and applied for all the test points. The maximum difference relative to 2700 K was 6,9% with an average of 3,2% for the eight test points excluding zero load at rated speed. This small variation was regarded as quite remarkable considering the heterogeneity of the combustion in a compression-ignition engine.

The shape of the curve for burnt zone temperatures was also regarded as unique. Figure 68 illustrates the curves of temperature for the burnt and unburnt zones and the bulk gas temperature for four engine torques varying from 50 to 200 Nm at rated speed. Each curve of burnt zone temperature exhibits a prominent sharp peak coinciding with the premixed phase of combustion. The occurrence of a second flatter peak conforming with the diffusion phase is governed by the relative loading on the engine and hence on the equivalence ratio. Thereafter all three curves merge. The following explanation is provided for these trends.

When combustion begins, the temperature of the burning zone increases rapidly to a maximum which is approximately the same as the adiabatic flame temperature under stoichiometric conditions. During the burning of the fuel-air mixture prepared earlier during the ignition delay, the temperature in the burning zone rises sharply to a maximum and then decreases in parallel with the rate of heat release. The sharp decrease in temperature of the burnt zone is the result of two factors. The first is the completion of burning of the initially prepared mixture, and the second is heat transfer from the burnt zone to the unburnt zone

which surrounds the burnt zone. Air entrainment into the burnt zone also contributes to the heat transfer effect and the reduction in average temperature of the burnt zone. Combustion then continues by a process of diffusion. After the initial temperature peak the temperature of the burnt zone either decreases at a slower rate, eventually merging with the bulk gas temperature, or it may increase slightly before decreasing because of a high equivalence ratio, resulting in a large portion of heat being released in the diffusion phase.

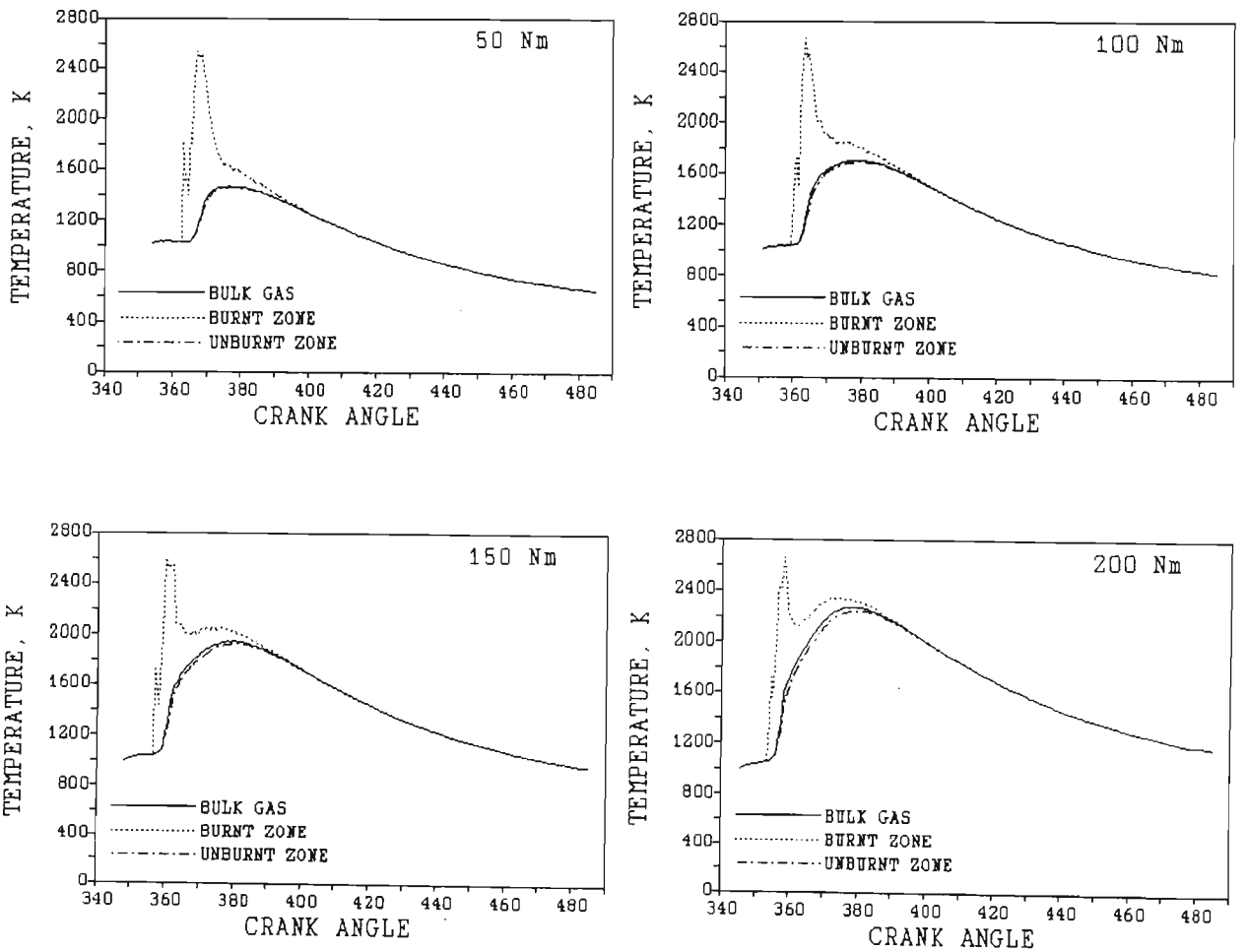

Figure 68 Variation of burnt zone temperature, bulk gas temperature and unburnt zone temperature with crank angle for different load settings.

The response in temperature of the unburnt zone when combustion begins is not immediate as this zone occupies the whole chamber

initially. An increase in average temperature of this zone occurs a few degrees of crank angle after combustion begins, at which time the temperature of the burnt zone is close to maximum. The unburnt temperature deviates from the bulk gas temperature initially as expected, but these two temperatures merge subsequently when what remains of the unburnt zone attains the overall temperature of products in the combustion chamber through heat transfer.

The burnt temperature spikes immediately after the temperature first rises are caused by small irregularities in the energy release at the start of combustion. They have a insignificant effect on the heat transfer.

It can be seen from Figure 68 that the burnt temperature deviates from the bulk gas temperature over a relatively small portion of the cycle. However, this portion includes the most pronounced changes in heat transfer and combustion.

The burnt and unburnt zone temperatures provide the basis for calculating the convective and radiative temperatures that are used to calculate the corresponding heat transfers. Hence it is important to establish their acceptability prior to computations of heat transfer. They are also largely responsible for representing the effects of combustion on the transfer of heat to the walls of the combustion chamber.

4.4.2 Convective heat transfer

The first important variable that had a significant influence on convective heat transfer was the convective temperature. This temperature which was calculated by the same method used by Morel and Keribar (1985) varied within the narrow constraints of the unburnt temperature and the bulk gas temperature. Initially it tended towards the unburnt temperature as was expected in the engine as initially unburnt gases were in contact with the walls. However, in the diffusion phase the convective

temperature tended towards the bulk gas temperature again representing what would have been expected with the gas temperatures in the vicinity of the walls approaching the bulk gas temperature.

In order to determine the variations in convective heat transfer from one section of the combustion chamber to another, the total heat transfer rates for the piston, liner and head were examined. These are illustrated in Figure 69 for rated speed and 200 r/min. The piston and head have convective heat transfer rates which are very similar with transfer to the head being slightly less than transfer to the piston. The work of Morel and Keribar (1985) showed the peak heat transfer to the head to be almost half that for the piston. This difference could be attributed to some extent to the higher overall wall temperatures specified in the model of Morel and Keribar (1985) for the head as a result of the high temperature of the valves. The valves also cover a significant portion of the head area.

The heat transfer rate to the liner is substantially less in total compared to the piston and head in Figure 69. Heat transfer is relatively low initially due to the low motoring pressure. Then with the piston shielding the liner as TDC is approached, the heat transfer almost reaches zero. After TDC there is a significant rise in heat transfer rate as more and more of the liner is exposed to the hot gases. The shape of the curve is in good agreement with the work of Morel and Keribar (1985).

A study of the breakdown of the total convective heat transfer from IVC to EVO for this load setting of 200 r/min at 2200 r/min indicated that approximately 47% of the heat was lost through the piston, 41% through the head and 13% through the liner. Morel et al. (1985) quoted figures for a conventionally cooled Cummins engine operating at rated conditions of 49% through the piston, 32% through the head and 19% through the liner. The differences between the two sets of figures therefore occur at the head and

at the liner with the present model predicting a greater heat loss through the head and a lower heat loss through the liner. Graphs by Assanis and Heywood (1986) that showed a breakdown of predicted convective heat transfer rates through the head, piston and liner indicate fairly good agreement with the predictions of this model.

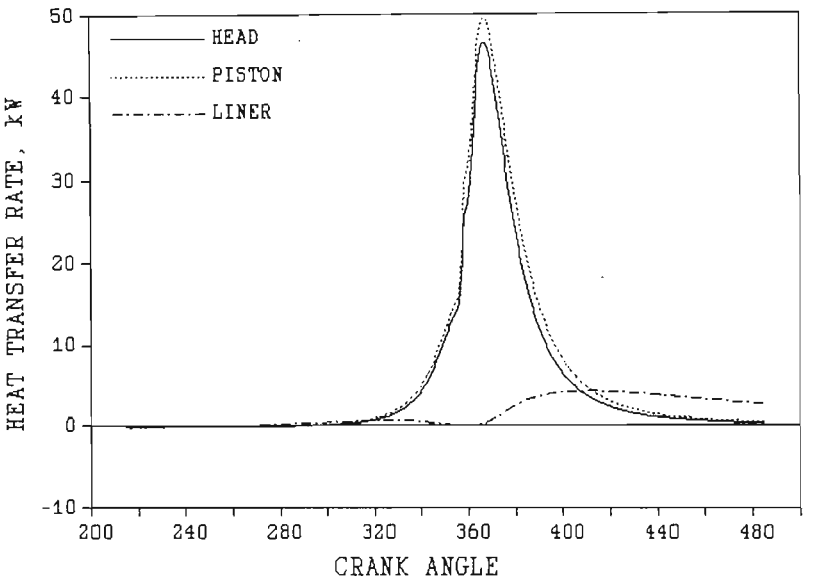

Figure 69 Convective heat transfer rates for the piston, liner and head at rated speed and 200 Nm.

Apart from the effect of the high temperature of the valves the shape and size of the piston bowl could also be responsible for the earlier differences. Hence these differences were regarded as being within the expectations of accuracy for this project. What was confirmed from these comparisons was the considerable variation in heat transfer rates that could occur between different locations within the combustion chamber. The division of the combustion chamber into several discrete sections was therefore imperative in order to achieve a higher level of accuracy in the prediction of convective heat transfer. While convective heat transfer represented the major form of heat loss, the contribution to heat loss from radiative heat transfer could not be ignored and therefore had to be included in the analysis.

4.4.3 Radiative heat transfer

With the motored engine tests it was possible to verify the convective heat transfer component of the model with particular reference to the gas flow characteristics in the combustion chamber. The fired engine tests provided heat flux data that could be used to verify the combined transfer of heat from convection and radiation. These tests allowed a further check of the overall combined heat transfer via an energy balance. Hence no direct means of verifying the radiative heat transfer component was included. However, as indicated earlier the contribution to the total heat flux of radiation was relatively small although still significant. The objectives in verifying the radiative heat transfer characteristics were to establish that the general shape and orders of magnitude of the emissivities and of the heat transfer rates were in acceptable agreement with published data. Also the radiative temperature should vary as predicted and measured by researchers.

The flame emissivity which was based on a combination of the soot and gas emissivities exhibited the trends illustrated in Figure 70 for different engine loads at rated speed. At all four loads there was a sharp increase in emissivity to a peak value and then a gradual decrease for the rest of the expansion stroke. The peak values of the emissivities were of approximately the same magnitude as measurements reported by Flynn et al. (1972) and Wahiduzzaman et al. (1987) for direct injection diesel engines. The general trends of the curves in Figure 70 were also in fairly close agreement with the results of these researchers.

The rate of decrease of flame emissivity after the peak value was dictated largely by the gas emissivity as shown in Figure 71. The soot emissivity has a dominant peak close to the crank angle of maximum energy release in the diffusion phase. The soot emissivity then subsides but the flame emissivity is then bolstered by the increasing gas emissivity.

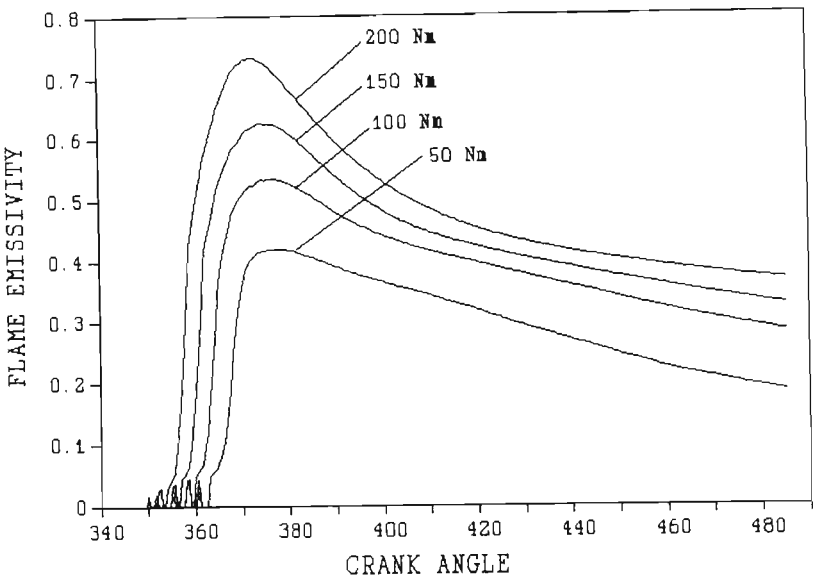

Figure 70 Flame emissivities varying with crank angle for different engine loads at rated speed.

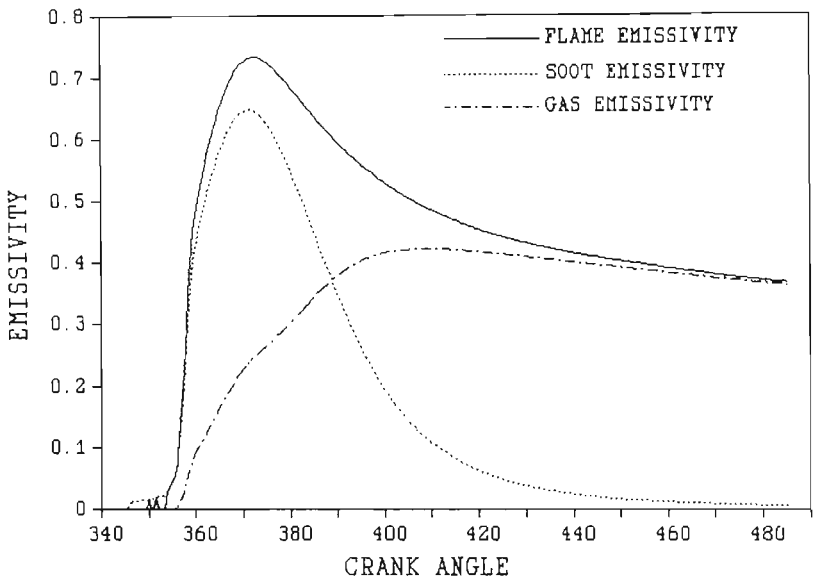

Figure 71 Gas, soot and flame emissivities at rated speed and 200 Nm.

Borman and Nishiwaki (1987) suggested that the apparent gray emissivity should be nearly zero at the end of combustion. This implied that the contribution from gas emissivity in the latter stages of combustion also approached zero especially as the combustion pressure decreased. However, the results of Kunitomo

et al. (1975) who were largely responsible for developing this model of radiant transfer, showed that the gas emissivity rose to a certain value and then stayed more or less constant.

One point of initial concern with the present predictions of gas emissivity was the magnitudes obtained as several researchers ignored gas radiation as a contributor to heat transfer. Owing to the difficulties of isolating gas emissivity from soot emissivity in measurements from diesel engines no published data could be found to verify the gas emissivity component. Nevertheless for the purposes of this model and the objectives of the project the emissivities were regarded as acceptable.

After verifying that appropriate emissivities were being generated, the next important variable in the determination of radiation heat transfer was the radiation temperature because of the fourth power relationship in the radiation formula. Figure 72 illustrates the variation with crank angle of radiation temperature in comparison to the bulk gas temperature for the four load settings. In all four cases the radiation temperature rises sharply in accordance with the burnt zone temperature reaching a maximum which is equivalent to 90% of the maximum burnt zone temperature. Beyond this maximum the radiation temperature continues to be linked to the burnt zone temperature but decreases in proportion to the angle of crank rotation that remains till EVO. This proportionality was set so that close to EVO the radiation temperature assumed the same value as the bulk gas temperature. The initial step down just after the maximum temperature indicated in Figure 72 is caused by the sharp decrease in burnt zone temperature after it reaches a peak. In accordance with the expectations of Borman and Nishiwaki (1987) the radiation temperature was initially close to the adiabatic flame temperature for a rich limit mixture and this temperature was relatively insensitive to load. The temperature then decreased almost linearly reaching the average gas temperature near the end of combustion.

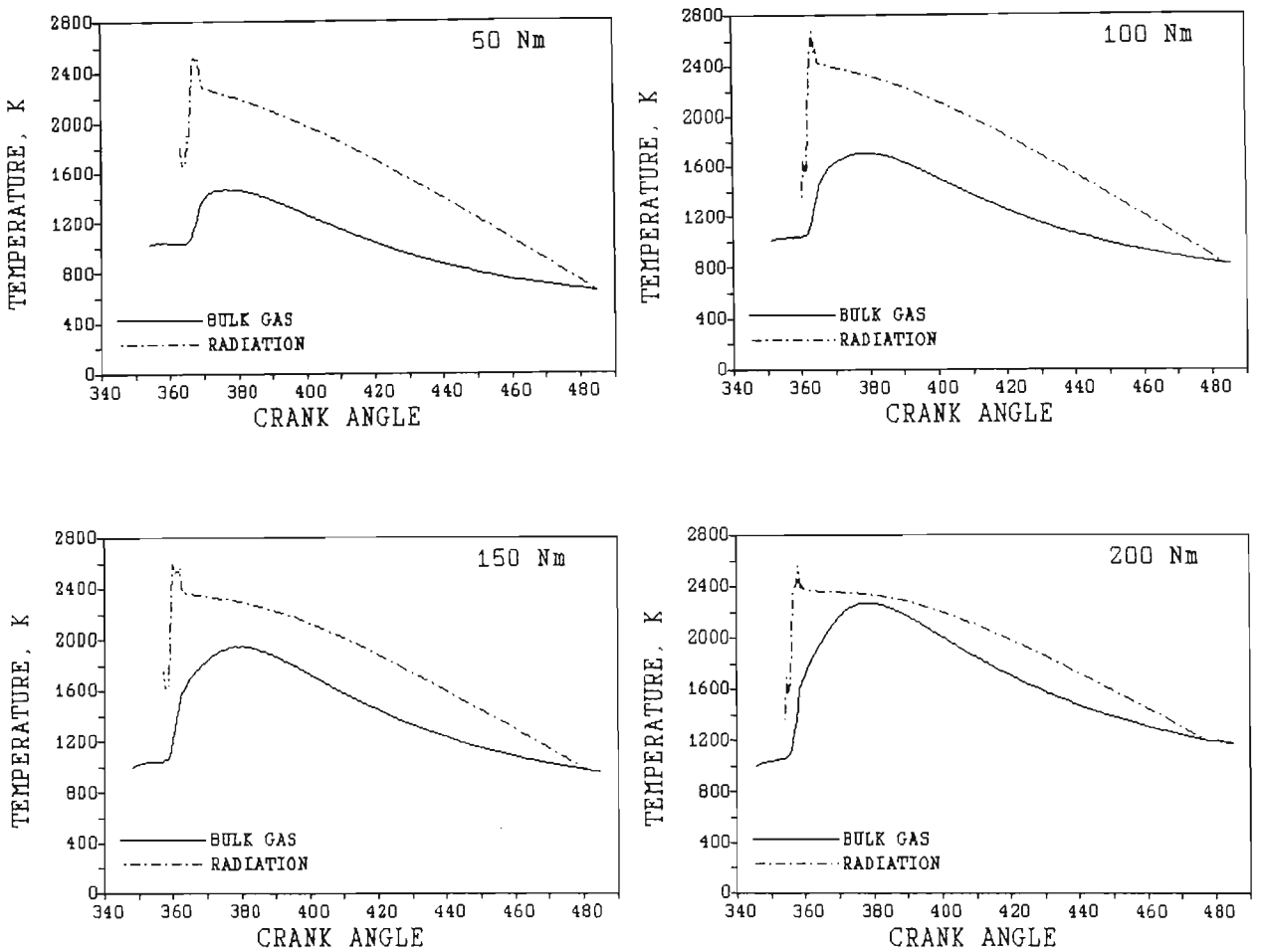

Figure 72 Variation of radiation temperature with crank angle for four load settings.

A graph presented by Dent and Sulaiman (1977) of a selection of flame temperature measurements in diesel engines performed by a number of researchers showed close agreement with the shape of the radiation temperature curves in Figure 72, with particular reference to the slight curve in the graphs as they decrease in the expansion stroke. More recent measurements of apparent radiation temperature by Wahiduzzaman et al. (1987) also support the trends and magnitude of the predicted radiation temperatures in Figure 72.

The predicted radiation heat transfer rates for the four loads at 2200 r/min are given in Figure 73. The curves which again are in close agreement with the results of Flynn et al. (1972), all rise sharply and reach a maximum close to the point of

maximum diffusion burning. Hence the premixed portion of the combustion produces little radiation in keeping with the conclusions of Borman and Nishiwaki (1987). Thereafter radiation decreases to a low value at EVO dictated to a large extent by the bulk gas temperature which represents the radiation temperature at that point. The radiant heat transfer rates in Figure 73 also decrease with load as would be expected. The soot concentration and the amount of carbon dioxide and water present decreased as the equivalence ratio was reduced thus reducing the heat transfer.

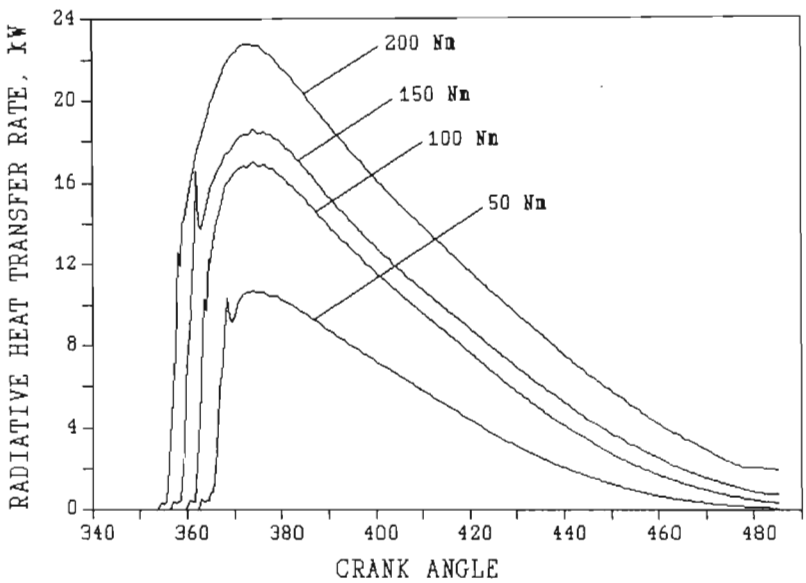

Figure 73 Radiation heat transfer rates varying with crank angle for four loads at 2200 r/min.

Radiation heat transfer was included in the overall model on the basis of inaccuracies reported by several researchers in heat release computations where it was excluded. In addition it was included in line with the objective of providing a combustion model that could be used to evaluate different fuels. Such fuels were likely to generate different amounts of radiation according to their structure and properties. As indicated in an earlier section this model takes into account the specific gravity of the fuel in the determination of soot emissivity. Callahan et al. (1985) indicated that the specific gravity tended to reflect the hydrogen content of the fuel. The diesel fuel used to verify the

present model had a density 0,853 kg/L giving an effective excess air ratio of 1,16 as measured from the graph of specific gravity versus effective excess air ratio published by Callahan et al. (1985). While the objectives of the project were achieved by examining the response of the model to only one fuel, the effect of a range of fuels of varying properties on radiation heat transfer should be examined in further projects involving this model. Such tests correlated with soot emissions would provide valuable information concerning the variation of radiation with fuel type.

From these results of radiation heat transfer it was concluded that the model provided an output with an accuracy that was acceptable in terms of the relative contribution of radiation to the total heat transfer. It was also necessary to analyse the results of the conduction component of heat transfer so as to complete the analysis of the individual components of heat transfer that were involved.

4.4.4 Conduction heat transfer

The main results generated from the conduction model that were of importance were the combustion chamber wall temperatures. In setting up the model it was necessary to establish suitable values for thermal resistances through each of the six demarcated walls of the combustion chamber. These values were determined by selecting the test point at 2200 r/min and 200 Nm and adjusting the resistances to obtain wall temperatures that were in agreement with trends and magnitudes of published data. It was recognised that a better level of accuracy could be achieved by using a more detailed resistance network. Nevertheless the objective for this model was to generate wall temperatures linked to the gas temperatures, gas-to-wall heat transfer coefficients and the oil and coolant temperatures that would vary in accordance with the operating conditions of the engine. Such a model was a substantial improvement over the assumption of one

wall temperature to represent all chamber surfaces under all operating conditions.

The variations of the average wall temperatures, gas temperatures and heat transfer coefficients are listed in Table 3 for all the load points and the one motored engine test point at 2200 r/min. The test point at rated speed with the engine idling is included as average conditions in the chamber are under consideration. The temperatures for the liner being surface 4 represent the values at the top of the liner which is in contact with the head. As described in an earlier section the liner temperature decays from this maximum value down to the coolant temperature at the bottom of the liner in line with BDC for the piston.

Table 3 Average temperatures and heat transfer coefficients for all the load points and for one motored engine test at 2000 r/min.

Variable	Test Results									
Speed (r/min)	2200	2200	2200	2200	2200	2200	2000	1800	1600	1400
Torque (Nm)	motor	0	50	100	150	200	200	200	200	200
Wall temp.(K) :										
Surface 1	373	395	413	433	453	482	474	464	452	444
Surface 2	374	401	423	446	470	503	494	482	468	459
Surface 3	374	401	422	445	469	502	493	480	467	459
Surface 4	362	385	400	417	436	464	455	447	436	429
Surface 5	363	394	415	438	464	500	489	477	464	457
Surface 6	365	401	425	452	481	523	510	496	481	475
Probe surface temp.(K)	414	438	465	495	537	590	578	555	543	533
Average HTC (W/m².K) :										
Surface 1	128	252	275	296	314	336	328	322	296	249
Surface 2	200	275	300	321	340	361	352	346	318	267
Surface 3	283	412	453	487	517	551	537	524	483	409
Surface 4	167	230	246	261	274	290	282	279	255	213
Surface 5	285	413	454	489	518	551	537	525	483	410
Surface 6	203	283	311	335	355	378	368	359	331	281
Average gas temp.(K)	397	506	571	637	707	800	775	744	724	743
Oil temp.(K)	368	368	372	375	378	380	381	378	375	373
Coolant temp.(K)	355	355	355	355	356	360	359	358	357	358

HTC - Heat Transfer Coefficient

After examining published data and the average surface temperatures at the probe for the test point of rated speed and 200 Nm, the target values for the five wall temperatures excluding the liner were 480, 500, 500, 500 and 525 K. The target value for the temperature at the top of the liner in

contact with the head was taken as 465 K. The values for 200 Nm and 2200 r/min listed in Table 3 varied a negligible amount from the target values after the thermal resistances had been adjusted. Figure 74 shows the predicted average temperature for the area of the head directly above the bowl and the surface temperature measured at the probe varying with equivalence ratio at the rated speed. The gradients of both curves are in close agreement with the probe temperature increasing at a slightly higher rate. The almost constant difference between the curves can be justified by the fact that the probe is situated in close proximity to both valves and is downstream of the exhaust valve relative to swirl rotation. Figure 75 shows the close correspondence for the same two temperature variables again but for varying speed at a constant load of 200 Nm. The same trends as for the test point at 2200 r/min and 200 Nm were obtained for the other predicted temperatures.

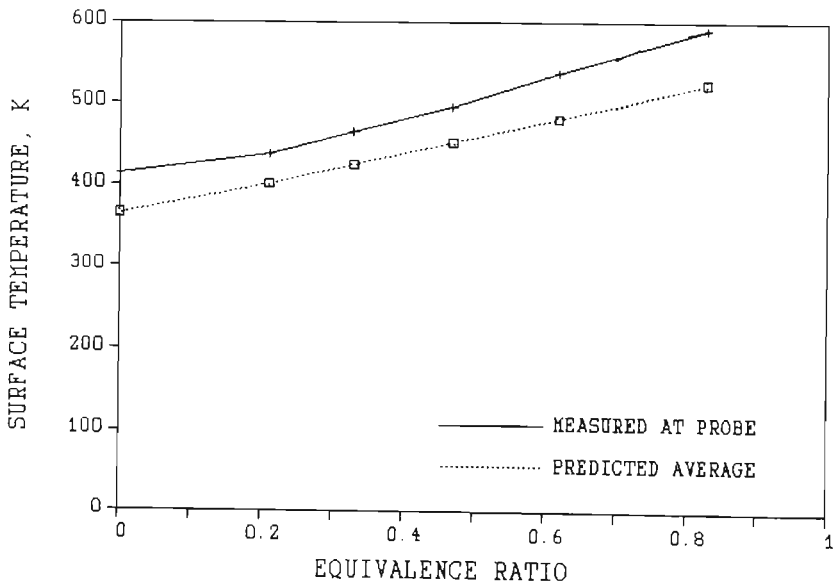

Figure 74 Variation with equivalence ratio of the predicted average temperature for the area of the head directly above the bowl compared to the surface temperature measured at the probe.

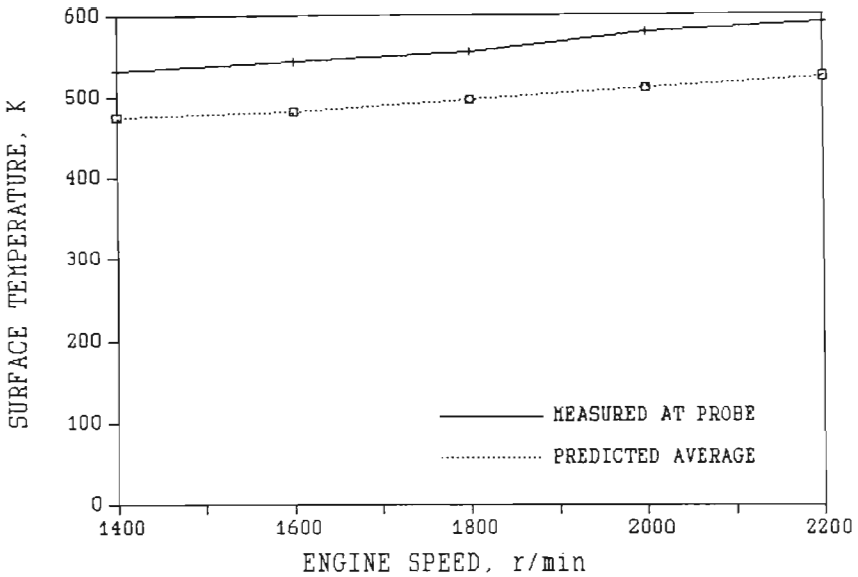

Figure 75 Variation with speed at a constant load of 200 Nm of predicted and measured surface temperatures for the area of the head above the bowl and the probe respectively.

A comparison of the average gas-to-wall heat transfer coefficients predicted for the piston at rated speed and 200 Nm with results published by Woschni (1979) and Woschni and Fieger (1979), indicated close agreement. The coefficients were slightly higher for the side of the bowl compared to the bottom of the bowl but there was a significantly higher coefficient for the piston crown.

The oil and coolant temperatures are included in Table 3 as they provide the temperature constraints on the outside of the combustion chamber. The coolant temperature remains relatively constant at all the test points while the oil temperature increases with load as would be expected.

It was concluded from these results that the conduction model although relatively simple was generating realistic wall temperatures that varied with accepted trends under different load and speed conditions. Such a model introduced an additional

step in the improvement of accuracy of the overall heat transfer and combustion analysis.

4.4.5 Combined Heat Transfer

The final phase of the verification process for the engine under fired conditions was to examine the combination of the heat transfer models. The verification was approached via two routes. The first route involved an analysis of the energy balance taking into account the energy release from the fuel and the heat transfer as compared to the energy input from the fuel. This analysis therefore provided a means of verifying the overall heat transfer from the combustion chamber linked to the combustion of the fuel. The second route was a comparison of the predicted and measured heat transfer at the heat flux probe.

Before proceeding with the details of the energy balance it is pertinent to illustrate the relative contributions of the convective and radiative heat transfers. Figure 76 shows the radiation, convection and total heat transfer rates at rated speed and 200 Nm. The radiation heat transfer forms close to 30% of the total heat transfer between IVC and EVO. This figure is in line with the predictions of a number of researchers. In addition the relative shapes of the curves in Figure 76 are in agreement with published results. Hence it was concluded that the convection and radiation heat transfer models were generating values that were of the right proportion and distribution relative to crank angle.

Referring to the results of the fired engine tests at the selected load and speed settings summarised in Appendix E the variable of particular relevance to the energy balance was the percentage of fuel mass burnt. This percentage represented the ratio of calculated fuel mass accounted for by the combustion model to the measured fuel mass injected into the cylinder.

At the constant load of 200 Nm and with varying speed the percentage was between 98 and 99% for the speed range of 1400 to 1800 r/min. This consistency close to 100% also indicated consistency in the prediction of heat transfer with varying speed. It also indicated that practically all the heat transfer was represented by the models. From 1800 to 2200 r/min the percentage decreased to 93,6 which, although relatively low, was still regarded as being acceptable.

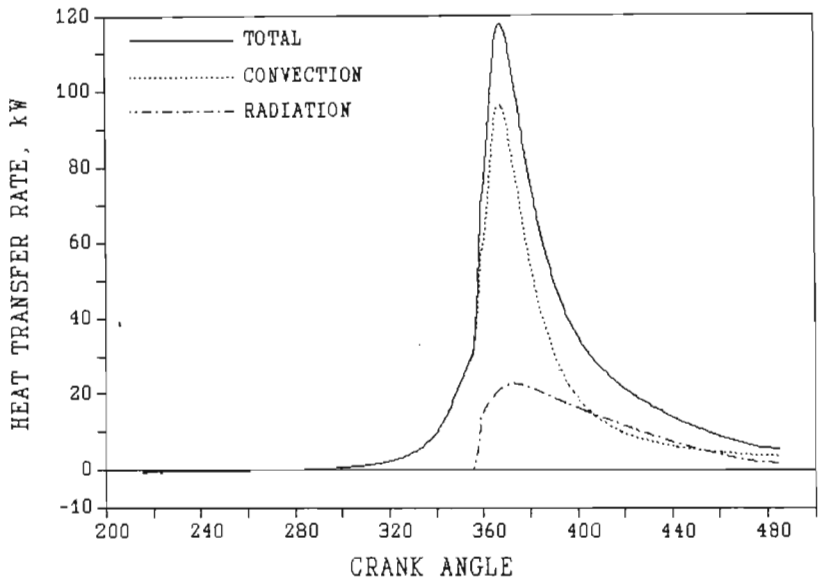

Figure 76 The variation of the radiation, convection and total heat transfer rates with crank angle at rated speed and 200 Nm.

The variation of the percentage of fuel mass burnt with load at constant speed was consistent for the torque range of 150 - 200 Nm. There was a slight increase at 100 Nm and then a significant decrease to 91% at 50 Nm. This latter decrease was attributed mainly to inconsistent combustion and irregular injection at the low load setting.

While the energy balance was selected as the most suitable method of evaluating the overall prediction of heat transfer in this project, it was recognised that the tests had been carried out in a four cylinder engine with combustion being monitored in only one cylinder at the front of the engine. Hence it was assumed

that the fuel was equally distributed among all four cylinders and that the indicated mean effective pressure generated in each cylinder was equal. Differences in these variables between cylinders could account for the variations in percentage of fuel mass burnt at the different loads and speeds. However, the energy balance still provided a useful verification of the overall heat transfer. The objective of the project was to provide a diagnostic model and therefore it should be applicable to production engines such as the ADE 236 engine used in this project.

Verification of the predicted heat transfer with the heat flux probe measurements was carried out with the resultant gas velocities at the probe site being specified as for the motored engine heat transfer predictions. As was discussed earlier with the motored engine tests the soot deposits had a significant influence on the heat flux measured at the probe. Therefore it was necessary to take into account the attenuation of the heat flux caused by the deposits. By comparing the heat flux before the start of combustion with the motored engine heat flux before and after the fired engine tests it was possible to establish the history of the soot deposition during the fired engine tests.

The effect of the soot deposition is best illustrated by examining the heat fluxes at 2200 r/min which are presented in Figure 77. Included in Figure 77 are the motored engine heat fluxes before and after the fired engine tests. It can be seen that the motored engine heat flux measured before correlates well with the heat flux measured with the engine idling at 2200 r/min. However, thereafter there is a distinct attenuation of all the curves before the start of combustion for the higher loads and in these cases the motored engine heat flux measured after the fired engine tests correlates well. This result implied that the initial deposits of soot had a significant effect on the heat flux but thereafter, assuming that further deposition did take place, no further attenuation of the heat flux occurred. The close correlation between the motored engine

heat flux after the fired engine tests and the portion of the heat flux measured before the start of combustion at constant load with varying speed also supported this observation.

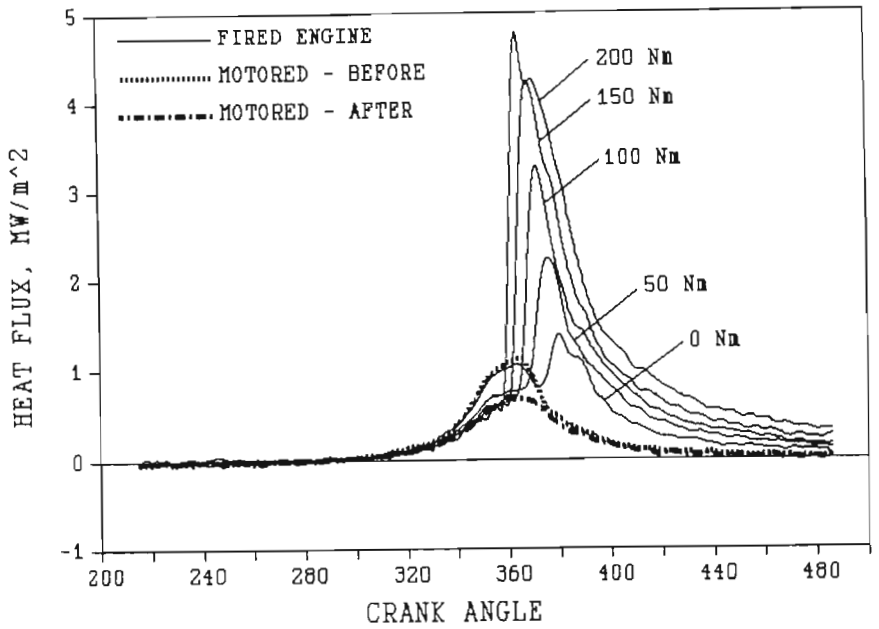

Figure 77 Variation of measured heat flux with crank angle for different loads and for a motored engine at 2200 r/min.

The attenuation of the heat flux by the soot deposits was counteracted by amplifying the heat flux measurements so that acceptable agreement with the predicted heat flux was achieved during the compression stroke. The predicted heat flux was determined using the same resultant velocity as computed for the motored engine tests discussed earlier. The latter predictions had been shown to correlate very closely with the measured heat flux from the clean probe.

As the heat flux probe was positioned just inside the bowl perimeter and therefore was exposed to the combustion events in the piston bowl and to radiation from the products of combustion it was necessary to incorporate radiation heat transfer into the total heat flux predicted at the probe site. In this case the area-averaged radiation heat transfer was used. In addition the convective temperature computed for the inner volume was applied in the calculation of convective heat transfer at the probe. The

wall temperature specified in these calculations was the same as the average surface temperature measured at the probe.

A comparison of the predicted and measured heat fluxes can be made by examining Figures 78 and 79. In each of the graphs three curves are shown which represent the measured heat flux, the predicted heat flux computed with the convective temperature for the inner volume and the predicted heat flux computed with the burnt zone temperature. The graphs in Figures 78 and 79 which are for constant speed and varying loads show some significant points of deviation of the predicted values from the measured values.

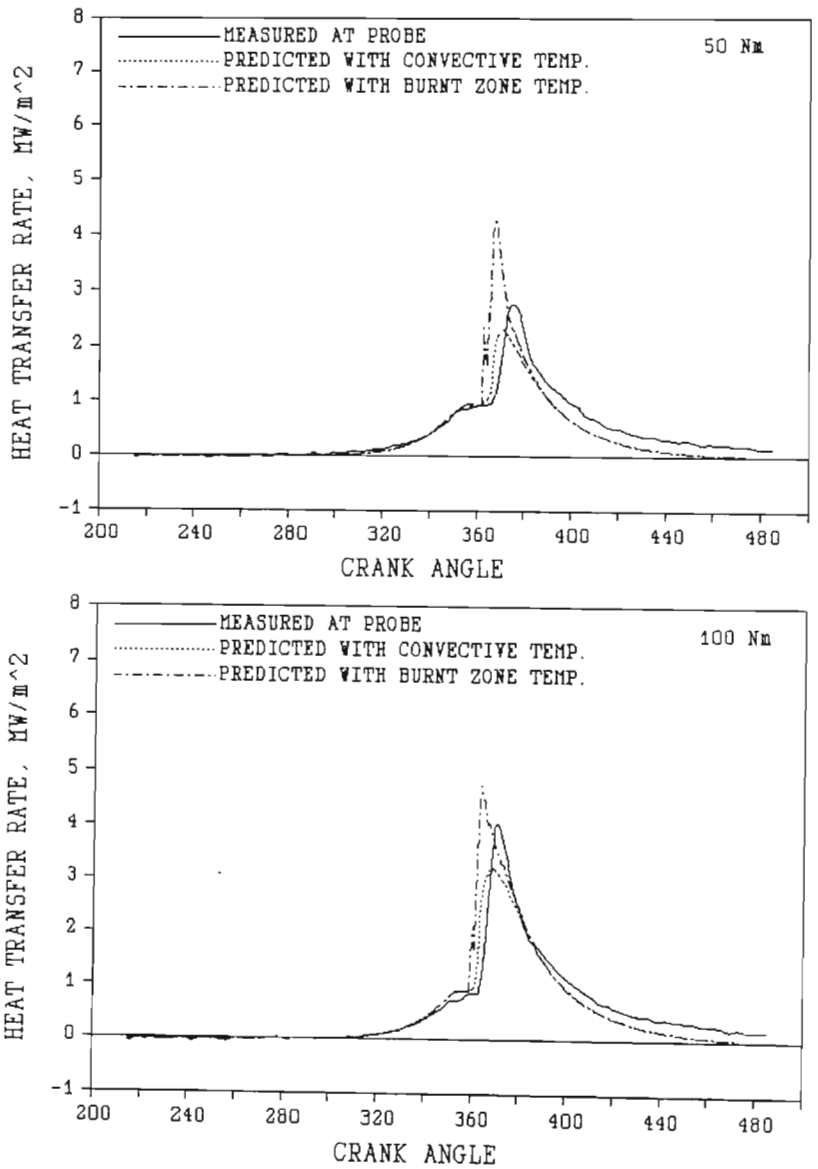

Figure 78 The predicted and measured heat fluxes varying with crank angle at 50 Nm and 100 Nm for rated speed.

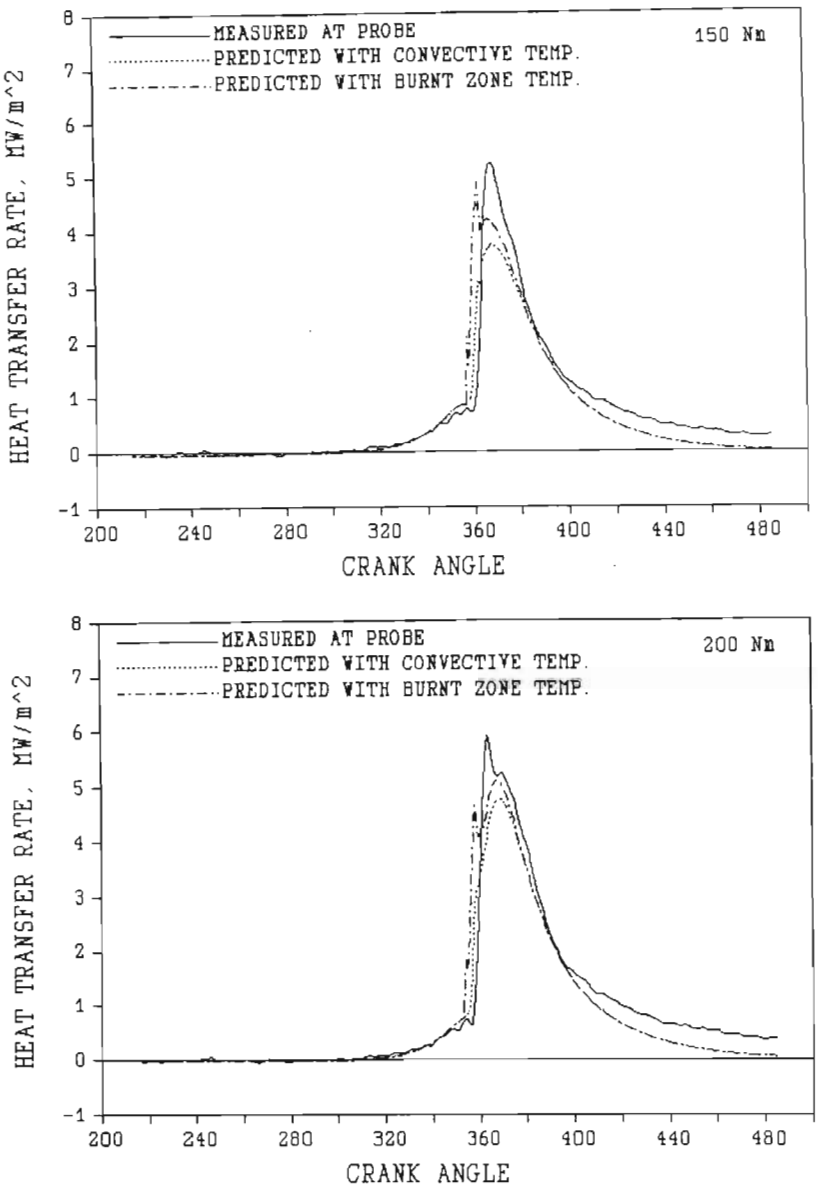

Figure 79 The predicted and measured heat fluxes varying with crank angle at 150 and 200 Nm for rated speed.

The first point of deviation was the crank angle at which the heat flux increased sharply as a result of the start of combustion. At all test points the rise in the measured heat flux was retarded compared to the predicted heat flux. However, the initial rates of increase of flux for the predicted and measured values were almost identical.

The second significant difference was the peak heat flux reached. Again in all cases the model predicted a lower peak than the

measured flux based on the convective temperature. In addition the heat flux measured at 2200 r/min and 200 Nm exhibited a prominent narrow peak followed by a second much smaller peak. Double peaks were also exhibited in the fluxes measured at 200 Nm with varying speed as shown in Figures 80 and 81. Annand and Ma (1970) reported double peaks in their measurements of heat flux and associated them with the premixed and diffusion phases of combustion. Dent and Sulaiman (1977) observed the influences of the two stages of combustion in their heat flux data as well.

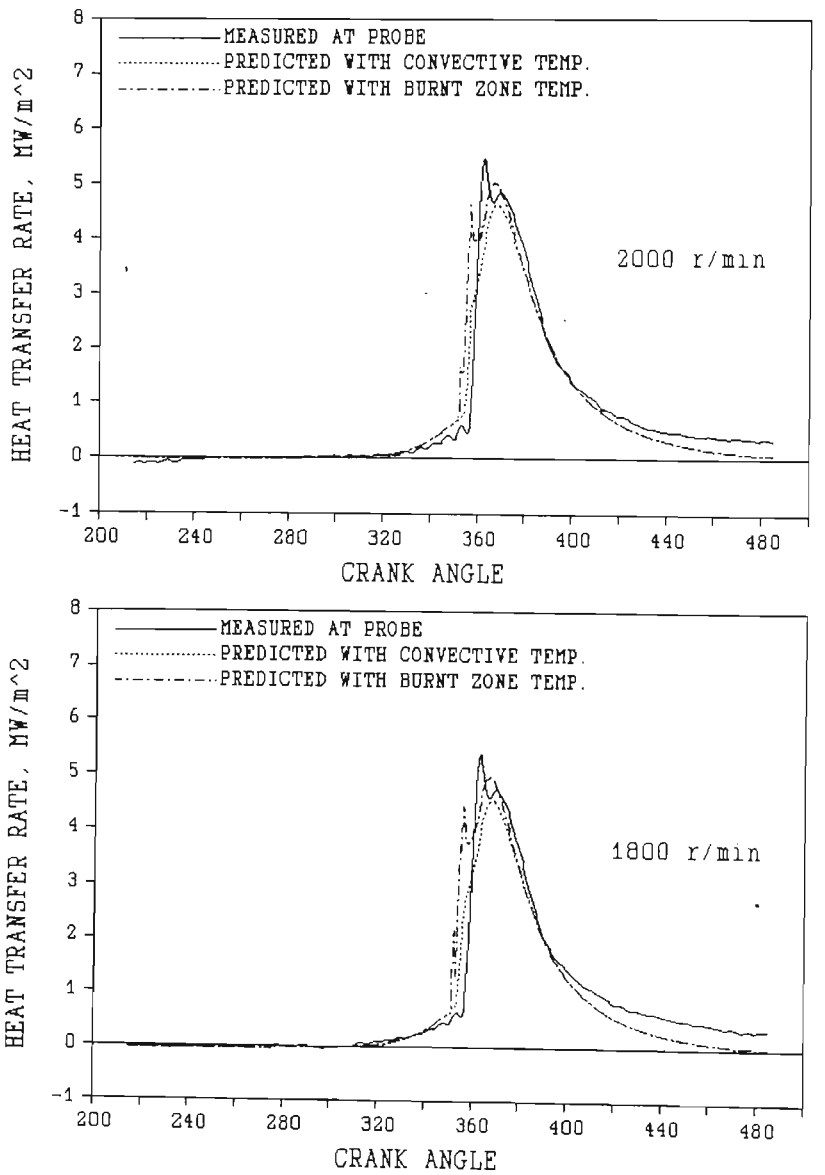

Figure 80 The predicted and measured heat fluxes varying with crank angle at 200 Nm for speeds of 1800 and 2000 r/min.

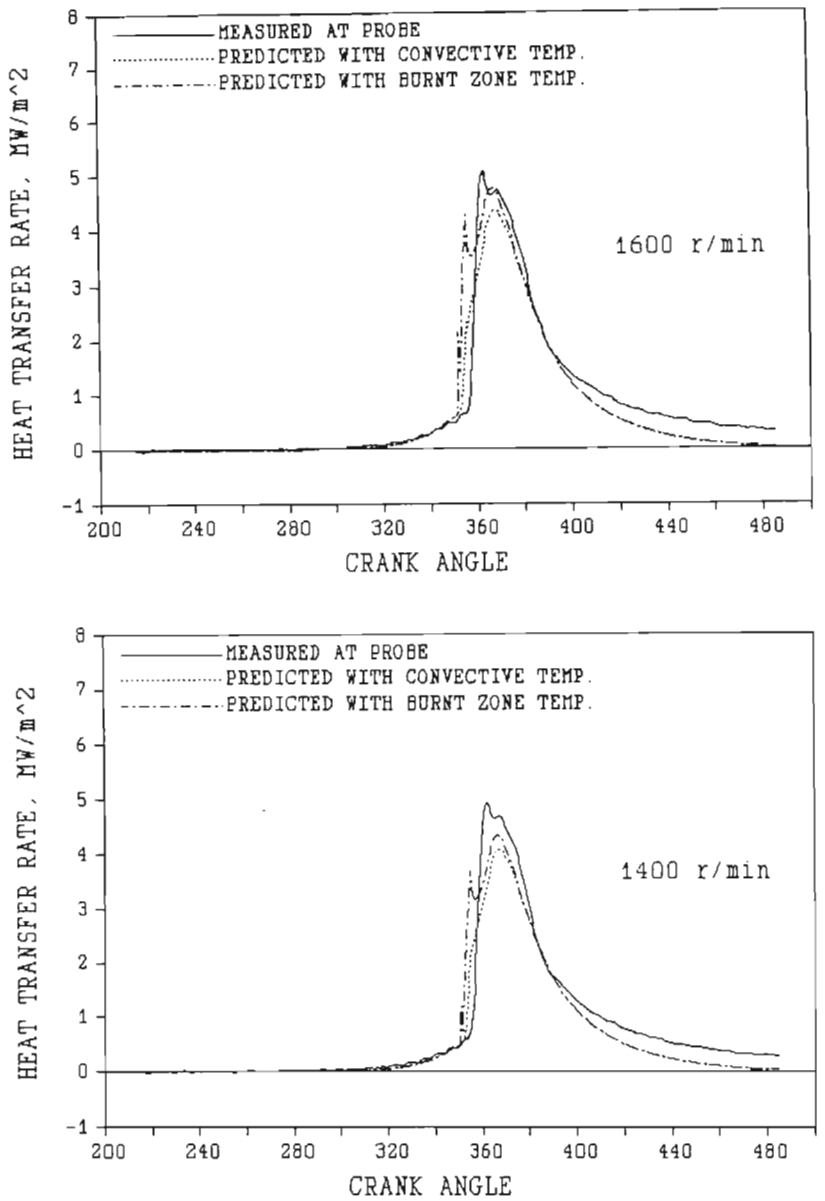

Figure 81 The predicted and measured heat fluxes varying with crank angle at 200 Nm for speeds of 1400 and 1600 r/min.

An initial study of the present set of data suggested that the two stages of combustion were responsible for both peaks. However, a closer examination of the heat fluxes measured at constant load and varying speed showed that the first peaks were all occurring within the narrow range of 362,5° to 365°CA. The positions of the peak rates of heat release at the same speeds for the same load varied between 355°CA and 358°CA. The initial sharp rise in measured heat flux at 1400 r/min and 200 Nm was

retarded relative to the predicted rise in heat flux by less than 2,5°CA. At 2200 r/min and 200 Nm this retardation was approximately the same. Hence in these measurements it was concluded that the first peak in the heat flux was not directly linked to the premixed phase of combustion.

An investigation of the peak heat fluxes for the motored engine tests at the same speeds for the clean probe indicated that these peaks also fell within a narrow band of 363° to 365°CA which corresponded very closely to the range observed for the first peak heat fluxes in the fired engine tests. The following explanation is put forward for the trends observed in the measured heat fluxes.

Starting off with the load setting of 50 Nm at 2200 r/min, injection timing was retarded and therefore start of combustion was somewhat retarded. A single peak of heat flux occurred which, taking into account the further retardation of the rise in measured heat flux, coincided with the end of the premixed phase and therefore with what could be regarded as the maximum rate of diffusion combustion. Increasing the load to 100 and 150 Nm resulted in the same single peak in each case but with corresponding increases in peak values. The peak heat flux at 150 Nm took place just before 370°CA. Again these peaks corresponded to the peaks in diffusion combustion rates.

At 2200 r/min and 200 Nm the start of combustion had advanced sufficiently so that the heat flux started to rise sharply after combustion just before TDC. This rise also signified a substantial rise in cylinder pressure. The result was that as the piston started its descent from TDC the reverse squish that was generated was boosted further by the hot, high pressure combustion gases flowing into the cooler, low pressure zones sandwiched between the piston crown and head. The boosted reverse squish then caused an increase in the heat flux particularly in the case of the measurements at the probe, which was situated at a point in the head where the hot gases were

likely to impinge as they found their way from the piston bowl into the clearance volume. This same reasoning could be applied to the measured heat fluxes shown in Figures 80 and 81.

The differences in the crank angles at which the heat fluxes began to rise after the start of combustion as well as the differences in the predicted and measured peak heat fluxes could be attributed partly to the location of the fuel spray plumes. Annand and Ma (1972) and Van Gerpen et al. (1985) stated that the position of the fuel spray plume relative to the surface thermocouple could have a significant effect on the measured heat flux.

An examination of the trajectories of the spray plumes for the ADE 236 engine indicated that there was one plume upstream of the probe relative to the direction of swirl. Figure 82 illustrates the approximate positions of the plumes compared to the head. The injection of fuel upstream of the probe would have meant that there would have been a time delay before the fuel reached the vicinity of the probe and also started burning. This factor was regarded as the main cause of the delayed response of the probe.

The effect of the position of the spray plumes highlighted the heterogeneous form of the combustion and therefore the localised differences in conditions in the combustion chamber. These differences were also likely to apply to the gas temperatures. It could be said that the temperatures at the probe could vary from the unburnt zone temperature to the burnt zone temperature as combustion took place. Therefore, for comparative purposes, the predicted heat flux based on the burnt zone temperature was included in Figures 78 to 81. At the lower loads of 50 and 100 Nm and at rated speed it was possible that an intermediate temperature between the convective temperature and the burnt zone temperature would be applicable. At 150 Nm even the predicted peak heat flux using the burnt zone temperature fell slightly

short of the measured peak heat flux. Nevertheless there was better correspondence when the burnt zone temperature was used.

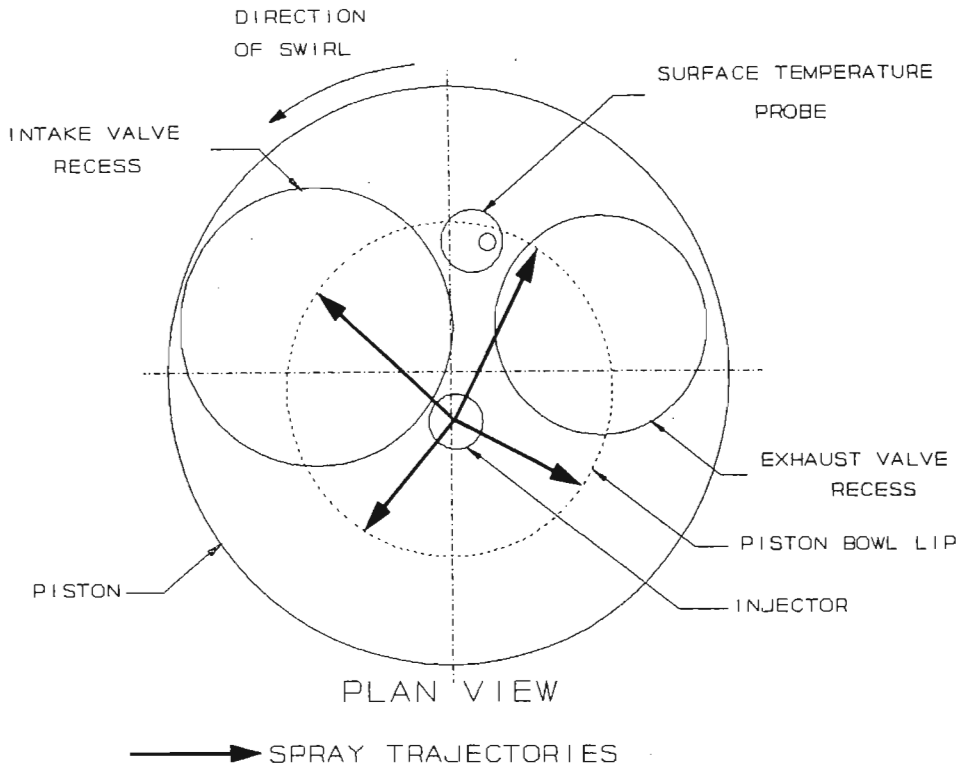

Figure 82 The plan view of the cylinder head and piston showing the approximate trajectories of the spray plumes.

At 200 Nm and 2200 r/min as well as at the lower speeds there was much closer agreement in the peak heat fluxes taking into account the temperature range being considered for the calculation of the predicted heat flux. It was therefore concluded that, apart from the selection of the appropriate gas temperature, the model was providing acceptable predictions of heat flux that were linked to the gas flow characteristics.

The results presented in this section show that, using fired engine data, the model generates heat transfer rates which can be defended not only on a global basis where the heat transfer rates through designated surfaces are averaged, but also in terms of point predictions in the combustion chamber. The results also

highlight the considerable variation in heat transfer that can occur from one point in the chamber to another. Such variations add considerable weight to the objective of moving away from a zero-dimensional model to a quasi-dimensional type where some predictions can be made on a more localised rather than global basis. For this type of prediction the well established global heat transfer models of Annand (1963) and Woschni (1967) are inappropriate because of their formulations and the variables upon which they are based with particular reference to the heat transfer coefficients.

5. CONCLUSIONS

On completion of the calibration and verification of the model it was possible to reach a number of important conclusions. These ranged from conclusions made concerning the individual sub-models to conclusions that were relevant to the overall model and the original objectives. They are presented in that order.

In the calibration and verification of the gas flow processes, excellent agreement with published data was achieved for the squish and swirl components of gas flow generated by the model. In addition these results were obtained for both a bowl-in-piston engine configuration typical of direct injection diesel engines and a flat piston configuration typical of spark ignition engines. It was concluded that the model was able to predict the dominant gas velocity components of squish and swirl for a broad range of engines with a precision that would provide a firm foundation for the calculation of convective heat transfer rates. This model could also be used as an effective tool for investigating the consequences of varying combustion chamber geometry on the gas flow processes. While emphasis was placed on diesel engine configurations, the model could be adapted easily for analysing swirl and squish processes in spark-ignition engines.

Verification of the turbulence intensities produced in the combustion chamber during the compression and expansion strokes proved to be less definitive than squish and swirl. Nevertheless with the aid of published data it was concluded that the right trends and orders of magnitude were being achieved with this component of the model.

The same conclusions were made concerning the resultant velocities and friction coefficients in the absence of published measurements of these variables. The role of these variables in the prediction of convective heat transfer rates was extremely

important as convective heat transfer dominated the modes of heat transfer occurring in the combustion chamber.

Measurements of heat flux and combustion pressure in the commercially marketed multi-cylinder ADE 236 direct injection diesel engine provided further confirmation of the precision of the model not only with respect to overall predictions of heat transfer but also to the gas flow predictions. The motored engine tests highlighted the ability of the model to predict gas velocities and hence convective heat transfer rates at particular locations in the cylinder. This level of precision had important implications in the study of locative thermal stresses particularly where boundary conditions for finite element analyses were required. The good agreement between predicted and measured heat transfer rates also confirmed the high accuracy of calibration of the gas flow models with particular reference to the corrective coefficients.

It was concluded from the results of the motored engine tests before and after the engine had run under fired conditions for approximately one hour that soot deposits attenuated the heat flux measurements significantly. Comparisons of these data with the fired engine heat flux measurements indicated that the soot was deposited within the first stages of firing but achieved an equilibrium fairly quickly with no further noticeable attenuation of the heat flux. It was therefore erroneous to neglect the effects of soot in the measurement of heat flux. However, only crude-oil derived diesel fuel was involved in these tests. It was likely that other fuels particularly the alcohols would generate different amounts of soot thereby causing a corresponding effect on the heat flux.

The output from the model for fired engine conditions was verified both on a global basis and for the single point measurement at the heat flux probe. The two zone combustion model provided a burnt zone geometry which varied as expected. The variations in the burnt zone temperature were credible and

conformed to what could be expected based on published data. The combustion chamber temperatures that were generated from the two-zone combustion provided significant inputs to the calculation of convection and radiation heat transfers. The effort in establishing the two-zone combustion model was justified on these grounds alone without considering any other uses of such a formulation.

Both the convective heat transfer and radiation heat transfer components for fired conditions followed expected trends and were of the right order of magnitude. Substantial variations in both instantaneous and total convective heat transfers to the piston, liner and head pointed again to the value of the quasi-dimensional approach in determining heat transfer rates. Although the radiative heat transfer rates could not be verified directly with the measurements that were made, the proportion of total radiative heat transfer could be reconciled easily with the proportion of total convective heat transfer. The soot and gas emissivities that were generated by the model were regarded as acceptable in terms of the objectives of the model. The radiation temperatures conformed well with predictions by a number of researchers.

The conduction heat transfer model, although relatively simple, provided a significant improvement in the prediction of wall temperatures over the use of single wall temperature values to represent the average temperature of all the chamber walls for all engine load conditions. This model responded to changes in engine load and speed and was also linked to oil and coolant temperatures which depicted the boundary conditions surrounding the combustion chamber.

In the final phase of the verification process where the combined heat transfer was examined, an energy balance taking into account energy released from the fuel and heat transfer showed that the model was providing acceptable predictions of the total heat transfer from the combustion chamber.

Predictions of heat flux at the probe did not approach the same level of agreement with measured heat flux as achieved under motored engine conditions. Nevertheless when compared to the correspondence of measured and calculated heat flux published by researchers, the predictions that were obtained were acceptable. The main cause of the deviations of the predicted heat fluxes from the measured values was localised variations in combustion as a result of the positions of the fuel spray plumes relative to the measurement point. It was also concluded that combustion affected the gas flow processes with particular reference to squish as the initial high rise in pressure at the start of combustion which tended to occur shortly before TDC created a substantial pressure differential between the piston bowl and the gas zone sandwiched between the piston crown and the cylinder head. The reverse squish was therefore amplified considerably. The present gas flow model did not include any terms that responded directly to this phenomenon as the cylinder pressure was assumed to be uniform throughout the cylinder. In further research with this model it is recommended that additional terms be introduced into the momentum flux equations to account for the effects of injection and combustion.

Another aspect of the model that could be refined further is in the production of turbulence. Extra terms taking into account turbulence generation and dissipation from shear at the boundary of the designated inner and outer volumes and shear at the cylinder walls could be included in the differential equations governing the production and dissipation of turbulence. Such terms could rely on an input from related terms used in the computation of swirl.

Only one fuel was used to verify the model for this project and it was concluded that this was adequate in terms of the objectives of the project. Future projects with the model should include the testing of a wide range of fuels that have different physical and chemical properties and hence different soot forming

tendencies. The response of the radiative heat transfer model to these fuels should provide useful information about these fuels with respect to this component of heat transfer.

A review of the overall predictions achieved with the model and their comparisons with measured data indicated that the main objectives of this research had been achieved with considerable success. Of particular note was the calibration and verification of the gas flow model which was regarded as the highlight of the overall exercise.

It was concluded that the different sub-models which were combined to form the overall model each contributed their individual strengths in relation to the level of accuracy dictated by their effect on the overall model.

In spite of the problems of modelling the heterogeneous combustion in compression-ignition engines, solutions for which are still being pursued by prominent researchers in this field, I believe that this model provides definite improvements over zero-dimensional models and over some of the more sophisticated quasi-dimensional models because of its ability to account for localised heat transfer with a high degree of accuracy.

6. REFERENCES

Abu-Romia, M.M. and Tien, C.L., 1967. Appropriate mean absorption coefficients for infrared radiation of gases. Trans. ASME, J. Heat Transfer, 89: 321 - 327.

Alkidas, A.C., 1986. The influence of partial suppression of heat rejection on the performance and emissions of a divided-chamber diesel engine. SAE paper 860309.

Alkidas, A.C., 1987. Combustion characteristics of a single-cylinder open-chamber diesel engine. Trans. ASME, J. Eng. for Gas Turbines and Power, 109: 419 - 425.

Annand, W.J.D., 1963. Heat transfer in the cylinders of reciprocating internal combustion engines. Proc. I. Mech. E., 177: 973 - 996.

Annand, W.J.D. and Ma, T.H., 1970. Instantaneous heat transfer rates to the cylinder head surface of a small compression-ignition engine. Proc. I. Mech. E., 185: 976 - 987.

Arcoumanis, C., Begleris, P., Gosman, A.D., and Whitelaw, J.H., 1986. Measurements and calculations of flow in a research diesel engine. Trans. SAE paper 861563, 95: 6.850 - 6.868.

Arcoumanis, C., Bicen, A.F. and Whitelaw, J.H., 1983. Squish and swirl - squish interaction in motored model engines. Trans ASME, J. Fluids Eng., 105: 105 - 112.

Arcoumanis, C. and Whitelaw, J.H., 1987. Fluid mechanics of internal combustion engines - a review. Proc. I. Mech. E., 201(C1): 57 - 74.

Assanis, D.N. and Heywood, J.B., 1986. Development and use of a computer simulation of the turbocompounded diesel system for engine performance and component heat transfer studies. SAE paper 860329.

Belaire, R.C., Davis, G.C., Kent, J.C. and Tabaczynksi, R.J., 1983. Combustion chamber effects on burn rates in a high swirl spark ignition engine. SAE paper 830335.

Benson, R.S. and Whitehouse, N.D., 1983. Internal combustion engines. Pergamon Press, Oxford, England.

Borgnakke, C., Davis, G.C. and Tabaczynski, R.J., 1981. Predictions of in-cylinder swirl velocity and turbulence intensity for an open chamber cup in piston engine. Trans. SAE paper 010224, 90: 964-978.

Borman, G. and Nishiwaki, K., 1987. Internal-combustion engine heat transfer. Prog. Energy Combust. Sci., 13: 1 - 46.

Brandl, F., Reverencic, I., Cartellieri, W. and Dent J.C., 1979. Turbulent air flow in the combustion bowl of a D.I. diesel engine and its effect on engine performance. SAE paper 790040.

Brehob, D.D. and Kittelson, D.B., 1988. A review of CI engine in-cylinder diagnostics for the investigation of soot loading, chemical composition, and temperature. SAE paper 880515.

Callahan, T.J., Yost, D.M. and Ryan, T.W., 1985. Acquisition and interpretation of diesel engine heat release data. SAE paper 852068.

Chang, S.L. and Rhee, K.T., 1983. Computation of radiation heat transfer in diesel combustion. SAE paper 831332.

CRC Handbook, 1986. Handbook of chemistry and physics. 66th Ed. CRC Press, Boca Raton, Florida, USA.

Dao, K., Uyehara, O.A. and Myers, P.S., 1973. Heat transfer rates at gas-wall interfaces in motored piston engine. SAE paper 730632.

Davis, G.C. and Borgnakke, Ck., 1982. The effect of in-cylinder flow processes (swirl, squish and turbulence intensity) on engine efficiency - model predictions. Trans. SAE paper 820045, 91: 176 -188.

Davis, G.C. and Tabaczynski, R.J., 1988. The effect of inlet velocity distribution and magnitude on in-cylinder turbulence intensity and burn rate - model versus experiment. Trans. ASME, J. Eng. for Gas Turbines and Power, 110: 509 - 514.

Davis, G.C., Tabaczynski, R.J. and Belaire, R.C., 1984. The effect of intake valve lift on turbulence intensity and burnrate in S.I. engines-model versus experiment. SAE paper 840030.

Dent, J.C. and Derham, J.A., 1974. Air motion in a four-stroke direct injection diesel engine. Proc. I. Mech. E., 188: 269 - 280, D61 - D68.

Dent, J.C. and Sulaiman, S.J., 1977. Convective and radiative heat transfer in a high swirl direct injection diesel engine. SAE paper 770407.

Durrett, R.P., Oren, D.C. and Ferguson, C.R., 1987. A multi-dimensional data set for diesel combustion model validation : 1 - initial conditions, pressure history and spray shapes. SAE paper 872087.

Eichelberg, G. 1939. Some new investigations on old combustion engine problems. Engineering, 148: 463 - 464, 547 - 560.

Faletti, J.J., Sorenson, S.C. and Goering, C.E., 1982. Energy release rates from hybrid fuels. ASAE paper 82-1548.

Fansler, T.D., 1985. Laser velocimetry measurements of swirl and squish flows in an engine with a cylindrical piston bowl. SAE paper 850124.

Flynn, P., Mizusawa, M., Uyehara, O.A. and Myers, P.S., 1972. An experimental determination of the instantaneous potential radiant heat transfer within an operating diesel engine. SAE paper 720022.

Foster, D.E., 1985. An overview of zero-dimensional thermodynamic models for IC engine data analysis. SAE paper 852070.

Goering, C.E., 1986. Engine and tractor power. PWS Publishers, Boston, Massachusetts, USA.

Gosman, A.D. and Harvey, P.S., 1982. Computer analysis of fuel-air mixing and combustion in an axisymmetric DI diesel. SAE paper 820036.

Grasso, F. and Bracco, F.V., 1983. Sensitivity of chamber turbulence to intake flows in axisymmetric reciprocating engines. J. AIAA, 21: 637 - 640.

Gülder, Ö.L., 1986. Flame temperature estimation of conventional and future jet fuels. Trans. ASME, J. Eng. for Gas Turbines and Power, 108: 376 - 380.

Gunn, M.E., 1987. Simulation of internal combustion engine processes. Bull. Energy Conversion and Utilization Technologies, DOE/ECU - 87/5: 1 - 11.

Haddad, S. and Watson, N., 1984. Design and applications in diesel engineering. Publ. Ellis Horwood Ltd., England.

Hansen, A.C., Taylor, A.B., Lyne, P.W.L. and Meiring, P., 1989. Alternative fuels combustion and performance monitor for C-I engines. Draft Final Report prepared for National Energy Council by Dept. of Agric. Eng., Univ. Natal, Pietermaritzburg, RSA.

Hayder, M.E. Varna, A.K. and Bracco, F.V., 1985. A limit to TDC turbulence intensity in internal combustion engines. A.IAA, J. Propulsion and Power, 1 (4): 300 - 308.

Heywood, J.B.., 1980. Engine combustion modeling - an overview. In combustion and Modeling in Reciprocating Engines, Ed Mattavi, J.N. and Amann, C.A., Plenum Press, New York, USA.

Hohenberg, G.F., 1979. Advanced approaches for heat transfer calculations. SAE paper 790825.

Holman, J.P., 1986. Heat transfer. 6th Ed. McGraw-Hill Book Co., New York, USA.

Johnston, S.C., Robinson, C.W., Rorke, W.S., Smith, J.R. and Witze, P.O., 1979. Application of later diagnostics to an injected engine. SAE paper 790092.

Kamel, M. and Watson, N., 1979. Heat transfer in the indirect injection diesel engine. SAE paper 790826.

Kouremenos, D.A., Rakopoulos, C.D. and Karvounis, E., 1988. Thermodynamic analysis of direct injection diesel engines by multi-zone modelling. In Analysis and design of advances energy systems : computer-aided analysis and design. Publ. ASME, AES - Vol 3 - 3: 67 - 77.

Krieger, R.B. and Borman, G.L., 1966. The computation of apparent heat release for internal combustion engines. ASME paper 66 - WA/DGp-4.

Kumar, S., Edsell, J., Milkins, E. and Watson, H., 1985. Modeling the heat and mass transfer and combustion processes of alternative fuels in diesel engines. Paper presented at Third Australasian Conference on Heat and Mass Transfer, University of Melbourne, Victoria 3052, Australia.

Kunitomo, T., Matsuoka, K. and Oguri, T., 1975. Prediction of radiative heat flux in a diesel engine. SAE paper 750786.

Lancaster, D.R., Krieger, R.B. and Lienesch, J.H., 1975. Measurement and analysis of engine pressure data. SAE paper 750026.

Launder, B.E. and Spalding, D.B., 1972. Lectures in mathematical models of turbulence. Academic Press, England.

Lawton, B., 1987. Effect of compression and expansion on instantaneous heat transfer in reciprocating internal combustion engines. Proc. I. Mech. E., 201(A3): 175 - 186.

Lilly, L.C.B., 1984. Diesel engine reference book. Publ. Butterworths, London, England.

Lipkea, W.H. and De Joode, A.D., 1987. A model of a direct injection diesel combustion system for use in cycle simulation and optimization studies. SAE paper 870573.

Lipkea, W.H., De Joode, A.D. and Christenson, S.R., 1987. The relationship between nitric oxide and work as influenced by engine operating conditions and combustion system parameters for a direct injection diesel engine. SAE paper 870269.

Martin, J.K. and Ahmad, T., 1986. Heat-release characteristics of an open-chamber diesel engine employing a wall-wetting combustion system. SAE paper 860420.

McCracken, D.D. and Dorn, W.S., 1964. Numerical methods and FORTRAN programming. Publ. John Wiley and Sons, Inc., New York, USA.

Monaghan, M.L. and Pettifer, H.F., 1981. Air motion and its effect on diesel performance and emissions. SAE paper 810255.

Morel, T., Fort, E.F. and Blumberg, P.N., 1985. Effect of insulation strategy and design parameters on diesel engine heat rejection and performance. SAE paper 850506.

Morel, T. and Keribar, R., 1985. A model for predicting spatially and time resolved convective heat transfer in bowl-in-piston combustion chambers. Trans. SAE paper 850204, 94: 2.77 - 2.93.

Morel, T. and Keribar, R., 1986. Heat radiation in DI diesel engines. SAE paper 860445.

Morel, T., Keribar, R. and Blumberg, P.N., 1988. A new approach to integrating engine performance and component design analysis through simulation. SAE paper 880131.

Morel, T., Wahiduzzaman, S. and Fort, E.F., 1988. Heat transfer experiments in an insulated diesel. SAE paper 880186.

Morel, T., Wahiduzzaman, S., Tree, D.R. and DeWitt, D.P., 1987. Effect of speed, load and location on heat transfer in a diesel engine - measurements and predictions. SAE paper 870154.

Murakami, A., Arai, M. and Hiroyasu, H., 1988. Swirl measurements and modelling in direct injection diesel engines. SAE paper 880385.

Murakami, A., Hiroyasu, H. and Arai, M., 1986. Time and space resolved measurement of air motion in a cylinder of direct-injection diesel engine. Trans SAE paper 861229, 95: 99 -108.

Nusselt, W., 1923. Dev Warmeubergang in der Verbrenungskraftmaschene, Z. Verdt. Ing., 67: 692 - 708.

Oguri, T. and Inaba, S., 1972. Radiant heat transfer in diesel engines. SAE paper 720023.

Olikara, C. and Borman, G.L., 1975. A computer program for calculating properties of equilibrium combustion products with some applications to IC engines. SAE paper 750468.

Oren, D.C., Durrett, R.P., Ferguson, C.R., Timar, J., Tree, D.R. and DeWitt, D.P., 1987. A multi-dimensional data set for diesel combustion model validation : II - fuel injection rate and boundary conditions. SAE paper 872088.

Peterson, R.C. and Wu, K.J., 1986. The effect of operating conditions on flame temperature in a diesel engine. SAE paper 861565.

Rao, V.K. and Bardon, M.F., 1985. Convective heat transfer in reciprocating engines. Proc. I. Mech. E., 199 (D3): 221 - 226.

Reynolds, W.C., 1980. Modeling of fluid motions in engines. In Combustion Modeling in Reciprocating Engines. Ed. Mattavi, J.N. and Amann, C.A., Plenum Press, New York, New York, USA: 41 - 68.

Saito, T., Daisho, Y., Uchida, N. and Ikeya, N., 1986. Effects of combustion chamber geometry on diesel combustion. SAE paper 861186.

Savage, L.D., 1982. Personal communication. Mech. Eng. Dept., University of Illinois, Urbana-Champaign, Illinois, USA.

Sitkei, G. and Ramanaiah, G.V., 1972. A rational approach for calculation of heat transfer in diesel engines. SAE paper 720027.

Strehlow, R.A., 1984. Combustion fundamentals. Publ. McGraw-Hill Book Co., New York, USA.

Szekely, G.A. and Alkidas, A.C., 1986. A two-stage heat release model for diesel engines. SAE paper 861272.

Tabaczynski, R.J., 1983. Turbulence measurements and modelling in reciprocating engines - an overview. Conference Proc. I Mech. E., C51/83: 51 - 59.

Tabaczynski, R.J., Trinker, F.H. and Shannon, B.A.S., 1980. Further refinement and validation of a turbulent flame propagation model for spark-ignition engines. Combustion and Flame, 39: 111 - 121.

Taylor, A.B., 1987. Combustion quality of selected compression-ignition fuels. Unpubl M Sc.Eng thesis, Dept. of Agric. Eng., Univ. Natal, Pietermaritzburg, RSA.

Taylor, A.B., Hansen, A.C., Lyne, P.W.L. and Meiring, P., 1989. Engine stress from combustion of alternative fuels in compression-ignition engines. Draft Final Report prepared for National Energy Council, Pretoria, RSA.

Tennekes, H. and Lumley, J.L., 1972. A first course in turbulence. MIT Press, Cambridge, Massachusetts, USA.

Theobald, M.A. and Alkidas, A.C., 1987. On the heat release analysis of diesel engines : effects of filtering of pressure data. SAE paper 872059.

Timoney, D.J., 1987a. Effects of important variables on measured heat release rates in a DI diesel. SAE paper 870271.

Timoney, D.J., 1987b. Problems with heat release analysis in DI diesels. SAE paper 870270.

Tsai, S., Lipkea, W.H. and De Joode, A.D., 1987. Use of an optimization procedure with a model of the combustion system in a direct injection diesel engine. ASME paper 87 - ICE - 34.

Van Gerpen, J.H., Huang, C. and Borman, G.L., 1985. The effects of swirl and injection parameters on diesel combustion and heat transfer. SAE paper 850265.

Wahiduzzaman, S., Morel, T., Timar, J. and DeWitt, D.P., 1987. Experimental and analytical study of heat radiation in a diesel engine. SAE paper 870571.

Way, R. J. B., 1977. Methods for determination of composition and thermodynamic properties of combustion products for internal combustion engine calculations. Proc. I. Mech. E., 190: 687 - 697.

Wong, V.W. and Hoult, D.P., 1979. Rapid distortion theory applied to turbulent combustion. SAE paper 790357.

Woschni, G., 1967. A universally applicable equation for the instantaneous heat transfer coefficient in the internal combustion engine. SAE paper 670931.

Woschni, G., 1970. Die Berechnung der Wanderverluste und der Thermischen Belastung der Bauteile von Diesel-motoren. MTZ, 30: 491 - 499.

Woschni, G., 1979. Prediction of thermal loading of supercharged diesel engines. SAE paper 790821.

Woschni, G. and Fieger, J., 1979. Determination of local heat transfer coefficients at the piston of a high speed diesel engine by evaluation of measured temperature distribution. SAE paper 790834.

Wotherspoon, D., 1988. Personal communication. Atlantis Diesel Engines (Pty) Ltd., Atlantis, RSA.

Yoshimitsu, T., Toyama, K., Sato, F. and Yamaguchi, H., 1984. Capabilities of heat insulated diesel engine. In The Adiabatic Engine: Past, Present and Future Developments, SAE/PT-84/28: 17 - 35.

7. APPENDICES

Appendix A Derivation of equations for radial and axial mass transportation of gases in the combustion chamber

For the determination of the radial transportation of mass due to squish the combustion chamber was divided into an inner and an outer volume as shown in Figure 30 with a boundary at the radius of the bowl. Assuming that the density is uniform throughout the cylinder it follows that:

$$\frac{m_1}{V_1} = \frac{m_0}{V_0}$$

where subscript 0 = total chamber
1 = inner volume
also 2 = outer volume.

Substituting for the volumes,

$$m_1/[\pi R_1^2.(l + h)] = m_0/(\pi R_2^2.l + \pi R_1^2.h)$$

hence $m_1 = [R_1^2.(l + h)/(R_2^2.l + R_1^2.h)].m_0$ -----(A1)

differentiating equation (A1) with respect to l,

$$\frac{dm}{dl}_1 = [- \frac{R_1^2.(R_1^2.l + R_1^2.h)}{(R_2^2.l + R_1^2.h)^2} + \frac{R_1^2}{R_2^2.l + R_1^2.h}].m_0$$

Re-arranging and simplifying:

$$\frac{dm}{dl}_1 = [R_1^2.(R_1^2 - R_2^2).h/(R_1^2.h + R_2^2.l)^2].m_0$$

For the determination of the axial transportation of mass into the bowl, the combustion chamber was divided into two volumes with a boundary at the entrance into the piston bowl as shown in Figure 31. Applying the same procedure as above:

$$\frac{m_4}{V_4} = \frac{m_0}{V_0}$$

where subscript 4 = piston bowl

then $m_4/(\pi R_1^2.h) = m_0/(\pi R_2^2.l + \pi R_1^2.h)$

or $m_4 = [R_1^2.h/(R_2^2.l + R_1^2.h)].m_0$ -----(A2)

Differentiating equation (A2) with respect to l,

$$\frac{dm_4}{dl} = [- R_1^2.R_2^2.h/(R_2^2.l + R_1^2.h)^2].m_0$$

Appendix B Derivation of ratio of burnt mass to total mass of gas in terms of the instantaneous proportion of CO_2 generated during combustion

Consider the general chemical equation:

$$C_xH_yO_z + a_1.O_2 + a_2.N_2 \rightarrow a_3.N_2 + a_4.CO_2 + a_5.H_2O + a_6.O_2 \text{---(B1)}$$

From the composition of air,

$$a_3 = a_2 = 3{,}76a_1 \text{---(B2)}$$

Equating the number of molecules on either side of equation (B1):

$$x = a_4$$
$$y = 2a_5$$
$$\text{and } z + 2a_1 = 2a_4 + a_5 + 2a_6$$

Initially let $a_6 = 0$ and $a_{1s} = a_1$ for stoichiometric conditions,

$$\text{then } z + 2a_{1s} = 2a_4 + a_5$$
$$\text{or } a_{1s} = a_4 + a_5/2 - z/2$$

Substituting for a_4 and a_5,

$$a_{1s} = x + y/4 - z/2 \text{---(B3)}$$

The equivalence ratio, ϕ is equal to the actual fuel-air ratio, F_a divided by the stoichiometric fuel-air ratio, F_s.

Using equations (B1) to (B3) it can be shown that:

$$F_s = 137{,}3.(x + y/4 - z/2)/(12x + y + 16z) \text{---(B4)}$$

For F_a , $a_6 > 0$

hence $F_a = a_1.137{,}3/(12x + y + 16z)$

where the value for a_1 represents the actual burning conditions in the cylinder.

Hence $a_1 = F_a.B = (\phi.F_s).B$ ---(B5)

where $B = (12x + y + 16z)/137,3$

Substituting for F_s in equation (B5) with equation (B4) and simplifying:

$$a_1 = \phi.(x + y/4 - z/2)$$

For actual burning conditions it can be shown from equation (B1) with substitution of a_1 to a_5 that:

$$a_6 = (\phi - 1).(x + y/4 - z/2)$$

Therefore the total exhaust output by mass, m_e is given by:

$$m_e = 28a_3 + 44a_4 + 18a_5 + 32a_6$$

Hence the total proportion of CO_2 by mass, m_{ct} can be obtained:

$$m_{ct} = 44a_4/m_e$$

The instantaneous ratio of burnt mass m_b to total mass m_t of gas in the cylinder during combustion can be calculated from the equation:

$$m_b/m_t = (m_{ci} - m_{cb})/m_{ct}$$

where

m_{ci} = instantaneous mass of CO_2 accumulated from combustion and calculated from the equilibrium composition of the cylinder contents

m_{cb} = mass of CO_2 present at the beginning of combustion as a residual.

Appendix C Derivation of geometrical constraints on burnt volume

The following geometrical constraints on the burnt volume were applied:

1. the burned zone is symmetrical relative to the axis of the piston, the bowl axis being assumed to coincide with the piston axis;
2. the distances from the burnt zone to the piston bowl bottom and to the head are equal;
3. the aspect ratios of the burnt zones in the clearance volume and in the bowl are equal to the aspect ratios of the whole clearance volume and of the whole bowl respectively.

In the initial stages of combustion the burnt zone will be largely confined to the bowl and therefore will not have expanded into the volume above the piston crown.

Referring to Figure C1 for $L \leq 2\delta$,

$(H + L)/2R_1 = \delta/X$ or $X = [2R_1/(H + L)].\delta$

Therefore

$$V_b = \pi(R_1 - X)^2.(L + H - 2\delta) \qquad \text{-----(C1)}$$

Multiplying out and expanding equation (C1), a third order equation for δ is obtained:

$$8\delta^3 - 12T.\delta^2 + 6T.\delta + T^2.V_b/\pi R_1^2 - T^3 = 0 \qquad \text{-----(C2)}$$

where $T = L + H$.

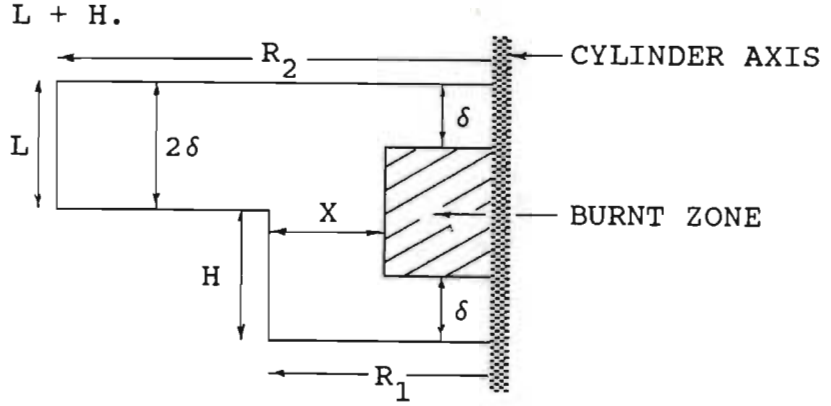

Figure C1 Geometry of the burnt zone when confined to the bowl

Referring to Figure C2, for $L > 2\delta$, assume that:

$$H/2R_1 = \delta/X \quad \text{or} \quad X = (2R_1/H).\delta$$

then $$V_c = \pi(R_1 - X)^2.H \qquad \text{-----(C3)}$$

where V_c = cylindrical burnt volume with smaller radius.

Also $$L/2R_2 = \delta/Y \quad \text{or} \quad Y = (2R_2/L).\delta$$

and $$V_d = \pi(R_2 - Y)^2.(L - 2\delta) \qquad \text{-----(C4)}$$

where V_d = cylindrical burnt volume with larger radius.

Hence total burnt volume is given by:

$$V_b = V_c + V_d$$

Combining Equations (C3) and (C4) and expanding into a third order equation :

$$A.\delta^3 - B.\delta^2 + C.\delta + D = 0 \qquad \text{-----(C5)}$$

where $A = 8R_2^2/L^2$

$$B = 4R_1^2/H + 12R_2^2/L$$

$$C = 4R_1^2 + 6R_2^2$$

$$D = V_b/\pi - R_1^2.H - R_2^2.L$$

Equations (C2) and (C5) were solved using the Newton-Raphson method.

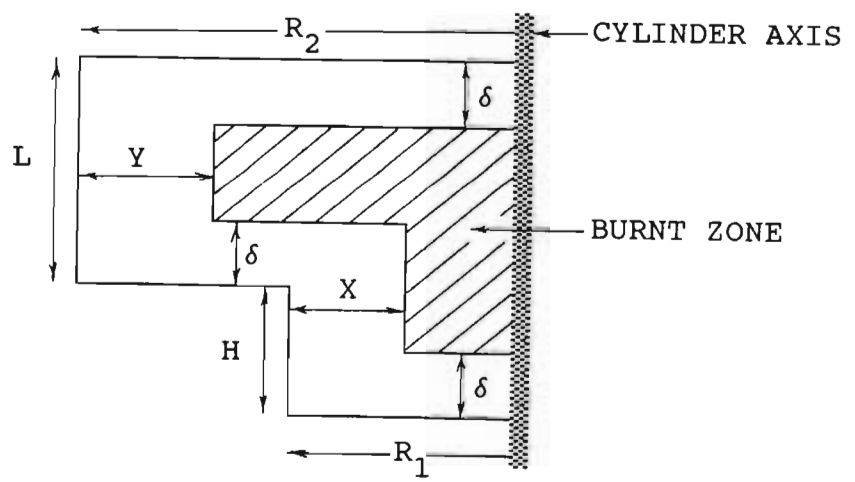

Figure C2 Geometry of the burnt zone when when expanded into the clearance volume.

Appendix D Calculation of Swirl Ratio at Inlet Valve Closing for the ADE 236 engine

The calculation of swirl ratio for the naturally aspirated ADE 236 engine was based on the Ricardo Momentum Summation Method for predicting engine swirl reported by Lilly (1984). This method relies on measurements carried out on a steady state flow rig. The following assumptions are made in this method:

a) The flow through the inlet port is incompressible and adiabatic on both the engine and the steady state flow rig.

b) The port retains the same characteristics under the transient conditions in an engine as it does under steady flow rig conditions.

c) The pressure drop across the port is assumed to be constant during induction.

d) Angular momentum is conserved and skin friction does not impede swirl.

e) Volumetric efficiency is 100%.

f) Flow occurs between inlet valve opening and closing so that flow is dependent on valve lift.

The swirl ratio R_s is defined as the ratio of the charge swirl speed at end of induction to the engine crankshaft speed. The Ricardo swirl ratio is determined from the equation:

$$R_s = \frac{L_d \int_{\alpha_1}^{\alpha_2} C_f . N_r \, d\alpha}{\int_{\alpha_1}^{\alpha_2} C_f^2 \, d\alpha} \qquad \text{-----(D1)}$$

where

C_f = flow coefficient = $Q/A.V_o$

A = valve throat area, m^2

Q = measured quantity of air flow, m^3/s

V_o = theoretical air velocity = $\sqrt{(2\Delta p/\rho)}$, m/s

Δp = pressure drop across valve, Pa

ρ = air density in inlet port, kg/m^3

N_r = non-dimensional rig swirl = $\omega_r . B/V_o$

ω_r = rig swirl as measured at any valve lift, rad/s
B = cylinder bore diameter, m
α_1 = crank angle at inlet valve opening, rad
α_2 = crank angle at inlet valve closing, rad
L_d = engine shape factor = $B.S/D^2$
S = stroke, m
D = inlet valve throat diameter, m

Measurements of swirl on a master cylinder head for the naturally aspirated ADE 236 engine for agricultural applications using a steady state flow rig were carried out by Atlantis Diesel Engines (Pty) Ltd. (Wotherspoon, 1988). In addition measurements of cam lift relative to camshaft rotation were supplied for this engine application by Wotherspoon (1988).

Values for C_f and N_r were determined from these data. A third order regression was used to obtain the correlation between flow coefficient and valve lift. Figure D1 shows that the regression curve is in good agreement with the data giving an R^2 value of greater than 99%. A greater scatter in the data for the swirl measurements was evident as illustrated in Figure D2. As a compromise a second order regression curve was fitted which provided an acceptable average swirl value when integrated over the valve lift angle.

Integration of the flow coefficient from IVO to IVC for the ADE 236 engine provided a mean flow coefficient of 0,308 which compared well with values quoted by Monaghan and Pettifer (1981) and Lilly (1984). In addition the curves in Figures D1 and D2 were of the right order of magnitude and shape.

The crank rotation from IVO to IVC was obtained from Wotherspoon (1988) for the Agric head of the ADE 236 being 5°BTDC to 35°ABDC giving a total value of 220° of crank rotation. From the profile of the cam lift in Figure D3 a small initial rise and final fall in lift can be seen. The clearance between the value and rocker will result in actual valve lift closer to the portion of the

curve which rises steeply. Hence the start of lift was adjusted so that 220° of total lift were obtained.

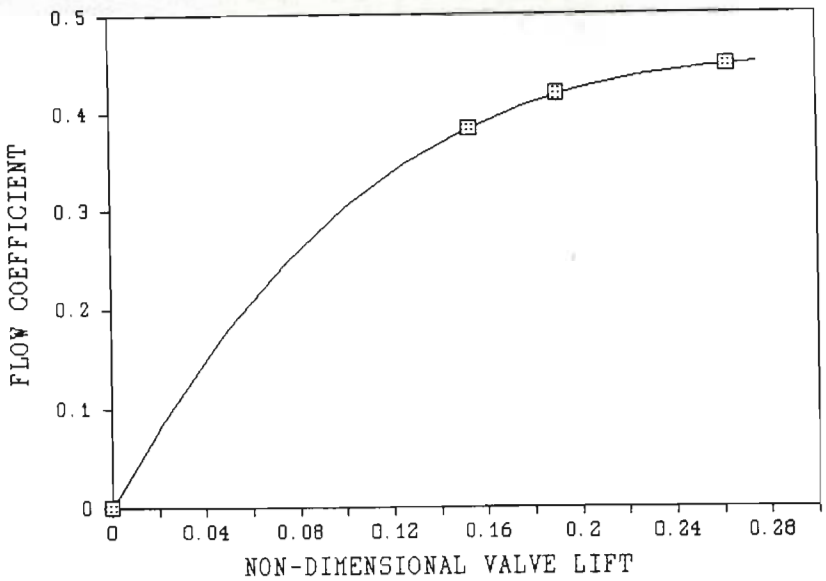

Figure D1 Non-dimensional inlet valve lift versus flow coefficient for the ADE 236 agricultural cylinder head.

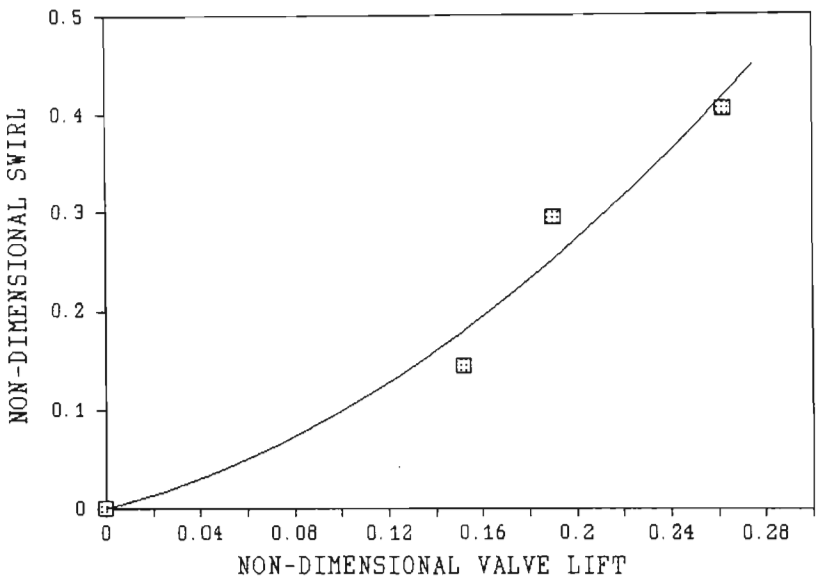

Figure D2 Non-dimensional inlet valve lift versus non-dimensional swirl for the ADE 236 agricultural head.

Measurements taken by Monaghan and Pettifer (1981) while comparing the vane swirl meter with the impulse swirl meter indicated that the vane swirl meter tended to underestimate by approximately 30% although the actual differences varied from port to port and was not obviously related to the type of port.

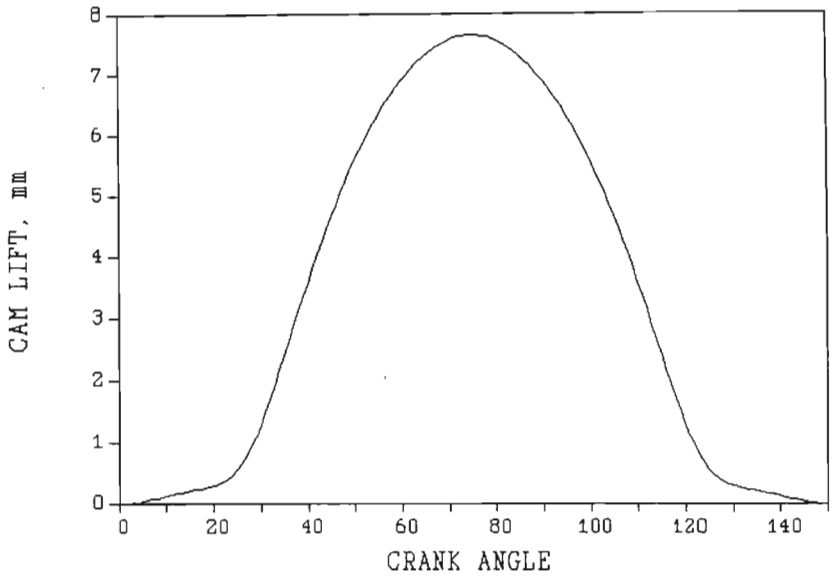

Figure D3 Cam angle versus cam lift for inlet valve.

Using equation (D1) the swirl ratio was determined as 1,72 from the vane swirl meter readings. By increasing this value by a factor of 1,3 to give 2,24 a more representative swirl ratio is obtained as recommended by Monaghan and Pettifer (1981) and Lilly (1984). In measurements carried out by Monaghan and Pettifer (1981) on a plain directed port similar to that of the ADE 236 engine, the vane swirl meter provided a Ricardo swirl ratio of 1,7 while the impulse meter value was 2,5. Hence it was concluded that the values obtained for the ADE 236 engine were acceptable for use in calculations of swirl flow during the compression and expansion strokes.

Appendix E A table of the results of the fired engine tests

VARIABLES	TEST RESULTS								
	1	2	3	4	5	6	7	8	9
ATMOS. CONDITIONS:									
Pressure (kPa)	92.8	92.8	92.8	92.8	92.8	92.8	92.8	92.8	92.8
Dry bulb temperature (°C)	30	30	30	30	30	30	30	30	30
Inlet air temperature(°C)	39.4	41.6	43.3	47.2	52.7	53.1	52.8	62.1	78.1
ENGINE PERFORMANCE:									
Speed (r/min)	2200	2202	2201	2202	2199	2003	1804	1603	1407
Torque (Nm)	0.4	50.2	100.3	149.4	200.4	199.6	199.5	199.2	199.4
BMEP (kPa)	1	163	325	485	650	647	647	646	647
Power (kW)	0.1	11.6	23.1	34.4	46.1	41.9	37.7	33.4	29.4
Fuel consumption (kg/h)	3.15	4.95	7.07	9.38	12.43	10.91	9.49	8.21	7.23
Spec. fuel cons (g/kWh)	***	427	306	272	269	261	252	245	246
Equivalence ratio	0.21	0.33	0.47	0.62	0.83	0.76	0.7	0.68	0.74
Volumetric efficiency (%)	78.8	78.8	78.8	78.8	78.8	82.2	87	87.2	80.3
Exhaust temperature (°C)	216	298	380	480	609	583	536	496	495
Bosch smoke	0.4	1	1.4	1.5	3.55	2.7	1.55	1	1.05
COMBUSTION ANALYSIS:									
IMEP (kPa)	157	321	487	634	826	817	785	748	732
FMEP (kPa)	156	158	162	149	176	170	138	102	85
Start of Injection (°CA)	357	354.5	351.5	348.5	346	346	346	345.5	345
Start of combustion (°CA)	365.5	361.5	359	355.5	352.5	352	351	351	350
Ignition delay (ms)	0.64	0.53	0.57	0.53	0.49	0.5	0.46	0.57	0.59
Max. dP/dt (MPa/s)	1621	3354	6091	8571	11470	10117	8624	7434	7357
@ (°CA)	373	367	363	360.5	357	356	355	354	354
Peak pressure (kPa)	4043	4808	5808	6611	7736	7918	8148	8255	8137
@ (°CA)	359	370	367.5	366	367.5	367.5	367	366	365.5
Fuel mass burned (%)	75.2	91	95.4	93.6	93.5	96.6	98.2	98.7	98

CA - Crank Angle